hGCP3 and Psoriasin: Is Their Interaction Biologically Significant in Human Breast Cancer?

by

Charlton M. Cooper

A Thesis submitted to the Faculty of Graduate Studies of

The University of Manitoba

in partial fulfilment of the requirements of the degree of

MASTER OF SCIENCE

Department of Biochemistry and Medical Genetics

University of Manitoba

Winnipeg

THE UNIVERSITY OF MANITOBA

FACULTY OF GRADUATE STUDIES

*****

COPYRIGHT PERMISSION PAGE

hGCP3 and Psoriasin:

Is Their Interaction Biologically Significant in Human Breast Cancer?

BY

Charlton M. Cooper

A Thesis/Practicum submitted to the Faculty of Graduate Studies of The University of Manitoba in partial fulfillment of the requirements of the degree

of

MASTER OF SCIENCE

In memory of my father

Abstract

An increasing body of evidence suggests that centrosomal dysfunction is a contributory factor, rather than side effect of early cancer progression. Our lab has identified psoriasin (S100A7) as an important player in promoting early breast cancer progression. To understand psoriasin's intracellular function we sought to identify putative psoriasin-interacting proteins with a yeast-2-hybrid (Y2H) assay. Therein we identified two centrosomal associated proteins as candidate psoriasin-interacting proteins. This has led us to hypothesize that psoriasin may promote cellular properties associated with cancer progression, in part, by influencing centrosomal function.

The aim of the current study was to determine whether one of these candidates, γ-tubulin ring complex protein-3 (hGCP3) physically interacts with psoriasin and whether this interaction is biologically relevant in breast cancer cells. To assess a biochemical interaction between these proteins by co-immunoprecipitation, Cos1 cells were transiently co-transfected with plasmids encoding psoriasin and His-hGCP3. A weak interaction was identified in some experiments but this could not be consistently reproduced. This may reflect the fact that immunofluorescent labeling of His-hGCP3 in transiently transfected cells did not display proper cellular distribution that is reported for its endogenous counterpart. To test whether psoriasin expression has a biological effect on endogenous hGCP3 function in the context of breast cancer cell line, we assayed two parameters of centrosomal function. The first being the effect psoriasin expression on normal mitotic microtubule spindle architecture, and the second, the ability to regrow microtubules from centrosomes that have been stripped of microtubules by pre-treatment

with nocodazole. It was found that psoriasin had no effect on the frequency or type of mitotic aberrations present in any cell line studied, nor on the capacity of naked centrosomes to regrow microtubules.

It is therefore concluded, that although an interaction between hGCP3 and psoriasin can occur in the Y2H system, it does not appear that this interaction is conserved in mammalian cells. Moreover, the absence of changes in centrosomal function when psoriasin is overexpressed supports this conclusion and suggests that a psoriasin-hGCP3 interaction is not biologically significant in human breast cancer.

Acknowledgements

I would like to begin with my sincerest thanks to Dr. Peter Watson for his guidance, help and advice, and his ability to 'rally the troops' during the course of this project when 'moral was low'. Thank you for your continuous support and forever positive comments as well as your insight and profound knowledge into the world of breast cancer.

I would like to convey my deepest appreciation to my committee members Dr. Bob Shiu, and Dr. Leigh Murphy for all their help and guidance. Thank you for imparting to me a strong sense of passion for science by simply being deeply-dedicated and contagiously-enthused about the work you're both doing. Thank you.

Next, I would like to thank Dr. Ethan Emberley, for without whom the foundation of the project would never have been laid and for your patient guidance during my early days of indoctrination into the lab. Thanks for all the laughs.

Molly, Andrea, Sylvia, Sandy, Adewale, Ladislav, Yulian, and Linda (I apologise for lumping you all together for each of you should be thanked individually, however) I thank you as a group, not only for your collective scientific knowledge that was a limitless source of answers to my questions, but additionally for making my experience within the Watson Lab more of a Watson family. Thanks for all the laughs.

I am deeply grateful to the GCCRD (Genomic Centre for Cancer Research and Diagnosis) at the Manitoba Institute for Cell Biology, University of Manitoba, for

without access to resources housed therein I certainly could not have completed the project.

Finally, thank you Nadalene for without your patience, support and love I would not have accomplished much.

Table of Contents

Index of Figures

List of Tables

List of Abbreviations

a.a.	amino acid
ADH	Atypical ductal hyperplasia
ALH	Atypical lobular hyperplasia
AmpR	Ampicillin resistance
BC	Breast Cancer
BSA	Bovine serum albumin
Ca^{2+}	Calcium cation
CAIX	Carbonic anhydrase IX
Co-IP	Co-immunoprecipitation
CIAP	Calf intestinal alkaline phosphatase
CIN	Chromosomal instability
CSN	COP9 signalosome complex
C-terminus	carboxy-terminus
DAPI	4',6-diamidino-2-phenylindole-dihydrochloride)
DCIS	Ductal carcinoma in situ
DMEM	Dulbecco's modified Eagle's medium
Dgrip	Drosophila γ-tubulin ring interacting protein
ER	Estrogen receptor-α
FBS	Fetal bovine serum
FEFAG	Fragment elution from agarose gel
FISH	Fluorescent in situ hybridization
GCP	γ-tubulin complex proteins
γTuC	γ-tubulin complex
γTuRC	γ-tubulin ring complex
γTuSC	γ-tubulin small complex
hGCP3	Human γ-tubulin complex protein 3
Hif1α	Hypoxia inducible factor 1α
IBC	Invasive breast cancer
IF	Immunofluorescent

IHC	Immuno-histochemistry
Jab1	c-Jun activating binding protein 1
LB	Luria-Bertani
LCIS	Lobular carcinoma in situ
MCS	Multicloning site
MRG	Microtubule regrowth assay
MM	Mouse monoclonal
MMP13	Matrix metalloproteinase 13
MSM	Mitotic spindle morphology
MT	Microtubule
MTOC	Microtubule organising centre
MW	Molecular weight
NiMa	Never in Mitosis
NS	Non-specific
N-terminus	Amino-terminus
OD	Optical density
ORF	Open reading frame
PCM	Pericentriolar material
RanBPM	Ran-binding protein M
RP	Rabbit polyclonal
rtTA	Reverse tet transactivator
SDM	Site directed mutagenesis
SDS-PAGE	Sodium dodecyl sulphate- polyacrilamide gel electrophoresis
SPB	Spindle pole body
TDLU	Terminal ductal lobular unit
TNT	Transcription and translation
VEGF	Vascular endothelial growth factor
Xgrip	Xenopus γ-tubulin ring interacting protein
Y2H	Yeast-2-hybrid

I. Introduction

1. Breast cancer

1.1. Breast Cancer Stats

The most common cancer among Canadian women is breast cancer, and it is estimated that this year alone 21,600 women will be diagnosed with the disease and 5,300 will succumb to its effects. In Manitoba, it is anticipated that 770 new cases will be diagnosed and 200 women will die of the disease. Although it is sometimes difficult to grasp the full impact of statistics based on a population as a whole, they translate into the fact that one in 9 women is expected to develop breast cancer during her lifetime and one in 27 will die of it (provided current diagnostic and treatment options remain the same.) These statistics may seem like grim news, however incidence rates for breast cancer have stabilized and death rates have declined since 1993. Arguably, this is largely the result of public awareness and increased communication about the disease that has ultimately led to more frequent screenings earlier in a women's life. As such breast cancers are being diagnosed at much earlier stages of the disease. (Source: Canadian Cancer society).

One such early stage lesion that is increasingly being diagnosed is ductal carcinoma *in situ* (DCIS) and the incidence rates have dramatically increased fivefold to six fold in the last quarter of the 20th century in North America (Ernster VL et al., 1996; Holland R et al., 1994). This increased detection rate is directly associated with more frequent mammogram screenings, that can detect microcalcifications associated DCIS (Holland R et al., 1994). Overall, it is estimated that 1 in every 1300 mammography examinations

leads to a diagnosis of DCIS (Ernster VL et al., 2002).This translates into the fact that nearly 20% of all breast cancers detected presently by screening in North America are DCIS (Ernster VL et al., 2002; Olivotto I et al., 2001).

1.2. DCIS-Types and Grading

DCIS refers to a category of breast lesions that are histopathologically, genetically and clinically dissimilar; however they are all morphologically characterized by uncontrolled proliferation of the glandular epithelium and having some, but not all cellular features of malignancy, namely the ability to invade surrounding tissue. As such, they are considered in place *(in situ)* as the tumour mass is contained within the milk-duct which in turn presents an intact basement membrane. In this sense, DCIS is considered pre-invasive, pre-malignant and even pre-cancerous (Allred DC et al., 2001). There are two major categories of DCIS that are distinguished by a pathologist based their appearance: non-comedo and comedo. The salient morphological feature distinguishing the later from the former is the presence of necrosis. There are many types of non-comedo DCIS and the most common are characterized as solid, cribiform, papillary and micropapillary depending on the morphological arrangement of cells.

Several histological grading systems have been developed to help determine a patients projected outcome (prognosis) in terms of risk for progression to invasive breast cancer (IBC) and risk to recurrence once the tumor is removed. The need for grading systems is based on the fact that well-differentiated DCIS probably gives rise to low-grade invasive breast carcinoma, which have a better long term clinical outcome than high-grade invasive breast carcinoma (Gupta SK et al., 1997). Grading systems are based on

malignant classifiers observed by a pathologist under the microscope who examines tumor cells obtained from biopsies, lumpectomies or mastectomies. These malignant classifiers include cellular as well as histological features such as the degree of cellular differentiation, cytonuclear malignancy grade, and degree of necrosis. Some tumor grading schemes have assigned scores to multiple malignant classifiers to generate prognostic indexes based on their combined score. For example, the Van Nuys grade is largely based on nuclear grade and presence of necrosis. In general all DCIS grading schemes typically use a three grade system ranging from Low grade (Grade 1) lesions, to Intermediate grade (Grade 2) to High grade (Grade 3) lesions. For example, the Van Nuys Prognostic index defines low grade lesions as those with small nuclei and no necrosis; intermediate grade lesions as those with intermediate size nuclei and with zonal necrosis; and high grade lesions as those with large abnormal nuclei and typically manifest associated necrosis. As such, increasing grade number reflects increasing tumor aggressiveness. Conversely, the likelihood of finding associated invasive carcinoma increases with the defined grade of DCIS (Bonnett M et al., 2002). In general, comedo-type DCIS are clinically more aggressive than non-comedo, and the presence of necrosis likely reflects a fast tumor growth rate. As such, there exist areas within comedo type lesions where cellular demands for oxygen and nutrients exceed the vasculature's ability to supply these essentials.

1.3 Breast Cancer Progression-DCIS is a direct precursor of IBC

It is widely accepted that malignant breast cancers arise from certain pre-existing lesions and develop over long-periods of time. By and large, breast cancers originate from rogue

members amongst the epithelial cells that delimit the milk ducts. More precisely, they arise within the area of the breast anatomically defined as the terminal ductal lobular units (TDLU), which are the structures containing the small milk producing glands located at the beginning of the milk-ductal system.

Breast pathologies encompass a variety of both benign and malignant disorders and pathologist have recognized for some time now a heterogeneous spectrum of morphological changes that occur both at the cellular and glandular levels associated with these different lesions. Epidemiological evidence has correlated which of these lesions have a tendency to progress to more aggressive and advanced forms of the disease. Of the many types of benign lesions, including non-proliferative disorders such as fibrocystic disease and fibroadenomas, as well as, proliferative disorders such as usual ductal hyperplasia without atypia, few have any significant potential associated with increased risk of developing invasive breast cancer (IBC). In contrast, pre-cancerous lesions described as hyperplasia with atypia, as well as bona fide carcinoma *in situ*, have long been recognized to significantly increase a women's risk of developing IBC. This has lead to a hypothetical model for the linear progression of breast cancer evolution based on the existence of certain precursor lesions. Although this histological model is undoubtedly oversimplified, it proposes that rogue stem cells in the normal TDLUs give rise to intermediate premalignant lesions, including the atypical hyperplasias (atypical ductal hyperplasia (ADH) or atypical lobular hyperplasia (ALH)), that progress to *in situ* carcinomas (ductal carcinoma *in situ* (DCIS) or lobular carcinoma *in situ* (LCIS)), which,

in the case of DCIS, eventually develop into the malignant invasive and metastatic cancers if left untreated (Allred DC et al., 2001).

Within this model, it is likely that most benign and pre-malignant lesions are not on a true biological continuum to the invasive disease in the sense that if left alone, individual cells within these low-risk lesions will acquire specific complement of genetic and epigenetic aberrations that will endow them with the gross phenotype of an invasive tumour. In fact, LCIS may only be a marker of increased breast cancer risk based on the observation that about half of associated synchronous invasive carcinomas are located in the opposite breast and many of these tumours are invasive ductal carcinomas (Allred DC et al., 2001). However, DCIS is thought to be a true and direct precursor of IBC; therefore, by definition is on the same biological continuum. Several lines of evidence support this notion. First, IBC is more common in breasts with synchronous DCIS than those without and the presence of DCIS is associated with a 10-fold increase in the risk of developing IBC (Allred DC et al., 2001). Moreover, if left untreated (or improperly treated), over long periods of time (10-40 years) a large percentage of even low-grade DCIS tumours will eventually present as synchronous invasive disease at the same site as the original DCIS (Sanders ME et al., 2005). In addition, DCIS shows almost the same degree of chromosomal instability as invasive ductal cancers (Hwang ES et al., 2004). However the most compelling evidence comes from cytogenic analysis revealing an almost identical genetic pattern (DNA gains and losses) in both invasive breast carcinoma and adjacent synchronous DCIS (Buerger H et al., 1999; Hwang ES et al., 2004; James LA et al., 1997).

1.4. Clinical Paradox

It is important to note that not all DCIS will progress to more advanced stages of the disease and in this light DCIS is thought to be a non-obligate precursor of invasive disease. It is not DCIS that kills, rather it is the invasive and metastatic phases of the disease that do. While early detection of invasive breast cancer is beneficial, the value of DCIS detection is currently a matter of debate. At present, based on the follow-up of small numbers of untreated cases that were originally misdiagnosed as benign and never treated, the best estimate for the risk of developing invasive cancer within 10 years of a diagnosis of DCIS is 10-25%, and over several decades or a lifetime is 25-40% (Sanders ME et al., 2005). Nevertheless, most DCIS are treated surgically, either by mastectomy or by lumpectomy with or without radiation while only a minority of DCIS (<2%) are not treated surgically (Ernster VL et al., 1997). This has lead to an interesting paradox in the clinical management of the disease based on the ability to diagnose these early lesions whose prognostic significance is at best, a matter of estimation. It is impossible at present to predict with one hundred percent certainty which DCIS will progress to the invasive disease from those that will not. Therefore, given that only a minority of DCIS will progress to invasive disease (provided current data on the subject is accurate), many DCIS are clinically insignificant but are nonetheless treated with invasive surgical procedures and radiotherapy. Thus a major challenge for the present and future clinical management of breast cancer is to distinguish those cases of DCIS that will go on to progress or recur from those that will not in order to identify those patients who require more invasive treatments from those who do not. This end is heavily dependent on our better understanding of the clinical, histopathological and genetic characteristics of DCIS

because the transition from preinvasive DCIS to the IBC is arguably the most critical biological event in breast cancer progression (Ernster VL et al., 1997).

One approach to resolve the DCIS clinical paradox is identify specific tissue-based markers that can serve as predictors for risk of recurrence and progression to invasive disease. Therefore it worthwhile to identify differential gene and protein expression that can be associated with clinical features of increased malignancy. Notable examples include ER-α status and Her2/Neu amplification status. Additionally, because the acquisition of invasiveness likely reflects a true biological continuum from DCIS lesion, changes in gene/protein expression between DCIS and adjacent synchronous IBC may in turn underscore specific proteins having participatory role in the acquisition of invasiveness.

1.5. Summary

The most common cancer among Canadian women is breast cancer. Fortunately, increased mammogram screenings, as well as earlier screenings in a women's life, have begun to detect the disease at increasingly earlier stages. This has greatly improved the survival rate as treatment options can be implemented much sooner in the natural progression of the cancer and is often implemented before the cancer has become invasive. One such early pre-invasive stage lesion that is increasingly being diagnosed is ductal carcinoma *in situ*. DCIS refers to a category of breast lesions that are histopathologically, genetically and clinically dissimilar. Nevertheless, DCIS is thought to be the direct but non-obligate precursor lesion to IBC based on histological, prognostic

and genetic evidence. It is important to note that not all DCIS (~50%) will progress to more advanced stages, and at present it is impossible to predict with one hundred percent certainty which DCIS will progress to the invasive disease. Nevertheless almost all cases of DCIS are treated surgically and with radiotherapy. Therefore many patients with DCIS are over treated as their DCIS was in fact clinically insignificant. To resolve this issue their has been a great need to identify genes and proteins that are differentially expressed, that can be associated with clinical features of increased malignancy and can serve as specific tissue-based markers that can better predict the risk of recurrence and progression to invasive disease.

2. Psoriasin and Breast Cancer

2.1. S100 family

2.1.1. Structure Function

To date, the S100 family of small (9-14 kDa), calcium-binding proteins comprises 21 members, all of which have in common two defining EF-hand type calcium binding domains; an imperfect one located in the N-terminus and classic EF-hand in C-terminus. S100s are exclusively expressed in vertebrates and not other metazoans. In humans, most genes encoding S100s (S100A1-S100A13) are found in a cluster on the long arm of chromosome 1. All members additionally share a common secondary protein structure where each calcium binding domain is flanked by alpha-helices and a linker region forms a hinge that separates the two helix-flanked EF-hands. Many of the members share significant amino acid sequence identity over the entire protein, however the hinge region as well as the extreme C-terminal sequence present the most divergent sequences. It is thought these latter two regions are responsible, in part, for specific biological effects associated with individual S100s. Additionally, non-redundant functions of S100s are attributable to a large degree of tissue/cell specific expression as no member is ubiquitously expressed, although some do appear to have functional overlap based on common target proteins in different cell types (Donato R, 2003).

The function of S100s was once thought to be predominantly in calcium homeostasis by virtue of their calcium binding properties. Although this may be true for specific

members, it now appears that S100s have pleiotropic functions independent of calcium homeostasis and have been implicated in the immune response, differentiation, cytoskeleton dynamics, enzyme activity, and growth. The mechanisms by which they exert their cellular effects are largely undefined, however it does appear they modulate the activity of specific target proteins through physical interactions. The activity of S100s is thought to be dependent on both their ability to dimerize and form homo- and/or heterodimers, as well as their ability to bind Ca^{2+}. Moreover their activity also seem dependent on their cellular localization as they have been described to have both intracellular and/or extracellular functions (Donato R, 2003).

2.1.2. S100s and Cancer

Several members of the S100 family are aberrantly expressed in cancer cells and in some cases are highly overexpressed (S100A4, S100A6, S100A7, S100B) while in others are markedly downregulated (S100A2). This suggests that specific S100 molecules may play a role in some aspect of tumorigenesis and/or tumor progression. Arguably, the aberrant expression of S100s in cancer cells could simply reflect deregulated cellular circuitry and therefore represent bystanders not directly implicated in the acquisition and/or promotion of cellular properties associated with cancer progression; however, this does not appear to be the case based on the evidence in the literature presented below.

For example, S100A4 has been implicated in invasion and metastasis of human tumor cells (Takenaga K et al., 1997b). S100A4 is upregulated in many cancer types and is associated with reduced survival in patients with breast (Nikitenko LL et al., 2000) and

bladder (Davies BR et al., 2002) cancers. In a model of human bladder cancer in rats, injection of cells expressing S100A4 preferentially form distant metastases over cells that do not express (Levett D et al., 2002). Moreover, by preventing S100A4 expression in the highly metastatic Lewis lung carcinoma cells by antisense RNA, the metastatic potential of these cells is significantly reduced as measured by *in vitro* motility and invasiveness assays (Takenaga K et al., 1997a). It is thought that S100A4 may exert its metastatic enhancing effect by modulating cytoskeletal dynamics (Lakshmi MS et al., 1993) and/ or through modulation of p53 activity (Grigorian M et al., 2001). Although the mechanism(s) of S100A4 action are ill-defined, S100A4 does appear to have a direct role in potentiating the metastatic behavior of cancer cells. Interestingly, S100A2 appears to have opposite effects to S100A4, and therefore not surprisingly, is downregulated in several cancers including that of the breast (Ilg EC et al., 1996), prostate (Gupta S et al., 2003) and lung (Feng G et al., 2001). It has been hypothesized that S100A2 may act as a tumor suppressor. Support for this latter assertion comes from experiments in which expression S100A2, or addition of extracellular S100A2 to the media had a significant inhibitory influence on cell motility and migration in human head and neck squamous cell carcinoma lines (Nagy N et al., 2001). This effect was attributed, in part, to modification in the polymerization/depolymerization dynamics of the actin cytoskeleton (Nagy N et al., 2001). Moreover, S100A6 has been implicated in the regulation key cellular processes that are sabotaged during neoplastic transformation, namely cell-cycle progression (Tonini GP et al., 1991) and proliferation (Breen EC et al., 2003). In addition, S100B expression is reported to reduce p53 transcriptional activity leading to reduced accumulation of the cell cycle inhibitor p21 (Lin J et al., 2001). Based on these

observations it has been speculated that S100B expression may contribute to cancer progression by inhibiting apoptosis (Lin J et al., 2001), although controversy exists in the literature whether or not this may be true (Sorci G et al., 2000). Finally, S100A7 has also been implicated in the progression of both skin and breast cancer and is further discussed in detail below (Section I-2.2).

2.1.3. S100s and the Cytoskeleton

It is of interest (to this thesis) that key targets of action for many S100s (in fact 13 out of twenty one) are elements of cytoskeleton including microtubules (MT), intermediate filaments and microfilaments, as well as specific molecular motors that travel along these elements. Growing evidence indicates a key role of S100s is in regulating the dynamics of specific cytoskeletal elements and as such influencing cell morphology and motility (Donato R, 2003). For example, S100B is found to associate with cytoplasmic MTs, mitotic spindles, as well as centrosomes (Donato R, 2001; Sorci G et al., 1998) and both S100A1 and S100B are able to cause a Ca^{2+} -dependent disassembly of cytoplasmic microtubules in a dose-dependent manner in U251 glioma cells and rat L6 myoblasts (Sorci G et al., 2000). Moreover, by modulating S100A4 expression in B16 melanoma cells it was found that increased S100A4 resulted in increased expression of unpolymerised tubulin (Lakshmi MS et al., 1993). This has led to the hypothesis that these S100s are involved in preventing excess tubulin polymerization and in MT remodelling, possibly in conjunction with cytosolic Ca^{2+} signalling (Donato R, 2001). Therefore it appears that regulation of MT dynamics is a key function of many S100s.

Although a large body of literature exists describing key functions of various S100s as they relate to other non-microtubule cytoskeletal elements (some of which have direct implications in cancer biology) in various cell models, they are not directly pertinent to this thesis; however, it is encouraged that the reader refer to an excellent review by Rosario Donato (Donato R, 2001) about this subject.

2.2. Psoriasin's Expression Profile during Breast Cancer Progression

As the monogram implies, psoriasin (S100A7) derives it's name from an association with psoriasis. In fact, psoriasin was first identified as a highly expressed, partially secreted protein in abnormally differentiated keratinocytes from psoriatic lesions of the skin (Madsen P et al., 1991). Since then it has become apparent that psoriasin is not only associated with specific inflammatory and hyperproliferative skin pathologies, but is also aberrantly expressed in several cancer types including squamous carcinomas of the skin (Alowami S et al., 2003), and bladder (Celis JE et al., 1996), as well as adenocarcinomas of the stomach (El Rifai W et al., 2002) and breast (Al Haddad S et al., 1999; Enerback C et al., 2002; Leygue E et al., 1996; Moog-Lutz C et al., 1995). Although psoriasin's normal function is not fully understood, there appears to be a strong association between its expression and specific pathologies of epithelial cell origin within the bladder, skin and breast.

Psoriasin was originally associated with breast cancer in 1995, when it was found that psoriasin mRNA is differentially expressed between primary breast cancers and nodal metastasis (Moog-Lutz C et al., 1995). However subsequent studies have identified the

key feature about psoriasin expression during breast cancer progression; psoriasin is markedly differentially expressed between pre-invasive DCIS and invasive stages of the disease. In healthy breast ducts, psoriasin is virtually undetectable; however several groups have shown that psoriasin mRNA and protein are massively up-regulated in many pre-invasive *in situ* lesions while levels of expression often drop off in invasive breast carcinomas (Al Haddad S et al., 1999; Enerback C et al., 2002; Leygue E et al., 1996). In fact, psoriasin is one of (if not the) most differentially expressed genes in high-grade ductal carcinomas in situ relative to normal ductal epithelial cells (Enerback C et al., 2002; Leygue E et al., 1996). This expression profile, coupled with the fact that transition from *in situ* to invasive carcinomas does appear to be a true biological continuum arising from clonal evolution of cells within in-situ lesions (see section I-1.3), suggests psoriasin may likely have a functional role that endows a pre-invasive cell to become invasive. Interestingly this expression profile mirrors that which is seen in skin tumorigenesis where psoriasin is rarely detected in normal epidermis but is highly expressed in many squamous carcinomas *in situ* with significantly reduced expression in invasive components (Alowami S et al., 2003). Although it is not fully understood why psoriasin expression often decreases in the invasive components, persistent expression is observed in roughly 15% of all invasive breast tumours (Emberley ED et al., 2003b). Moreover, several studies have shown psoriasin expression in both preinvasive DCIS and invasive breast carcinomas is significantly associated with markers of poor prognosis. The most compelling and consistent association is with estrogen receptor-α (ER) negative status, while other associations include higher nuclear grade, node positive status, necrosis and in some studies an increase in presence of inflammatory infiltrates (Al Haddad S et al.,

1999; Emberley ED et al., 2003b; Emberley ED et al., 2004; Enerback C et al., 2002). Moreover it is found in those patients with both ER-negative and psoriasin positive invasive tumours, they have a shorter time to progression and poorer survival than those patients with ER-negative tumours where psoriasin is absent (Emberley ED et al., 2003b). Taken together, these results provide compelling correlative data that suggest psoriasin, although not implicitly required for the acquisition of invasiveness and malignancy, significantly exacerbates the situation and, simply put, turns an already bad situation (i.e. ER-negative status) into a worse one.

2.3. Psoriasin Expression is Associated with more Aggressive Breast Cancer Phenotypes *in vitro* and *in vivo*

Although *in vivo* correlations are compelling between psoriasin expression and markers of poor prognosis in human breast tumours, it does not provide an answer as to whether psoriasin is definitively involved in the acquisition and/or promotion of cellular properties associated with cancer progression. To this end, our lab has taken a direct approach to studying the biological effects of psoriasin expression in cultured breast cancer cells. It is found that by engineering psoriasin into the ER-negative breast cancer line, MDA-MB-231, these cells grow faster, have increased invasiveness and decreased adhesion by *in vitro* assays as compared to their parental counterparts (Emberley ED et al., 2003a). Moreover, promotion of these malignant features is dependent on the level of psoriasin expression as observed in clones with high and low levels of psoriasin expression. Additionally, psoriasin expressing MDA-MB-231s are more resistant to apoptosis induced by loss of substrate attachment (Emberley ED et al., 2005), which is

thought to be a necessary biological property associated with invasiveness. The effect of psoriasin expression on tumour growth *in vivo* was also analysed by injecting high and low psoriasin expressing MDA-MB-231, as well as vector control and parental MDA-MB-231 into the mammary fat pad of nude mice. In either case, psoriasin significantly increased the tumorigenicity of MDA-MB-231 cells, and tumours appeared sooner and overall size were much larger than either control cell tumours (Emberley ED et al., 2003a). It was also noted that in 20% of mice injected with psoriasin expressing MDA-MB-231, abdominal lymph node metastases developed whereas control cells did not form metastases (Emberley ED et al., 2003a). Taken together, these data provide compelling evidence indicating psoriasin confers a more aggressive behaviour both *in vitro* and *in vivo*, and these results are consistent with correlative data in human breast tumours that indicate psoriasin is associated with markers of poor prognosis and more aggressive tumours.

2.4. Biological Functions of Psoriasin

The normal function of psoriasin is unknown. In the skin, psoriasin may be involved in the host immune/ inflammatory response as it has been found in granulocyte extracts associated with inflammatory skin pathologies (Algermissen B et al., 1996) and is chemotactic for CD4+ cells *in vitro* (Jinquan T et al., 1996). Moreover, interleukin-22, a cytokine known to have proinflammatory activities, up-regulates in a dose-dependent manner the expression of S100A7 in cultured human epidermal keratinocytes (Boniface K et al., 2005). Additionally, psoriasin may protect the skin from E.coli infection as it has been found to have E.coli killing properties and is induced and secreted by

keratinocytes when exposed to E.coli (Glaser R et al., 2005). In contrast, psoriasin expression in skin cancers does not appear to be associated with an increased numbers of inflammatory cell infiltrates suggesting psoriasin may have alternative function in neoplastic disease as opposed to inflammatory skin diseases (Alowami S et al., 2003). In breast cancer, some reports have either observed increased inflammatory infiltrates when psoriasin is present (Al Haddad S et al., 1999; Emberley ED et al., 2004) while others have failed to identify a significant association with inflammatory cell infiltration (Emberley ED et al., 2003b; Enerback C et al., 2002). Although these results may provide a putative biological role for secreted forms of psoriasin, they do not explain its intracellular function. To this end it has also been suggested that psoriasin may be involved in epithelial cell differentiation based on its association with altered keratinocyte differentiation (Martinsson H et al., 2005; Olsen E et al., 1995; Van Ruissen F et al., 1996) and increased frequency of occurrence at specific stages of cancer progression that are synonymous with dedifferentiation (Al Haddad S et al., 1999; Alowami S et al., 2003). Moreover, it is found that psoriasin can be induced in MCF10A mammary epithelial cells by various environmental stresses (that are likely to occur *in vivo* within high-grade DCIS) including loss of attachment to the extracellular matrix, growth factor deprivation and confluent conditions suggesting it may be involved in some aspect of stress-response (Enerback C et al., 2002). A role in apoptotic resistance has been suggested by some based on the observation that keratinocytes derived from psoriatic lesions are more resistant to apoptosis (Wrone-Smith T et al., 1997). Based on observation in our lab (and in the context of a breast epithelial cell) psoriasin also appears

to have a role in pro-survival/growth and pro-invasive pathways that confer more aggressive biological behaviour in ER-negative breast cancer cells (see I-2.3).

How psoriasin exerts these seemingly pleiotropic functions at the molecular level is not completely known at present. In skin, psoriasin is found to co-immunoprecipitate and co-localize with epidermal fatty acid binding protein and it is found that upon calcium stimulation both proteins redistribute from the cytoplasm to focal adhesion like structures (Ruse M et al., 2003). However, the biological function of this interaction and how it relates to inflammatory skin pathologies, hyperproliferative skin disorders or epithelial skin differentiation is not known. In breast cancer, recent evidence suggests that psoriasin may exert its biological effect, in part, through a physical interaction with Jab1 (c-jun activation domain binding protein 1) thereby modulating and increasing the activity of this latter protein via promoting its translocation to the nucleus (Emberley ED et al., 2003a). Jab1 is a multifunctional protein involved in increasing the specificity of AP-1 protein target gene activation; several of which have been implicated as key factors in breast tumor progression including VEGF (vascular endothelial growth factor), and MMP13 (matrix metalloproteinase 13). Moreover, Jab1 is found to enhance the activity of HIF-1α (hypoxia inducible factor 1α), thereby enhancing the cell's central defense mechanism against hypoxic stresses. Additionally, Jab1 is a component of the COP9 signalosome regulatory complex (CSN) involved in protein degradation by the Ub-26S proteosome (Chamovitz DA et al., 2001). In this way Jab1 is intimately associated with, and influences many cellular pathways involved in integrin, steroid hormone and Erb-2 signaling, as well as in cell cycle control. Work done in our lab (largely by Dr. E.

Emberley) has convincingly demonstrated that when psoriasin is expressed in MDA-MD-231 cells, these cells have increased nuclear localization of Jab1 resulting in increased AP-1 activity, increased expression of AP-1 and Hif-1α dependent genes (including VEGF, MMP13, CAIX (carbonic anhydrase IX)), and reduced expression of the negative cell-cycle regulator $p27^{Kip1}$. Induction of some of these proteins, and decreased steady-state levels of others may explain, in part, the promotion of more aggressive biological features associated with psoriasin expression. For example, it is thought that reduction in p27 levels may explain why these cells grow faster; however, they fail to give definitive causal effect as to why psoriasin expressing cell are less adherent and more invasive. Therefore it is likely, based on the molecular behavior of other S100s which have multiple target proteins, psoriasin does as well, even within the context of an individual breast epithelial cell. Simply stated, the ability for psoriasin to interact with Jab1 does not preclude the possibility that psoriasin can interact with other proteins to promote more aggressive cellular behavior. This later assertion is the premise of this thesis.

2.5. Summary

S100 proteins are a multigenic, functionally diverse family of small calcium binding proteins of which several members have been implicated in promotion of cellular properties associated with more aggressive tumour behaviour. They act by forming complexes with target proteins to modulate target protein activity thereby exerting their biological effect. A key function of this family appears to be in the regulation of cytoskeletal dynamics. One member of this family, psoriasin/S100A7 is aberrantly expressed during breast and skin cancer progression. The prominent feature about

psoriasin's expression profile in early breast cancer progression is it is not expressed in normal breast ductal epithelium but is highly expressed in many in situ ductal carcinomas with slightly reduced expression in the invasive components of these cancers. However, persistent levels of high psoriasin expression in invasive tumours are significantly associated with poor prognosis. These patients have a shorter time to progression and decreased survival versus those patients with invasive carcinomas that do not express psoriasin. Additionally when psoriasin is engineered into breast cancer cells that normally do not express psoriasin, these cells grow faster, are less adherent, and are more invasive both in *in vitro assays* and *in vivo* animal models. This has led our lab to hypothesise that psoriasin is an important diagnostic marker and player in promoting invasiveness in pre-invasive tumour cells. How psoriasin is able to do this is unknown, however it may exert its effects, in part, by modulating Jab1 function, however activity of other target proteins are likely to be modulated by psoriasin.

3. hGCP3 and the γ-TuRC

3.1. Microtubules and the Microtubule Cytoskeleton: The Diversity and Organization

Eukaryotic cells have evolved a highly-organized and dynamic microtubule cytoskeleton. The microtubule cytoskeleton can be organized into many diverse and specialized structures. These include the mitotic spindle apparatus in mitotic cells, basal motors in ciliata, apical-basal bundles in epithelial cells, in addition to the canonical radial array of MTs extending from the centrosome in interphase cells. As such MTs are fundamentally required for many defining eukaryotic cell processes including: chromosome segregation during cell division, cytokinesis, cellular morphogenesis, cell motility, and intracellular vesicle trafficking (Kellogg DR et al., 1994).

To a large extent, the dynamic nature of the MT cytoskeleton is owing to intrinsic biochemical properties of microtubules. Microtubules are long, hollow cylindrical, rigid structures (25nm in diameter) formed from the non-covalent polymerization of α and β-tubulin heterodimers. Each microtubule is a polar structure with β-tubulin at one end α-tubulin at the other. The former end gives rise to the so-called "plus" or fast growing end, while the latter is the so-called "minus" or slow growing end. The formation of microtubules occurs in a two-step process and involves a rate-limiting nucleation step followed by polymer elongation in which GTP-bound tubulin molecules are added to the plus end. Assembled MTs are highly dynamic, showing spontaneous length fluctuations in which individual MT transit between phases of elongation and shrinkage.

Organizing the MT cytoskeleton additionally requires the orchestration of many cellular factors that co-ordinately modulate individual microtubule dynamics (Murphy SM et al., 1998). These include proteins that work on already polymerized MTs and function to either sever, stabilized, destabilize, or bind and sort microtubule polymers (Martin OC et al., 1998). In addition, eukaryotic cells exert profound control over where and when MTs grow with the aid of specialized organelles generically known as microtubule organizing centres (MTOCs) (Zhou J et al., 2002) (Murphy SM et al., 1998). In animal cells, the centrosome is the major microtubule organizing centre while in yeast it is known as the spindle pole body (SPB). MTOCs are structurally quite different between evolutionary distant eukaryotes; however despite morphological diversity, the principle function of all MTOCs is to generate de novo microtubule growth. (Fava F et al., 1999; Young A et al., 2000). In fact, a number of proteins directly involved in catalyzing MT nucleation have been identified, many of which are invariably conserved across eukaryotes. The most well-studied of these include the ubiquitous γ-tubulin while other proteins, found in γ-tubulin containing protein complexes have been identified. These latter proteins, known as γ-tubulin complex proteins (Gaps), define a protein super family and show varying degrees of evolutionary conservation. Thus at the molecular level, the mechanism of MT nucleation has been conserved, by and large, throughout evolution. This is a reflection of how fundamentally important MTs are to eukaryotic cells and the critical role that MT nucleation has on overall control of MT dynamics. (Murphy SM et al., 1998; Schnackenberg BJ et al., 1999).

3.2. Centrosome and γTuRC: Structure and Function

In animal cells, the centrosome is composed of a pair of orthogonally positioned centrioles that are surrounded by relatively undefined pericentriolar material (PCM). Once thought to be an amorphous mass of electron dense material, recent evidence now suggests the PCM is a highly organised matrix in which large coiled-coil proteins (including pericentrin, kendrin, and ninein) form a unique lattice surrounding the centrioles proper (Dictenberg JB et al., 1998; Schnackenberg BJ et al., 1999). Microtubules are oriented with the minus ends at the centrosome, embedded in the PCM, and the plus ends growing away from the centrosome (Bergen 1980). As such, microtubules are organised (for the most part) into a polarized radial array with the centrosome at its focus. It is important to note that centrioles themselves do not appear to play a direct role in microtubule nucleation, as evidenced by the fact that in plants, acentriolar structures are competent to nucleate microtubules (Canaday J et al., 2000).

The PCM is the site within the centrosome where MTs are nucleated and begin to grow. Embedded within the PCM are large (25-32S) ring shaped protein complexes containing γ-tubulin known as the γ-tubulin ring complex (γTuRC). In higher eukaryotes γTuRCs, are the intracellular particles responsible for the template driven mechanism of MT nucleation from centrosomes. Several lines of evidence have led to this inescapable conclusion. First, purified γTuRC can nucleate MTs *in vitro* with much faster kinetics and at tubulin concentrations that are too low to promote spontaneous microtubule nucleation *in* vitro. γTuRCs are also observed to localize and cap the minus, slow growing end of microtubules in vitro (Zheng Y et al., 1995). Moreover, spontaneously

generated microtubules *in vitro* are structurally abnormal whereas in the presence of γTuRCs, *in vitro* nucleated MTs are structurally normal (Evans L et al., 1985; Zheng Y et al., 1995). Second, high resolution electron immunolocalization of γ-tubulin reveal that γ-TuRCs are localized within the PCM of centrosomes and associated with MTs (Vogel JM et al., 1997). Finally, direct evidence comes from complementation assay in which the nucleating capacity from centrosomes that have been rendered non-functional under stringent salt conditions can only be restored when γTuRCs are reintroduced into the system (Moritz M et al., 1998).

A large pool, roughly 70-80% of all γTuRCs are located in the cytoplasm, and are not associated with centrosomes (Khodjakov A et al., 1999). Cytoplasmic γ-tubulin is also present in a smaller complex (~10S), termed the γ-tubulin small complex (γTuSC) and is presumably a component of the full size complex. Despite apparent heterogeneity in sizes of γTuRCs between different metazoans (Debec 1995; Moudjou 1997; Detraves 1997), electron microscopic images taken of highly purified, large γ-tubulin-containing complexes from Xenopus (Zheng Y et al., 1995), Drosophila (Moritz M et al., 2000; Oegema K et al., 1999) and humans (Murphy SM et al., 2001) has revealed remarkably similar structures (Figure 1). γTuRCs are modular mega-complexes (~$2.2x10^6$ D) with defined structural-subunit composition presenting a capped lock-washer, ring-like appearance with a cross-section similar to a that of a microtubule (~25nm) (Murphy SM et al., 2001; Oegema K et al., 1999; Zheng Y et al., 1995). Images obtained from electron microscopy tomography and platinum shadowing reveal a repeated U or V-shaped structural subunit that forms the ring (Figure 1) (Moritz M et al., 2000). It is thought this

repeated ring-subunit is the γTuSC and is composed of γ-tubulin and two additional gamma-tubulin complex proteins (GCPs). In Drosophila, both the γTuSC (9.8S, 280kDa) and the much larger ring shaped complex (35.5S, $2.2x10^6$Da) have been purified and characterized (Oegema K et al., 1999) and it was found that the γTuSC is unable to nucleate microtubules as efficiently as the holistic complex. In addition to 6-7 γTuSCs, the entire γTuRC contains additional polypeptides that form a globular cap that sits asymmetrically on the ring and are presumably required for complete MT nucleating function. (Moritz M et al., 2000) In contrast to higher eukaryotes, S *.cerevesia* utilize a much simpler ~6S (300kDa) γ-tubulin containing complex whose composition is analogous to the γTuSC (see below). There is no evidence to suggest that a more complex or higher order cytoplasmic form of γTuC exist in yeast. This has lead some to hypothesise that the γTuSC may represent the minimal functional nucleating particle that has been conserved, in evolutionary terms, from yeast to higher eukaryotes (Murphy SM et al., 2001).

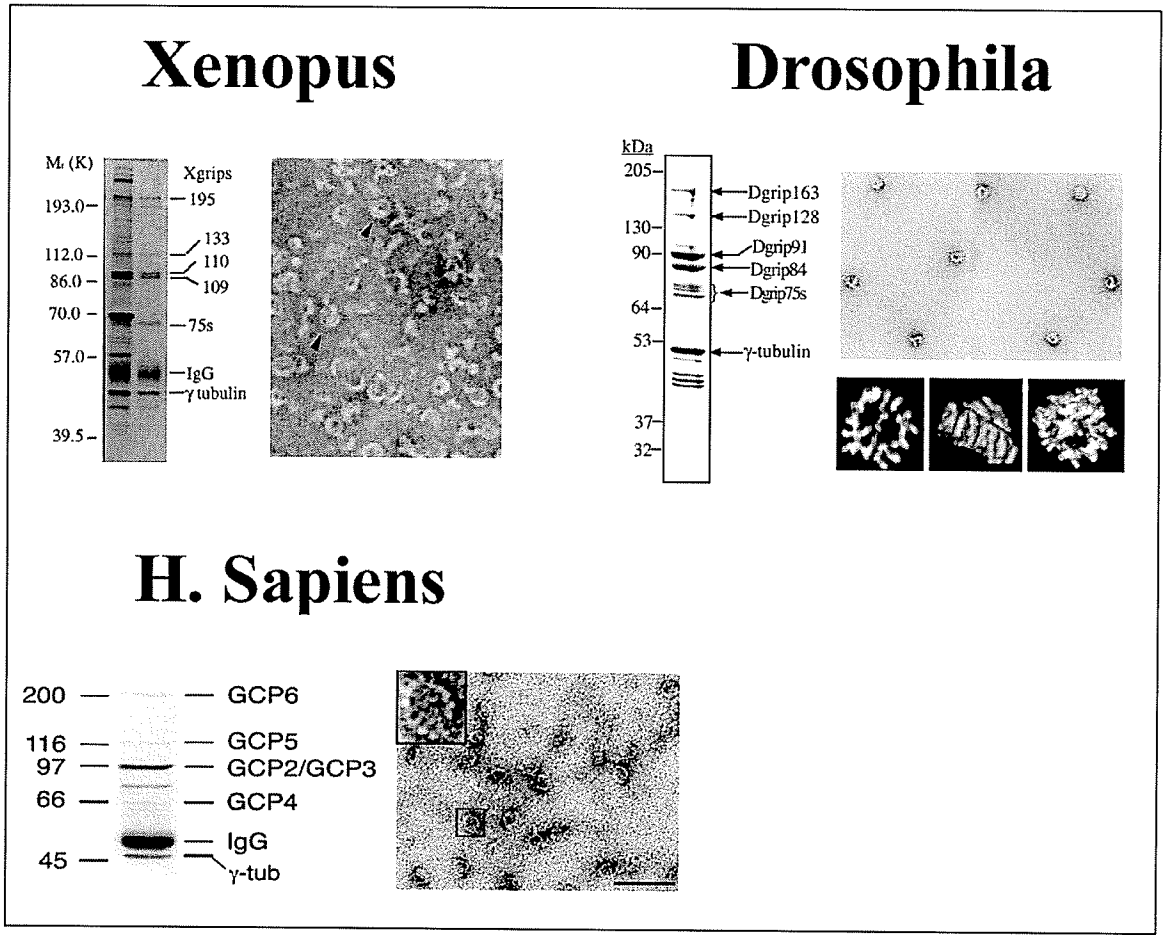

Figure 1: Overall polypeptide composition and morphology of γTuRCs is conserved across metazoans. In addition to γ-tubulin, at least five additional proteins compose the core γTuRC as shown by PAGE analysis of highly purified complexes from Xenopus (Zheng Y et al., 1995), Drosophila (Moritz M et al., 2000; Oegema K et al., 1999) and Humans (Murphy SM et al., 2001) (left panels). Morphological comparisons of cytoplasmic γ-TuC show a conserved ring structure with a diameter of ~25nm (right panels). Detailed images obtained tomographic analysis of Drosophila γ-TuRC reveal a capped-lock washer structure as shown from the bottom, the side, and from on top. Highlighted in red is the contour of one γTuSC presenting an inverted V-shape and which is composed of two molecules of γ-tubulin and one molecule each of GCP2 and GCP3 (Moritz M et al., 2000; Oegema K et al., 1999).

3.3. Temporal and Spatial Regulation of γTuRC Activity

At the onset of mitosis, levels of γTuRCs associated with centrosomes increase at least 3 fold from interphase to metaphase and rapidly decrease in late anaphase (Fava F et al., 1999; Khodjakov A et al., 1999). This transient recruitment to the centrosome is reflected by a 5 to 10 fold increase in the number of MTs associated with mitotic versus interphase centrosomes (Khodjakov A et al., 1999). Temporal activation of γTuRC activation likely reflects centrosomal maturation during the cell cycle. Centrosomes accumulate pericentriolar material, such as pericentrin, and enlarge from G1 until mitosis, followed by rapid disassembly as the cell exits mitosis (Dictenberg JB et al., 1998) . A model has been proposed in which a large complex (~3 MDa) consisting of a pericentrin sub-complex and two γTuRCs represent the assembly competent co-complex that is formed in the cytoplasm and recruited to the centrosome by the microtubule motor, Dynein, along microtubules (Dictenberg JB et al., 1998; Young A et al., 2000). Biochemical evidence for this model comes for sucrose gradient sedimentation, gel filtration and co-immunoprecipitation (Co-IP) analysis showing that the pericentrin-γTuRC co-complex is distinct from the γTuRC (Dictenberg JB et al., 1998). Moreover it was shown by IF microscopy in live cells that particles containing endogenous pericentrin and γ-tubulin move along microtubules and dock at centrosomes and this effect could be blocked with microinjection of anti-Dynein antibodies(Zimmerman WC et al., 2004). It should be noted that although this model for γTuRC recruitment to the centrosome is compelling, controversy exits in the literature over whether or not recruitment of γTuRCs to the centrosome is dependent on microtubules as others have reported recruitment of γ-tubulin to the centrosome is independent of microtubules (Khodjakov A et al., 1999; Young A et

al., 2000). Moreover this model additionally relies on the fact that other unidentified proteins mediate the assembly of pericentrin subcomplex and γTuRCs in the cytoplasm in a cell-cycle dependent manner in order for recruitment to the centrosome to occur in a temporally defined manner.

Less is known however of the mechanism in which γTuRC activation is spatially restricted to the centrosome. *In vivo*, cytoplasmic γTuRCs are not competent to nucleate microtubules. Several mechanisms have been proposed to explain how γTuRC activity is spatially restricted, although at present no single mechanism is known for certain (Figure 2). One possibility is that additional factors located at the centrosome are required for γ-TuRC activation. These may include cell-cycle-dependent centrosomal-localized kinases, although this would suggest a phosphorylation cue is required (Tassin AM et al., 1999). This has not been experimentally confirmed. Moreover, activity of γTuRC may be spatially regulated through the binding of guanosine nucleotides enriched at the centrosome (Roymans D et al., 2001). This is based on the observation that γ-tubulin is competent to nucleate microtubules only when saturated with GTP (Oegema K et al., 1999). It has also been proposed that the proteins located in that 'mature' centrosome may activate nucleation function of γTuRCs through conformational changes induced by interaction. Additionally the proteins located at the centrosome may simply stabilize microtubule nuclei. This latter possibility would suggest that cytoplasmic γTuRC are active, however the cytoplasmic environment simply is not permissive in stabilizing MT growth. Alternatively, factors found in the cytoplasm may inhibit the nucleation activity. Evidence supporting this latter possibility comes from a recent report describing a small

polypeptide purified from both cultured neuronal cells and bovine brain, MINUS, that effectively suppresses microtubule nucleation in vitro (Fanara P et al., 1999). It should be noted that the *in vivo* cellular localization of MINUS is not known. It is also possible that a combination of inhibition in the cytoplasm coupled with activation at the centrosome work in concert to regulate the spatial and temporal activation of γTuRCs (Figure 2).

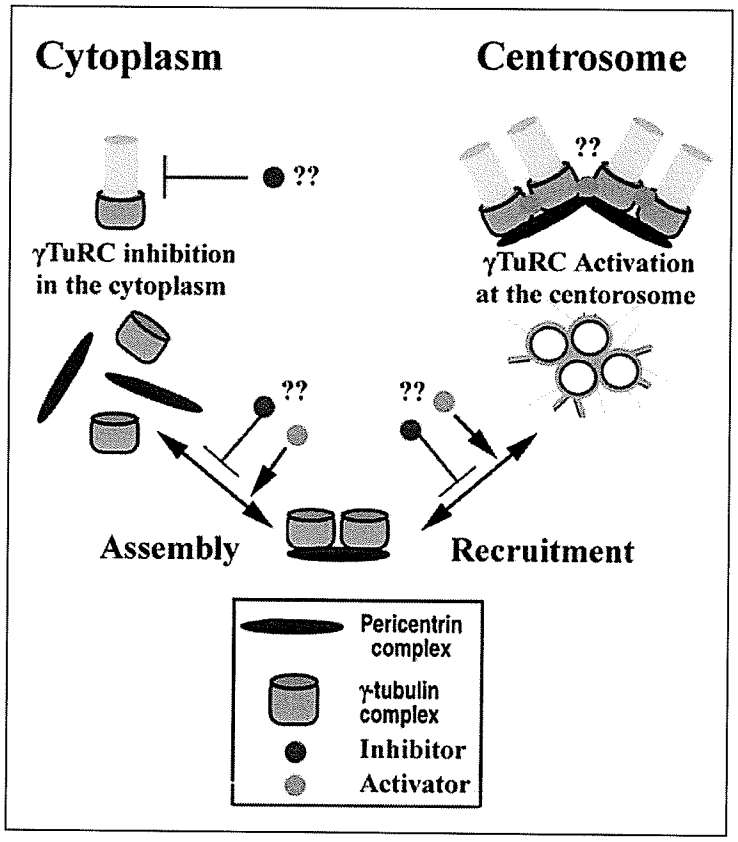

Figure 2: Proposed model for γTuRC activation at the centrosome and/or inhibition in the cytoplasm (adapted from (Dictenberg JB et al., 1998)). The majority of γTuRC are found in the cytoplasm (70-80%) and are not competent to nucleate MTs perhaps due to inhibitory factors found in the cytoplasm. To meet the cellular demands for increased MTs at the onset of mitosis, γTuRCs are assembled into a recruitment-competent co-complex with a pericentrin. In this model, the pericentrin-γTuRC co-complex is cargo for Dynein microtubule motors that shuttle their cargo along microtubules and dock at centrosomes where γTuRCs are able to nucleate MTs. Assembly, as well as recruitment of pericentrin-γTuRC co-complexes may in turn be regulated by both inhibitory and/or activating molecules in the cytoplasm. At the centrosome it is thought that additional proteins may induce γTuRC activation and/or provide a permissive environment that stabilizes MT nuclei.

3.4. γTuRC Composition:GCP3 is essential

Bioinformatic analyses have revealed that specific core proteins that constitute the γ-tubulin complex from evolutionarily distant eukaryotes are related and therefore define GCP orthologues. This is not surprising considering the morphological and functional conservation of γTuCs across metazoans and eukaryotes respectively. More intriguing perhaps is that different GCPs within the same complex are related to each other and show regions with significant homology (Murphy SM et al., 2001). As such it has been proposed that proteins that constitute γTuC define a unique superfamily of proteins called the GCP superfamily (Murphy SM et al., 2001).

For clarity, nomenclature proposed by Murphy et al 1998 to describe the evolutionary relationship between members of the GCP superfamily will be used. GCP followed by a number will refer to a family of orthologues within the GCP superfamily otherwise the species defined GCP nomenclature will be employed (see Table 1).

To date, the prototypic γTuSC from *Saccharomyces cerevisiae* is simplest known γ-tubulin complex. It is composed of two molecules of γ-tubulin and one molecule each of Spc97p (GCP2) and Spc98p (GCP3) (Geissler *et al.*, 1996; Knop *et al.*, 1997). Interestingly, the γTuSC within higher eukaryotes, like the yeast complex, consists only of γ-tubulin and GCP2 and GCP3 orthologues suggesting that these three proteins form a conserved functional core unit (Moritz M et al., 2000; Murphy SM et al., 2001). GCP2 and GCP3 are conserved ubiquitously through evolution from fungi (Knop M et al., 1997b), plants (Erhardt M et al., 2002) and animals (Murphy SM et al., 1998) and based

on biochemical and genetic characterization in various organisms, γ-tubulin, GCP2 and GCP3 play an indispensable role (Fujita A et al., 2002) (see Table 1). In contrast to the yeast, γTuRCs from the fly to humans, all of which present the same overall polypeptide composition, are significantly more complex and contain at least five different proteins (GCP2-6) in addition to γ-tubulin. In terms of evolutional conservation, orthologues to GCP4-6 are less widespread. Nevertheless, a complete set of orthologues to all known human GCPs, including γ-tubulin, and hGCP2-6, have been characterized in the fly, the frog and in humans suggesting that the mechanism of microtubule nucleation is conserved across metazoans.

Table 1: Summary of GCP composition of γTuCs from Yeast to Humans including species specific names and molecular weights. γ-Tubulin, GCP2 and GCP3 are ubiquitously conserved across eukaryotes and form the core MT nucleating unit.

S cerevesia		Drosophila		Xenopus		Homo sapiens	
Name	MW	Name	MW	Name	MW	Name	MW
------	------	*Dgrip16*	163	*Xgrip210*	210	hGCP6	244
------	------	*Drip128*	128	Xgrip133	133	hGCP5	118
------	------	Drip75	75	Xgrip75	75	hGCP4	76
Spc98p	**98**	**Dgrip91**	**91**	**Xgrip109**	**109**	**hGCP3**	**104**
Spc97p	**97**	**Dgrip84**	**84**	**Xgrip110**	**110**	**hGCP2**	**103**
Tub4p	**52**	**γ-Tubulin**	**53**	**γ-Tubulin**	**50**	**γ-Tubulin**	**48**

(Spc, spindle control body; Dgrip, Drosophila γ-tubulin interacting protein; Xgrip, Xenopus γ-tubulin interacting protein; MW, molecular weight)

3.5. Structure and Function of hGCP3 within the γTuRC

Human gamma-tubulin complex protein 3 (hGCP3/hsSpc98p) was first identified and characterized in 1998 by two groups independently trying to find human orthologues to spindle pole body components in S. cerevesia that interact with γ-tubulin (Murphy SM et al., 1998; Tassin AM et al., 1998). hGCP3 was found to co-localize with γ-tubulin, both in the cytoplasm and at the centrosome, was able to rescue a γ-tubulin null mutation in S. pombe, co-immunoprecitpitated with γ-tubulin in mammalian cell extracts, and co-sedimented with γ-tubulin in a sucrose density gradient (Murphy SM et al., 1998). Moreover, antibodies directed against hGCP3 inhibited microtubule nucleation from isolated centrosomes as well as in microinjected cells (Tassin AM et al., 1998). Within a single γTuRC, GCP2, GCP3 and γ-tubulin are found to be more abundant than the other GCPs (GCP4-6) which is consistent with the proposed model (described above) that GCP2-3 and γ-tubulin form the repeating γTuSC of the ring while the other less abundant proteins compose the lid (Fava F et al., 1999; Murphy SM et al., 1998; Murphy SM et al., 2001). Taken together these results indicate hGCP3 is intrinsically associated with γ-tubulin and is found within the same complex (γTuRC) and is indispensably required for nucleating MTs.

hGCP3 gene encodes a protein 907 amino acids long that shares no significant homology with other known protein motifs. It does however have 5 regions showing significant homology (31-44% similarity) with other hGCPs as well as the yeast GCP orthologues spc97p and spc98p (Murphy SM et al., 1998; Murphy SM et al., 2001). Moreover, spanning two of these conserved regions (regions III and IV), is a highly conserved

domain found in all GCP3 orthologues from Homo sapiens, Xenopus, Drosophila, zebrafish and plants (Tassin AM et al., 1999). It has been hypothesized that the five conserved domains might have a role in folding the proteins in the correct conformation or in GCP-GCP subunit interactions within the complex (Murphy SM et al., 2001). Moreover the presence of a highly conserved central region within all GCP3 across evolutionary distant eukaryotes suggests that this region is indispensable for GCP3 function and may be involved in γ-tubulin binding (Tassin AM et al., 1999) (Figure 3).

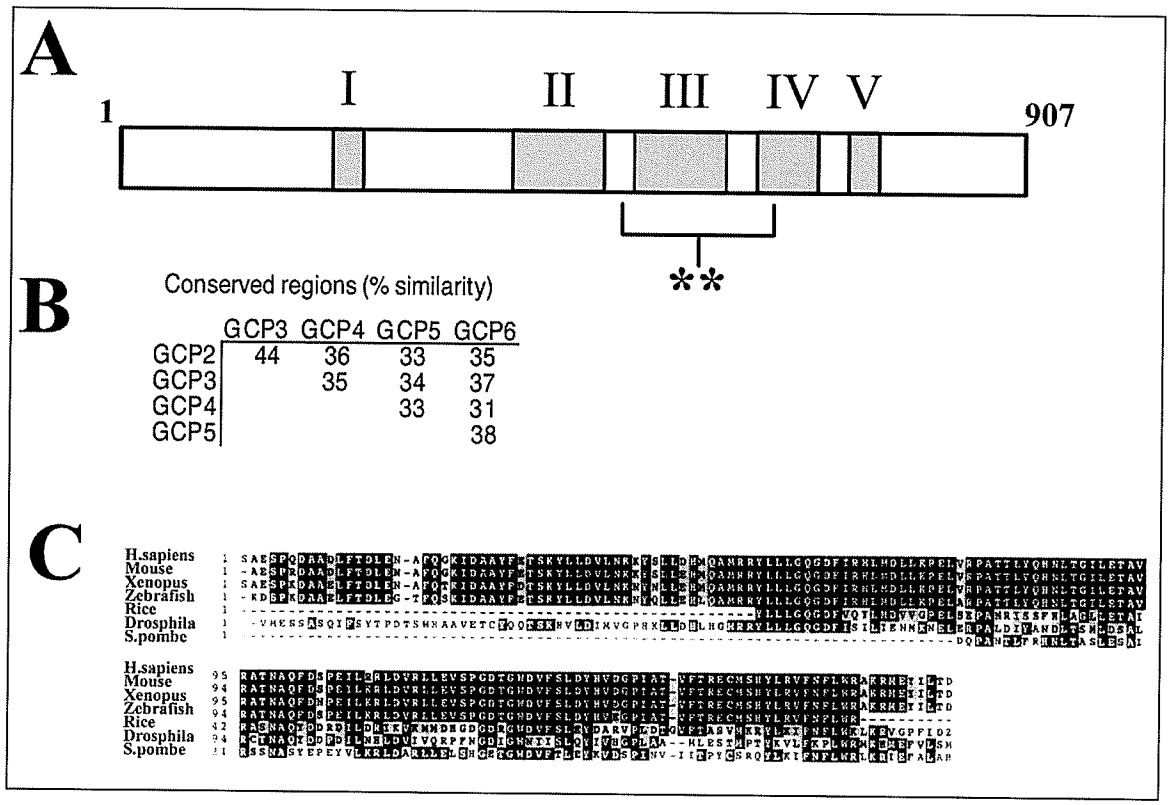

Figure 3: (A) Diagrammatic structure of hGCP3 showing relative position of the five domains (I-IV) having significant amino acid similarity amongst all hGCPs as shown in (B) (adapted from (Murphy SM et al., 2001). Region highlighted by the double asterix is the putative GCP3 γ-tubulin binding domain that is highly conserved across eukaryotes as shown in (C) (adapted from(Tassin AM et al., 1999).

It has been speculated that within the γTuRC, hGCP3 may simply serve a structural role that positions γ-tubulin molecules in the proper orientation in order to create a 'tubulin seed' necessary for MT polymerization to take place. Although this may be true, data obtained from both mutational and biochemical immunodepletion studies, as well as recent reports describing human proteins that interact with hGCP3 suggest that hGCP3 is the molecule within the complex that tethers the complex to PCM. First, mutations in the Drosophila GCP3 orthologue, Dgrip91 significantly reduces the levels of γ-tubulin associated with the centrosome while in Xenopus, specific immunodepletion of Xgrip109 prevented γ-tubulin from being recruited to the centrosome (Barbosa V et al., 2000; Martin OC et al., 1998). Moreover in animal cells, hGCP3 was found to co-immunoprecipitate with several large coiled-coil protein that constitute the pericentriolar matrix including CG-NAP/AKAP450 (Takahashi M et al., 2002), kendrin/pericentrinB (Takahashi M et al., 2002) and pericentrin (Zimmerman WC et al., 2004). Taken together these results suggest that GCP3 is necessary for proper localization of γTuRCs to the centrosome which is consistent with a role in anchoring the compexes to the PCM.

3.6. Additional γTuRC Functions: MT Capping, Centrosome Duplication and Cell Cycle Progression

It is clear that γTuRC are responsible for de novo growth of microtubules from MTOCs and catalyze the nucleation reaction. However, other roles are slowly being ascribed to γTuRCs that are either independent of its nucleation function or possible downstream

consequences of aberrant γTuRC function. The most compelling additional γTuRC function supported by direct evidence in the literature is in capping the minus end of MTs and regulating minus end dynamics. Evidence for this comes from the finding that γTuRCs prevent minus-end growth on the microtubules it nucleates, as well as on preformed microtubules to which it binds (Wiese C et al., 2000). Evidence also exists that γTuRC function is required for centrosomal stability and structural maintenance as well as in cell-cycle progression, although these functions may be the result of indirect γTuRC activity. First, inhibiting mono-ubiquitination of γ-tubulin by the BRCA1/Bard1 complex using mutant γ-tubulin K48R or overexpression of a γ-Tubulin binding region of BRCA1 causes a marked amplification of centrosomes and results in the accumulation of mitotic cells with abnormal spindles and induces apoptosis (Hsu LC et al., 1998; Hsu LC et al., 2001; Starita LM et al., 2004). Additionally, mutation of the Drosophila GCP3 orthologue resulted in a centrosomal phenotype characterized by an accumulation of pericentriolar material, and centrosomes missing centrioles. As for a role in cell cycle progression it is found that by inhibiting anchoring of γTuCs at the centrosome by overexpression of GCP2/3 binding domain of pericentrin, a checkpoint response is activated that prevents mitotic entry and triggers apoptotic cell death. In contrast, temperature sensitive GCP2/3 (Alp4/6) mutants in fission yeast, are found not to arrest in mitosis despite extensive spindle defects at the restrictive temperature; rather, at the permissive temperature mutants cells are hypersensitive to MT destabilizing agents and viability is lost at the first mitosis (Vardy L et al., 2000). From this it was concluded that Alp4/6 are required in the fission yeast to activate the spindle checkpoint in order to initiate mitotic arrest (Vardy L et al., 2000). Finally Zhou and colleagues observed upon

transient overexpression of γ-tubulin in mammalian cells, cells abnormally exit mitosis despite having failed to form normal bipolar spindles, and immediately reduplicate their DNA (Zhou J et al., 2002). From this it was suggested that the number of nucleation sites and/or γ-tubulin itself may play a role in the cell cycle progression in mammalian cells (Zhou J et al., 2002). Taken together, although not conclusive, these results suggest that γTuC function is required for not only MT nucleation, but may additionally be required for centrosomal stability as well as normal activation of mitotic checkpoints and normal cell cycle progression.

3.7. Association with molecules involved in cancer progression

The majority of molecules found to interact with components of the γTuRCs have been identified as proteins involved with PCM, however three reports indicate that γTuRCs do associate with specific proteins involved in tumour suppression and/or cancer predisposition syndromes. The first is Elac2, a candidate prostate cancer susceptibility gene that interacts with γ-Tubulin ring complex predominantly in the cytoplasm (Korver W et al., 2003). Elac2 immunoprecipitates contain γ-tubulin and both hGCP2 and hGCP3. Elac2 overexpression delays G2/M progression as indicated by an accumulation of cells with a 4N DNA content and cytoplasmic localized cyclin B and inactive cdc2. (Korver W et al., 2003). It is proposed that ELAC2 interacts with the gamma-tubulin complex and perturbation of ELAC2 might promote tumorigenesis through irregular cell division, although this has yet to be confirmed experimentally (Korver W et al., 2003). Secondly, γ-Tubulin colocalizes and coimmunoprecipitates with Nm23-h1/Nm23-R, the main enzyme involved in GTP synthesis and a tumour metastasis suppressor gene. Point

mutations in NM23-H1 have been detected in several advanced tumours of childhood neuroblastoma however the molecular mechanisms by which NM23 exert its functions are still unknown (Roymans D et al., 2001). Although it is not reported whether GCP2 or GCP3 were also in the immunoprecipitates it should be kept in mind that γ-tubulin appears solely to function in complexed forms as purification of functional monomeric gamma-tubulin has not been successful so far (Shu HB et al., 1995; Vassilev A et al., 1995; Zheng Y et al., 1995; Zhou J et al., 2002). Finally the most compelling interaction in the context of breast cancer is an interaction with BRCA1. BRCA1 is a cancer suppressor gene with pleiotropic biological functions, that when mutated leads to the susceptibility of tumorigenesis in breasts and ovaries. BRCA1 localizes with the centrosome during mitosis and coimmunoprecipitates preferentially when hypophosphorylated with γ-tubulin (Hsu LC et al., 1998). Overexpression of a γ-tubulin binding region of BRCA1 (a.a. 504-803) or treatment with okadaic acid (an inhibitor of PP1 and PP2A that results hyperphosphorylation of BRCA1) interferes with the BRCA1/ γ-Tubulin interaction and results in the accumulation of mitotic cells with multiple centrosome and abnormal spindles inducing apoptosis.(Hsu LC et al., 2001). Moreover γ-tubulin is a specific ubiquitinated substrate of BRCA1/Bard1 complex and is ubiquitinated at lysines 48 and 344. Inhibition of γ-tubulin ubiquitination using mutant γ-tubulin K48R causes a marked amplification of centrosomes. It was noted that monoubiquitination of γ-tubulin did not disrupt the γTuRC as inferred by presence of the unmodified γ-tubulin associated with the monoubuiquitinated γ-tubulin. Additionally, monoubiquitination of γ-tubulin likely serves another function other than signalling it for

degradation as the proteosome machinery recognizes proteins only with four or more ubiquitin chains (Starita LM et al., 2004).

Taken together, these results suggest that modulation of γTuRCs by specific molecules associated with cancer suppression and/or tumorigenesis is not an improbable phenomenon. How these interactions contribute to the progression and/or acquisition of the disease is not known; however, like so many other players in cancer progression it is likely that coordinated deregulation of the normal cell circuitry rather than a single sabotaging event is responsible for the acquisition and progression of the disease.

3.8. Summary

In summary, γTuRC are responsible for initiating microtubule growth from centrosomes and therefore are the active particle that defines one major aspect of centrosome function- the ability to generate MTs. Within these complexes hGCP3 is an indispensable core protein as it has invariably been conserved throughout evolution, and is the second most (next to γ-tubulin) abundant protein within the complex. As such, hGCP3 is intrinsically required for centrosome function. How γTuRC are specifically activated to catalyze MT nucleation at the centrosome and in a cell cycle dependent manner is not completely known. It is likely however that due the central function of γTuRC in establishing MTs that several layers of regulation are in place to avoid aberrant MT growth. Finally, evidence in the literature suggests that γTuRCs are the targets for molecules associated with cancer suppression and/or progression including Elac2, NM23-H1, and BRCA1.

4. Centrosome Dysfunction and Cancer Progression

4.1. Theodor Boveri: An Old Theory Revisited

The term 'centrosome' was first coined by Theodor Boveri in1888, and it was he that first recognised a potential link between centrosomal abnormalities and human cancers. (Nigg EA, 2002; Rieder CL et al., 2001). Through his work with sea urchin embryos, he was able to observe the generation of aneuploidies, reminiscent of those seen in tumours when an egg was double fertilized with two sperm (Salisbury JL, 2001). The resulting zygote contained twice the number of centrosomes and gave rise to multipolar zygotic spindles. Ultimately, the developing zygote would divide asymmetrically and daughter cells would receive unequal genome contents. From this, Boveri proposed that chromosomal abnormalities resulting from multipolar mitosis may be the causal basis for the origin of malignant tumours that are characterized by aneuploidies and loss of cellular/tissue architecture (Salisbury JL, 2001). It would take over three-quarters of a century before the necessary technological advances would enable his hypothesis to be tested and it appears that he may have been correct.

4.2. Types of Aberrations

It is now recognised that centrosomal abnormalities are common-place and occur in tumours of multiple origins. These alterations not only include structural and numerical defects, but also functional alterations in their ability to initiate microtubule growth. Characteristic structural abnormalities include: increase in centrosome number and volume, accumulation of excess pericentriolar material, centrosomes with supernumerary

centrioles, centrioles of various sizes and shapes, and centrosomes having inappropriate phosphorylation status (Salisbury JL et al., 2004). In addition, centrosomes also show functional abnormalities in tumour cells including inappropriate centrosome duplication during the cell cycle and nucleation of unusually large microtubule arrays (Salisbury JL et al., 2004).

4.3. Sources of Centrosomal Abnormalities

The underlying biological mechanisms leading to the formation of centrosome defects are not clear, although several distinct (and not necessarily mutually exclusive) possibilities have been proposed. These include: alterations of checkpoint controls allowing for accumulation of cells with centrosome defects that would otherwise be eliminated; initiation of multiple rounds of centrosome replication within a single cell cycle through the uncoupling of DNA replication and centrosome duplication cycle; and finally, failure to complete cytokinesis leading to tetraploid cells with multiple centrosomes (Nigg EA, 2002). Changes in proteins associated with centrosomal defects are found to be involved in cell cycle control, centrosome structure or function, and in DNA-damage repair (Nigg EA, 2002).

For example loss of the tumour suppressor, p53, is thought to be a player in the promotion of cells with supernumerary centrosomes , but is not absolutely required for this process (Nigg EA, 2002). Support for this idea comes from the fact that mutation or elimination of p53 (Fukasawa K et al., 1996) or it's downstream effectors $p21^{Waf/Cip1}$ (Tarapore P et al., 2001) and GADD45 (Wang XW et al., 1999), or overexpression of

negative p53 regulators (Mdm2) (Carroll PE et al., 1999) induces supernumerical centrosome abnormalities in some experimental models; however other studies have failed to reveal a correlation between p53 mutation and centrosomal amplification and chromosomal instability (CIN) in archived breast and prostate tumour samples (Lingle WL et al., 2002; Pihan GA et al., 2003). Similarly, alteration in the levels of centrosome-associated-kinases from the aurora family of kinases have been implicated in centrosomal amplification and generation of chromosomal instabilities in a wide range of tumours (Goepfert TM et al., 2002; Hu W et al., 2005). Additionally, mutation or functional disruption of several proteins involved in DNA repair including the breast and ovarian cancer susceptibility genes BRCA1/BRCA2 can lead to numerical centrosome aberrations (Starita LM et al., 2004; Tutt A et al., 1999). Although the mechanisms by which these proteins regulate centrosome numbers are not completely known, in the case of BRCA1 it appears that it regulates centrosome number via it's ubiquitinating activity of γ-tubulin (Starita LM et al., 2004) as discussed in section I-3.7.

Numerical amplification of centrosomes frequently coincides with structural abnormalities. In vivo, centrosomes from tumour cells are visibly much larger as observed by immunofluorescent or electron microscopy (Lingle WL et al., 1999) and display an accumulation of PCM proteins including pericentrin (Pihan GA et al., 2001), and γ-tubulin (Lingle WL et al., 1998), as well as centriole-associated proteins including centrin (Lingle WL et al., 1998). Conversely, overexpression of several PCM such as pericentrin (Pihan GA et al., 2001), TACC (Gergely F et al., 2000), CEP135 (Ohta T et al., 2002) and C-NAP1 (Mayor T et al., 2002) in cultured cells results in structural

abnormalities characteristic of those seen in tumours. In fact, overexpression of pericentrin in primary prostate cancer cells induces phenotypic characteristics of prostate tumours including CIN and loss of cellular architecture (Pihan GA et al., 2001).

4.4. Central Paradigm: Centrosome Dysfunction and Cancer Progression

Centrosomal dysfunction is strongly correlated with the concomitant loss of genomic stability and change in cellular/tissue architecture that characterize many (if not all) aggressive carcinomas (Lingle WL et al., 1998; Pihan GA et al., 1998). How centrosome dysfunction is able do this can be understood by fully appreciating the dichotomous roles centrosomes play in mitotic and interphase cells.

During mitosis in somatic cells, two centrosomes and their orchestrated bipolar microtubule spindles are responsible for the faithful and equal partitioning of the tetraploid-G2 DNA content into two daughter cells. It is easy to conceptually understand how dysfunction, and in particular the formation of multipolar spindles, can lead to chromosome missegregation. As such, it is believed that aberrant centrosome function can confer a mutator phenotype via increasing genomic/ chromosomal instability (Lingle WL et al., 1999). Although, most mutated progeny will not be viable, occasionally some progeny will be endowed with a particular selective advantage, and over time, result in viable cancer cells that have accumulated proto-oncogene mutations, and lost alleles to tumor suppressor genes (Pihan GA et al., 2003). From a Darwinian model for the genomic evolution in cancer cells, CIN is thought to be an important and key mechanism that potentiates a more aggressive tumor state (Lengauer C et al., 1998). Experimentally,

using immunohistochemical detection for centrosomal abnormalities from archival tumor samples, and fluorescence *in situ* hybridization (FISH) analysis to quantify the degree of chromosomal instability, several groups have confirmed in both prostate (Pihan GA et al., 2003) and in breast tumors (Lingle WL et al., 2002), that chromosomal instability and centrosomal defects occur together and show a positive, linear, statistically significant correlation.

In the context of an interphase tumour cell, it may be more difficult to conceptually grasp how centrosome dysfunction may contribute to cancer progression. However, considering centrosomes are implicitly involved in defining cell polarity , shape and motility, (Pihan GA et al., 2003) it is conceivable that centrosome dysfunction also contributes to cancer progression through actions in interphase cells. The former two properties (cell polarity and shape) have direct implication on tissue organisation, while changes in motility may directly impact the invasive properties of a cell. In normal breast tissue, the degree of ductal organisation largely reflects particular cytoarchitectural features of individual epithelial cells. Luminal epithelial cells present a cuboidal cell morphology where the nuclei are typically located in the basal region of the cell and polarity is maintained by a centrosome located in the apical region often near lateral junction complexes (Lingle WL et al., 1999). In contrast, individual tumour cells within invasive adenocarcinomas (for example) have skewed cell polarity and are characterized by a loss of structural differentiation that ultimately results in tissue disorganisation (Lingle WL et al., 1999). To this end, centrosome defects have been found to correlate with histological/cytological grade of the in situ and invasive lesions, both in prostate (Pihan GA et al., 2003) and

breast tumours (Lingle WL et al., 2002). In prostate, the frequency of centrosome defects increases in invasive tumours with increasing Gleason grade (Pihan GA et al., 2001). The Gleason grade is one of the best predictors for prostate cancer progression and reflects changes in cytoarchitectural features associated with tumour progression. In invasive breast carcinomas, increased centrosome function (nucleation capacity) is significantly associated with increasing histological grade (Nottingham grade) which is in turn an indicator of poor prognosis and associated with shorter disease-free survival and overall survival. These results support the assertion that centrosome dysfunction contributes to cellular, and therefore glandular disorganisation, that is reflected by higher histological grade of tumours (Pihan GA et al., 2003).

4.5. Cause or Consequence

A growing body of evidence suggests that centrosome aberrations serve a causal role rather than that of a bystander during cancer progression; although, this point remains hotly debated. Several lines of circumstantial evidence support this notion. First, centrosome defects are frequent and have been detected in nearly almost all cancers surveyed to date including prostate (Pihan GA et al., 2001), brain (Weber RG et al., 1998) , colon (Ghadimi BM et al., 2000), head and neck (Gustafson LM et al., 2000), lung (Pihan GA et al., 1998), pancreas (Sato N et al., 2001) and breast (Lingle WL et al., 1998). Additionally, centrosome aberrations are not exclusive to late stages of tumor progression, rather they occur early in *in situ* carcinomas such as the uterine cervix, prostate and breast (Lingle WL et al., 2002; Pihan GA et al., 2003). I*n vivo,* the frequency of centrosome abnormalities dramatically increases during cancer progression in animal

models (Shono M et al., 2001). Finally, the degree of centrosome defects is associated with increasing aggressive phenotypes in tumours and is strongly associated with the concomitant loss of genomic stability and change in cellular/tissue architecture as previously discussed (Section I-4.3) (Lingle WL et al., 1999; Pihan GA et al., 2001). Together results suggest a stepwise progression of centrosome defects occurs during cancer progression *in vivo*. Although they do not explicitly answer the question of whether centrosome defects are a cause or consequence of cancer progression, taken with the centrosome's normal cellular roles, they certainly provide compelling evidence to suggest a direct link between centrosome dysfunction and phenotypic hallmarks of many tumors.

4.6. Summary

Centrosome defects are frequent and characteristic of many tumours, including those of the breast. Characteristic abnormalities include numerical, structural and functional aberrations. They are found early during cancer progression in human tumours and in animal models and as such are thought to represent an early event in the evolution of the malignant disease. Correlative data suggest that centrosomal abnormalities are an important causal agent for chromosomal instability early in cancer progression. In turn, CIN is thought to be important and key mechanism that potentiates a more aggressive tumour state whereby cancer cells acquire a mutator phenotype that endows a particular subset with selective advantages by accumulating proto-oncogene mutations, and losing alleles to tumour suppressor genes. Moreover modifications of the microtubule cytoskeleton, owing to centrosome dysfunction, are thought to contribute directly to

cellular, and therefore glandular disorganisation and lead to higher histological grade of tumours (Pihan GA et al., 2001). Centrosome aberrations may originate from several fundamentally distinct mechanisms and proteins involved in cell cycle control, centrosome structure or function, and in DNA-damage repair have been implicated in the acquisition of centrosome dysfunction (Nigg EA, 2002).

5. Study Rational

5.1. Background/ Rational

To better understand psoriasin's intracellular function, and possible avenues with which psoriasin may potentiate a more aggressive breast cancer state, our lab (largely through the work of Dr. Ethan Emberley) searched for interacting proteins in a normal breast cell library using a yeast-2-hybrid (Y2H) screen. From a screen of $17.3x10^6$ clones, 4 were identified as true positives based on their ability to activate the LacZ reporter gene and grow on Tryp-/Leu-/His- media.

Two of these psoriasin-interacting candidates were identified at the time as centrosome associated proteins and included RanBPM (Ran binding protein M) and hGCP3 (see Figure 4). This immediately raised question as to whether psoriasin exerts its biological effect during breast cancer progression via altering some aspect of centrosome function. As discussed in section I-4, a growing body of evidence suggests that centrosome

dysfunction is major contributing factor in neoplastic transformation and promotion of more aggressive tumour phenotypes. Our laboratory initially pursued the relevance of RanBPM where it was shown to interact with psoriasin in-vitro but an interaction was not confirmed in-vivo (Emberley ED et al., 2002). My interest lies with the second centrosome-associated psoriasin-interacting candidate hGCP3.

5.2. Hypothesis

It is my hypothesis that psoriasin physically interacts with hGCP3 and this interaction has downstream effects on centrosomal function mediated by hGCP3. Moreover, altered psoriasin expression is able to influence cellular properties associated with cancer progression, in part, through a physical interaction with hGCP3. There were three goals for the study: First, to clone hGCP3 into appropriate mammalian expression vectors; second, to confirm the yeast-two-hybrid GCP3-psoriasin interaction data using biochemical means and direct visualisation with immunofluorescent microscopy; third, to determine if psoriasin expression has a bearing on centrosomal function. Ultimately, the goal of this project was to answer the question: Is an interaction between psoriasin and hGCP3 biologically relevant in breast cancer?

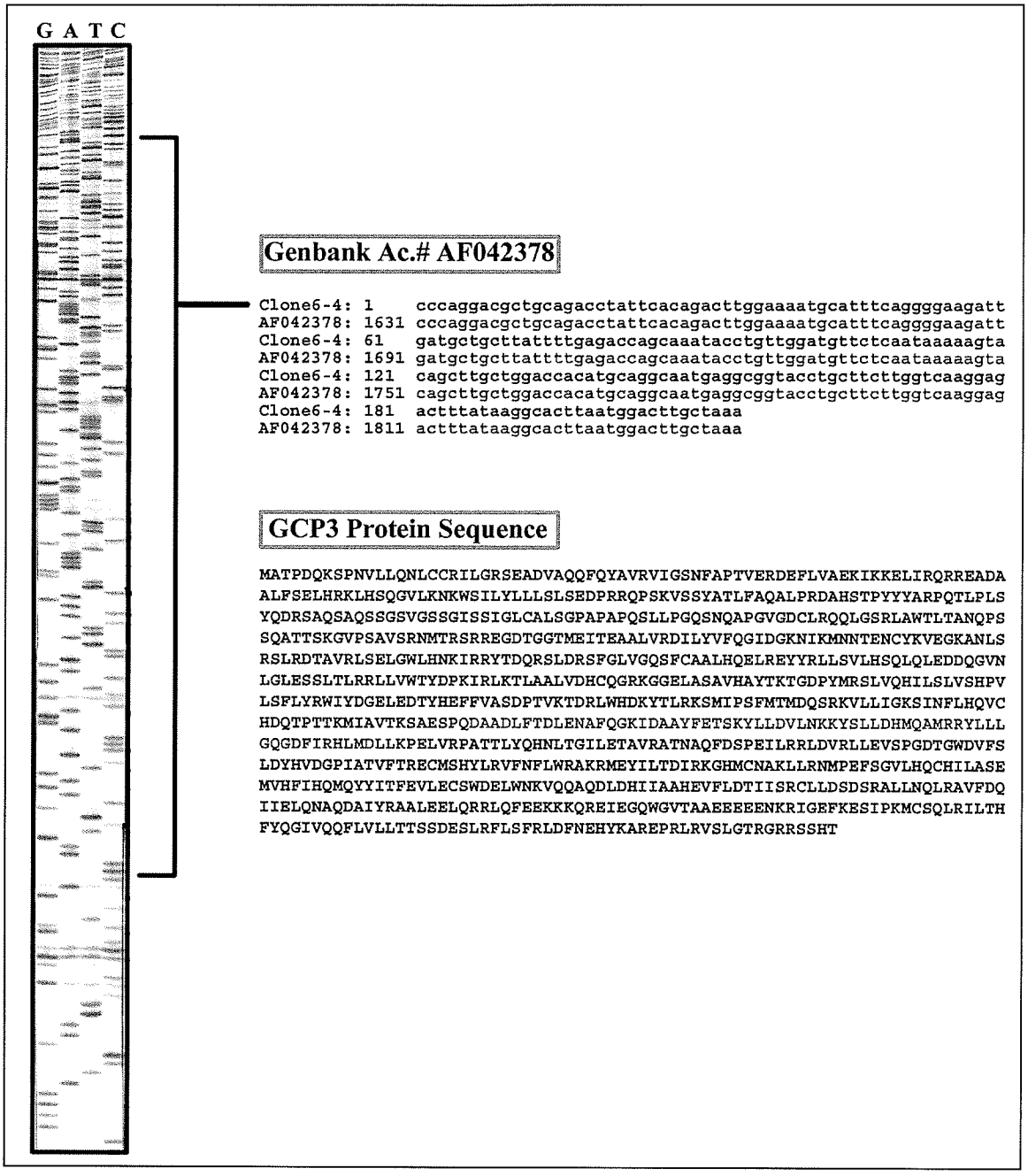

Figure 4: Psoriasin interacting Yeast-2-Hybrid clone 6-4 is hGCP3. Nucleotide sequencing of clone 6-4 (Left) reveals 100% alignment with Genbank sequence AF042378 from nucleotides 1631-1840 (highlighted in red; right-top). This region corresponds to a partial hGCP3 protein fragment (highlighted in red) located in the central region of the protein (right-bottom). This region is that identified to be the putative γ-tubulin binding region (see Figure 3).

II. Materials and Methods

1. Cell Culture

1.1 Bacteria Culture

All bacterial cultures (E.coli-DH5α) were grown in standard Luria-Bertani (LB) broth and agar. LB broths were stored at room temperature until required and was supplemented with carbenicillin (Sigma) at a final concentration of 20μg/mL. Before poring LB agar plates, the agar was cooled to >55^{0}C before supplementing it with 40μg/mL carbenicilllin. LB-agar plates were stored at 4^{0}C until needed. For bacteria cryo-cultures, actively growing bacteria in the presence of selective agent were scraped from an agar plate with sterile toothpicks and transferred to cryovials (Nalgene) containing 500μl sterile 20% glycerol. Cryo-cultures were vortexed for 10 seconds to dissolve clumps then stored at –70^0 C.

1.2 Mammalian Cell Culture

Cells were cultured in Dulbecos modified Eagles medium (DMEM) supplemented with 5% Fetal Bovine Serum (Cansera), 0.35% glucose (Fisher), 2mM L-glutamine (Gibco) and 1000 units pencillin/streptomysin (Gibco). All cell manipulations were conducted in a Labgard laminar flow biological safety cabinet (NuAire Inc.). All cell lines were grown in a water-jacketed incubator at 37^{0}C with a humidified atmosphere containing 5% CO_2 (Forma Scientific). Cell lines used in study are summarized in Table 2. For induction of genes regulated by minimal tetracycline promoter, cells were cultured for one week in

5% Tet-approved FBS-DMEM (Hyclone) prior to supplementing the media with doxycycline (1μg/mL; Sigma) for 48hrs.

Table 2: Cell lines used in this study

Name	Origin	Clone	Feature
MCF7	Human mammary adenocarcinoma-Epithelial	wild type	Endogenous psoriasin negligible
MCF7-clone89*	Human mammary adenocarcinoma-Epithelial	Mag01	Psoriasin inducible- non-expressor with Dox
		Mag06	Psoriasin inducible-expressor with Dox
		Mag07	Psoriasin inducible-expressor with Dox
MDA-MB-231	Human mammary adenocarcinoma-Epithelial	wild type	Endogenous psoriasin negligible
		1A1	Psoriasin non-expressor
		Fa3	Psoriasin expressor
		Fd3	Psoriasin expressor
MDA-MB-468	Human mammary adenocarcinoma-Epithelial	wild type	High levels of endogenous psoriasin
Cos1	Green Monkey Kidney-Epithelial-	wild type	Easy to transfect
Hela	Human cervix carcinoma-Epitheloid	wild type	Endogenous psoriasin negligible
		Hela.12	Psoriasin non-expressor
		Hela.16	Psoriasin expressor

*(Venditti M et al., 2002) –MCF7 clone 89 that stably expresses rtTA

2. Generating cDNA for PCR amplification of hGCP3

2.1. RNA Preparation from Cell Lines:

To extract total RNA from cultured cells, cells were cultured in 10cm diameter dishes under standard conditions till reaching a confluency of 80%. Growth media was then removed and 1ml of Trizol (Invitrogen) was added to the entire surface of the plate. A cell scraper was used to scrape cells from plate and the Cell/Trizol slurry was then transferred to a sterile 1.5ml Eppendorf tube and either processed for RNA extraction immediately or stored at -70^0C for a maximum of 1 month. RNA extraction was performed according to manufacturers instructions. Briefly, to 1ml Trizol/cell slurry 0.2ml chloroform (Fisher) was added, mixed, and incubated at room temperature for 3-5 minutes. Samples were then centrifuged at 12000g for 15 minutes at 4^0C and the aqueous phase (top layer) was transferred to a fresh 1.5ml Eppendorf tube. Next, 0.5ml isopropanol (Fisher) was added to the isolated aqueous layer, mixed, and incubated 5-10 minutes at room temperature followed by centrifugation at 12000g for 15 minutes at 4^0C. The supernatant was then carefully decanted and the remaining RNA pellet was washed with 1ml 75% ethanol followed by centrifugation at 7500g for 5 minutes at 4^0C. The ethanol supernatant was then carefully decanted and the RNA pellet was air dried for 10 minutes at room temperature. Finally the pellet was resuspended in 100μl DEPC-water and stored at -70^0C before quantification.

2.2. Quantification of RNA Concentration

Stock RNA samples were removed from -70^0C storage and immediately placed in a 65^0C water bath for 5 minutes, mixed gently, then centrifuged for 5 seconds at maximum speed

and put on ice. One μL of total RNA was added to 199μL DEPC treated water (1:200 dilution) in a 500μL Dnase and RNase free tube (Eppendorf). Samples were gently mixed and centrifuged at maximum speed for 5 seconds. All manipulations were done one ice as much as possible. Entire 200μL was then transferred into a well of a non-UV absorbing clear bottom 96-well plate (Falcon) and 200μl DEPC water was used as a blank. Optical density (OD) measurements were taken at 260nm using a Spectra Max 190 spectrophotometer (Molecular Devices) and SoftMax Software. RNA concentration was calculated using the following equation: RNA μg/μL = (ODxdilutionx40)/1000.

2.3. Dilution of Total RNA for Reverse Transcription

Stock samples of RNA that have had their concentrations previously determined were removed from –70^{0}C storage and immediately placed in a 65^{0}C water bath for 5 minutes, before being mixed gently and centrifuged for 5 seconds at maximum speed. All subsequent manipulations were performed on ice as much as possible. All stock RNA samples were diluted to a concentration of 1μg/μL in a DNase and RNase free 500μl tube with DEPC water and placed on ice.

2.4. Reverse Transcription Reaction with Thermoscript (Invitrogen)

cDNAs were synthesized using total RNA isolated from MDA-MB-468 cells, Thermoscript (Invitrogen) reverse tanscriptase was used as specified by the manufacturer's instructions. All RNA manipulations were performed on ice as much as possible. Briefly, an RNA master mix and a Thermoscript master mix were made in 500μl tubes and contained the following:

RNA Master Mix	Thermosript Master Mix
5μL 1μg/μL RNA	4μL 5X cDNA Synthesis Buffer
1μL 50μM Oligo$(dT)_{20}$ primer	1μL 0.1M DTT
2μL 10mM dNTP Mix	1μL 40U/μL RNaseOUT™
4μL DEPC H_2O	1μL 15U/μL ThermoScript
	1μL DEPC H_2O

The RNA mix was then placed in a 65^{0}C water bath for 5 minutes, then on ice before 8μL of Thermosript master mix was added. The total volume per reaction was 20μl. Each reaction was mixed by gently pipetting the solution up and down before being briefly spun to collect the contents at the bottom of the tube. The cDNA synthesis reaction were performed in a PTC 100 PCR machine (MJ Research) using the following program: [55^{0}C for 55 minutes] + [85^{0}C for 5 minutes] + [4^{0}C, hold].

2.5. PCR amplification of hGCP3 ORF from MDA-MB-468 cDNA

A PCR-based approach was used to amplify full-length hGCP3 open reading frame (ORF) for cloning purposes. PCR primers (GCP3-U/L-ORF, Table 4) were designed to flank and contain both start and stop codons reported to delimit hGCP3 open reading frame (ORF) (Genbank accession number AF042378). Using a high fidelity DNA polymerase, Platinum Pfx (Invitrogen), a 2750bp product was amplified from a MDA-MB-468 cDNA library (section II-2.4) using the following PCR cycle: [94^{0}C, 4min] + [94^{0}C, 30 sec; 65^{0}C, 30sec; 68^{0}C, 190sec]x34 + [72^{0}C, 7min]. Two μL of starting cDNA

was used as a template and reactions were carried out in 1X final concentration of Pfx enhancer solution (Invitrogen) according to the manufacturer's instructions. Taq polymerase (Invitrogen) was added to the last cycle [72^{0}C, 7min] in order to incorporate a single deoxyadenosine to the 3´-ends of amplified fragments.

3. Cloning & Subcloning hGCP3

3.1. pcc001(pGEM T-easy: hGCP3*)

hGCP3 ORF PCR product (2μL from step II-2.5) was ligated into pGem T-Easy (Promega) (hereafter referred to as pGem) utilizing single 3´-T overhangs at the insertion site according to manufacturer's instructions and electroporated into E. coli DH5α (see II-4.6). Transformed E. Coli were selected on Amp-plates and recombinants were screened, based on the insertional inactivation of the α-peptide coding region for β-galactosidase that flanks the multiple cloning site of pGEM, by blue/ white colony selection on X-Gal agar plates.

3.2. pcc002 (pcDNA4.0His/MaxA-hGCP3*)

To generate a mammalian expression vector that expresses an N-terminal epitope tagged hGCP3, hGCP3 insert from pcc001 was ligated into pcDNA4His/Max utilizing compatible Not1 sites. Briefly, to prevent self-ligation of Not1-restricted-pcDNA4-plasmid, 5'-terminal phosphate groups were removed using calf intestinal alkaline phosphatase (CIAP 2U/μL, Amersham) according to the manufacturer's instructions.

Phenol extracted and ethanol precipitated products were then OD'ed, and used as 'vector' for ligation. The hGCP3 insert was prepared by co-restriction of pcc001 with Not1 and Pvu1 followed by fragment isolation using a FEFAG protocol (see II-4.5). Not1 removes the hGCP3 cassette from the pGem multicloning site (MCS), while Pvu1 uniquely cuts the pGem backbone allowing for the hGCP3 cassette to migrate slower during agarose del electrophoresis than vector fragments, thereby facilitating isolation and extraction from the gel. Phenol extracted and ethanol precipitated product was OD'ed, and used as 'insert' for ligation. Ligation were performed with T4 DNA ligase (Invitrogen) at a 90:30 (Insert:vector) fmol ends ratio according to the manufacturer's protocol. Transformed colonies that were able to grow on Amp plates were screened by rapid PCR protocol (see II-4.4) for the presence of the hGCP3 insert .

3.3. pcc003 (pcDNA4.0His/MaxA-hGCP3)

The 'Transformer site-directed-mutagenesis' kit (Clontech) was used to reverse the single missense mutation at Phe51 in pcc002 according to the manufacturer's instruction. The following primers were designed for this purpose: GCP3-REV-MUT and APA1-MUT (Table 4).

3.4. pcc005 (pTreHygro-His-hGCP3)

His-tagged hGCP3 from pcc003 was subcloned into a tetracycline inducible expression vector pTre2-Hyg (Promega) using a similar approach previously described for the subcloning of hGCP3. The His-hGCP3 insert was prepared by co-restriction of pcc003 with Pme1 and Apa1 followed by fragment isolation using a FEFAG protocol (see II-

4.5). Pme1 removes the His-hGCP3 cassette from the pcc003, while Apa1 specifically cuts the pcc003 vector backbone at multiple sites. The vector was prepared by digesting pTRE2-Hyg with EcoRV, followed by CIAP treatment. Blunt-end ligations were performed with T4 DNA ligase (5U/μL) (Roche). Ligations were either diluted 1/5 or left undiluted before 1ul was electroporated into DH5α. Transformed colonies that were able to grow on Amp plates were screened by rapid PCR for the presence of the His-hGCP3 insert.

Table 3: Plasmid constructs generated for this study

Name	Size (Kb)	Parent vector	Insert	Purpose
pcc001	5773	pGEM-T Easy (Promega)	hGCP3*	Easy to clone and Sequence PCR products
pcc002	8050	pcDNA4/HisMax (Invitrogen)	His- hGCP3*	Constitutive eukaryotic expression of epitope tagged (HisMax) mutant hGCP3
pcc003	8050	pcDNA4/HisMax (Invitrogen)	His-hGCP3	Constitutive eukaryotic expression of epitope tagged hGCP3
pcc005	8462	pTRE2hyg (Clontech)	His-hGCP3	Tetracycline Inducible eukaryotic expression of His-hGCP3

hGCP3*-contains a mutation a Phe51

3.5. Sequence Analysis

All vector constructs were verified by rapid PCR-screen and diagnostic restriction analysis, as well as by sequencing to ensure that the nucleotide sequence was correct. Table 4 summarizes all sequencing primers used in this study. DNA was sequenced at the University of Calgary Core DNA Facility, Calgary Alberta (http://dnaservices.myweb.med.ucalgary.ca/UCDNAServicesHome.html). Automated

sequencing was performed with an ABI Prism 377 DNA Sequencer (Applied Biosystems). For sequencing reaction, 5μg of template double stranded plasmid DNA was diluted in a total volume of 10μl and submitted in a DNase and RNase free 500μl Eppendorf test tube. The specific sequencing primer was submitted at a concentration of 3.2 pmol/μL in 5μl total volume in a separate DNase and RNase free 500μl Eppendorf test tube. Sequencing results were downloaded from the Core DNA Facility's FTP server. Sequencing results were submitted to BLAST (http://www.ncbi.nlm.nih.gov/BLAST/) for identification of mutations.

Table 4: Primers used in this study for cloning, quantifying, sequencing and site-directed-mutagenesis

Purpose	Name	Seq 5'→3'
PCR-Quant	GCP3-U-Quant	AGCGTGGGCAGCAGTGGCATCAGCAGCATT
	GCP3-L-Quant	CTCACCTCCTTTCCTTCCTTGGCACTGGTC
PCR of hGCP3 cDNA	GCP3-U-ORF	CACGGCTCCGGGCGAGGAT
	GCP3-L-ORF	GGGAGGACCGCGAGCTTCACG
Sequencing	T7	TAATACGACTCACTATAGGG
	SP6	GAATTAGGTGACACTATA
	GCP3-2	CCCAGGACAGTCTAATCAAG
	GCP3-3	GACCACTGCCAAGGAAGGAA
	GCP3-4	GGACTTGCTAAAACCAGAAC
	pTRE-3'Seq	CCATTCTAAACAACACCCTG
	pTRE-5'Seq	CGCCTGGAGACGCCATC
	GCP3-5'-OUT	ACGTTCGGCGACTTCTGGTC
	GCP3-3'-OUT	GTTACTGACGACCAGCTCTGACG
S.D.M	GCP3-REV-MUT	p-GAGATGAATTTTTAGTAGCTG
	APA1 MUT	p-GTCTAGAGGTACCGTTTAAAC

S.D.M., site-directed-mutagenesis; mutagenic nucleotides are underlined

4. General Methods used in Cloning and Subcloning

4.1. Plasmid Preparation

Single, isolated colonies of E. Coli DH5α containing the desired plasmid were picked from freshly streaked Amp-plates and transferred with a sterile toothpick to 2ml Amp-broth. Overnight cultures were grown for ~16hr at 37^0C and were processed with the High Pure Plasmid Isolation Kit (Roche) according to the manufacturers directions. The DNA is eluted in a final volume of 100μl TE buffer. One 2ml bacterial culture typically yields >10μg of plasmid DNA.

4.2. Phenol Extraction and Ethanol Precipitation:

In order to remove protein contaminants or ethidium bromide from DNA, phenol extraction was performed prior to ethanol precipitation only when the DNA would be used for subsequent ligation reactions. Otherwise ethanol precipitation was exclusively performed to concentrate plasmid samples and to purify plasmid from elution buffer salts. Briefly, equal volume of phenol:chloroform (1:1) was added to samples and vortexed twice for 20 seconds with 20 seconds incubation in between. The aqueous layer was transferred to a new 1.5ml Eppendorf tube and the DNA was precipitated with 1/10 the volume of 3M NaAc pH5.2 and 2X the volume with ice cold 100% ethanol. Samples were vortexed and incubated at -70^0C for 15 minutes followed by centrifugation (10000g for 15 min. at 4^0C). The supernatant was then removed and the pellet washed with 200μl 70% ethanol before removing the 70% ethanol and air drying the pellet for 20 minutes.

The pellet was then resuspended in 10-20μl sterile distilled water (for sequencing), or TE pH 7.5 (for transfection or cloning).

4.3. Quantification of Plasmid DNA Concentration

One μL of ethanol precipitated plasmid DNA was added directly into a well of a non-UV absorbing clear bottom 96-well plate (Falcon) containing 199μL ddH_2O (1:200 dilution). As a blank 1μL of TE or ddH_2O was added to 199μl ddH_2O. All wells were pipetted up-and-down three times to ensure proper mixing. Optical density was measured with a Spectra Max 190 spectrophotometer (molecular Devices) using a wavelength of 260nm. The concentration of double stranded plasmid DNA(μg/μL) was calculated with the following equation: μg/μl = (OD x 50x dilution factor)/1000 where an optical density 1 = 50μg/μL, and a dilution of 1/200 was used. The purity was determined by the ratio of readings taken at 260 nm and 280 nm wavelengths and typical purities varied between 1.5-1.8.

4.4. Rapid Screen of Transformed E.coli for hGCP3 Recombinant Constructs by PCR

Five µl from a 2mL overnight culture was combined in an 0.5mL PCR tube with 40µl of ddH_2O. Cells were pelleted by centrifugation (12500 r.p.m. for 30sec) and supernatant was removed. Cell pellets were resuspended in 20µl ddH_2O before being boiled at 100^0C for 5min. Cell debris was pelleted by centrifugation (10000 r.p.m. for 3 min at 4^0C) before 1µl of supernatant was added to a standard PCR mix using GCP3-U/L-Quant

primer set (Table4) for PCR. The following PCR cycle was used [95^{0}C for 4min] + [95^{0}C, 30 sec; 65^{0}C, 30sec; 72^{0}C, 45sec]x35 + [4^{0}C,hold].

4.5. Fragment Elution from Agarose Gel (FEFAG)

Prior to loading agarose gel, large-scale restriction digests were performed in which 100 μL of mini-plasmid preparations were digested with the appropriate restriction endonuclease (10μL) in the manufacturer's specified buffer (50μL). The final volume was brought to 500μL with ddH_2O. Following completion of restriction digest (1.5hr at 37^{0}C), restriction products were ethanol precipitated (see II-4.2) and resuspended in 20μL ddH_2O. Two μL of 10X DNA Loading Dye was added before ethanol-precipitated plasmid fragments were loaded and separated in a 0.5% agarose gel made with TAE containing ethidium bromide. Samples were electophoresed in TAE buffer at 100V for 40-70mins or until the band to be isolated was well resolved and separated from other bands. Bands were visualized briefly using a hand-held long-wavelength UV light. Next, 3MM Whatman paper and dialysis tubing (Fisher) were cut to the same size and were roughly two and half times the width of a loading well. A slit was cut into the gel all the way through with a scalpel just below the DNA fragment to be isolated and the pre-cut piece of Whatman paper/tubing was inserted together into the slit (the paper closest to the fragment). The gel was additionally run for 15 minutes at 110V. Next, the paper/tubing were removed from the gel and put into a 500μl tube (cap removed) that has had a hole poked in the bottom with an 18.5g needle. It is important that paper/tubing is not packed in bottom of tube. Next, the 500μl tube was inserted into a 1.5ml tube that has had its cap removed and 100μl Elution Buffer (EB) was added. The EB was then pipetted up and

down 5 times making sure the filter paper is well washed followed by centrifugation for 10 seconds at 500g in a bench top centrifuge. The EB that has collected in the bottom of the 1.5ml tube was transferred to a new 1.5ml tube. Washing, centrifugation and collection steps were repeated 2 more times, with the last centrifugation step at maximum speed for 30 seconds. Pooled EB (~400-500µl/well) containing isolated DNA fragment was then subjected to phenol:chloroform extraction (see II-4.2) to clean the insert, and ethanol precipitation to concentrate the sample, before resuspending in 10µl of ddH_2O.

4.6. Electroporation

Electroporation chambers with a channel gap of 0.1cm (BioRad) were placed on ice for 15 minutes prior to electroporation. Meanwhile, tubes containing 30μl of electrocompetent DH5α were placed on ice and allowed to thaw before being combined with the appropriate amount of plasmid DNA (1µl of pure plasmid or 2µl of 1/5 dilutions from ligation reactions). Bacteria DNA mixtures were pipetted between electrode surface of the electroporation chamber. Electroporations were performed using a Gene Pulser (BioRad) under the following conditions: 400 ohms, 25μFD and 1.25V. Bacteria were then transferred to 1ml LB and incubated at 37^0C with shaking (200rpm) for 1hr. Finally, 10 to 200μL (depending on the source of DNA) was bacteria plated onto amp-plates and grown overnight at 37^0C.

5. In vitro TNT

In vitro transcription and translation of ^{35}S-Met labelled His-hGCP3 protein was performed using a rabbit reticulocyte lysate kit (Promega) according to the manufacturer's instructions with 1μg of pcc003 as template plasmid. Samples were electrophoresed through a 10% SDS-polyacrylamide gel as previously described. The gel was then dried and autoradiography (overnight exposure) was used to detect labelled protein.

6. Transfection

6.1. Effectene

For stable transfection of MCF7 cells, Effectene reagent (Qiagen) was used according to the manufactures instructions at a ratio of 1μg DNA: 8μL Enhancer: 25μL Effectene. Plasmid DNA was prepared in TE buffer at a concentration of at least 1μg/μl, and DNA/ Effectene complexes were added dropwise to the surface of the dishes. Transfections were performed in 100mm culture dishes and with 2μg of plasmid.

6.2. Lipofectamine2000

For transient transfection experiments in Cos1 cells, Lipofectamine2000 (Invitrogen) was found to be an effective transfection reagent. In preparation for transient transfections, cells were plated 48h-72h in advance and allowed to attain 75-90% confluency and 16-24hr prior to transfection the media was replaced with antibiotic-free media.

Transfections were performed according to the manufacturer's protocol at a ratio of 3ul Lp2000:1ug DNA and Opti-MEM reduced serum media (Invitrogen) was used as a DNA and Lipofectamine2000 diluents. However one key difference between the recommended protocol and that used in this study was the combined DNA-Lipofectamine2000 complexes were added directly to the surface of the cells for one minute prior (and not after) to adding the rest of the plating volume of Opti-MEM. This was found to yield a far better transfection efficiency. For His-hGCP3 overexpression studies(see III-4), Cos1 cells were grown in 6cm dishes and transfected with 4μg of pcc003. For co-immunoprecipitation studies (see III-2.1; III-5.1), Cos1 cells were grown in 10cm dishes and transfected with 12 to 24 μg of total of plasmid DNA. To reduce cytotoxicity attributable to prolonged incubation with polycationic lipid transfer agents, the transfection media was removed 6-8hr post-transfection, and the cell surface washed several time (3-5X) with PBS before regular media containing serum and antibiotics was added.

7. Stables and inducibles

7.1. Stables

MCF7 cells were seeded at $1x10^5$ per 10cm dish, 24h before transfection. Six dishes were transfected with 1ug of pcc003 using Effectene Reagent (Qiagen) according to manufacturer's protocol (see II-5.1). Two non-transfected dishes serve as selection control. Zeocin (Invitrogen; 450ug/mL) was used as the transfection selection agent as pcc003 encodes a zeocin resistance gene, and selection was started 24h after transfection.

Selection media was changed every other day and continued for the duration of the experiment till western analysis. Approximately two and a half weeks after zeocin selection, control plates were devoid of living cell save for a few isolated cells with granular, vacuolized, swollen appearance. To get a range of fast growing and slow growing clones, over the next four weeks, colonies of zeocin resistant MCF7 were isolated. This was accomplished by the 'cloning-ring method.' Briefly, after removing the media from the dish and washing cells with PBS, sterile Cloning Rings (Fisher) (which are coated on one edge with silicon vacuum grease) were placed firmly on the plate such that individual colonies were in the middle of the ring. The ring was then flooded with Trypsin-EDTA (Invitrogen) and incubated at 37oC for 5 minutes. Contents of the ring were then gently pipetted up and down to break apart the colony and then transferred to a well in a 96-well plate. Growth media containing selective agent was added to the well. Clones were ramped-up to the T25 flask stage over the next two to four weeks before western analysis with Anti-His antibodies was performed.

7.2. Inducibles

The protocol used to generate an inducible 'Tet-On' His-hGCP3 MCF7 cell model is essentially that described above (see II-7.1). However, several key differences include: using MCF7-89 cells expressing the reverse tetracycline transactivator (rtTA) (courtesy of Dr. Shiu, Department of Physiology, University of Manitoba) (Venditti M et al., 2002), culturing cells in 'Tet-Approved' media (Hyclone) two week prior to transfection and throughout the duration of cloning exercise, using Hygromycin (Sigma) selection (500μg/mL), and using linearized pcc005 vector for transfection. Xmn1 restriction

uniquely cuts pcc005 within AmpR gene and linearilized products were purified using MiniElute Reaction Cleanup Kit (Qiagen) before transfection. Linearilized vector are thought to integrate into the genome better circular plasmids.

8. Western Blot

8.1. Extraction of Protein from Culture Cells

Total cell lysates were prepared by washing cells (cultured in 60mm or 100mm dishes (Costar)) twice in ice cold PBS and were lysed with SIB (60-150μL). Cells were scraped off the surface of dish with a plastic cell scraper (Costar) and transferred to a 1.5ml Eppendorf tube on ice. All protein lysates were sonicated with a Sonic Dismembranator (Fisher Scientific) for 2 pulses of 10 seconds at setting of 4 to sheer genomic DNA. All sonicated proteins lysates were stored at -20^0C.

8.2. Protein Assay

Protein concentrations from total cell lysates were determined using the Micro BCA Protein Assay Kit (Pierce) according to the manufactures instructions. The equation for Standard Curves were generated by plotting values for protein concentration (X-axis) vs. absorbance at 562nm (Y-axis) in Graph Pad Prism statistical software (Graph Pad). Linear regression statistics were performed to calculate the equation for the best fit line (not forced through the origin 0,0). The Y-intercept and the slope of the line was used to calculate the protein concentration of the unknown samples using Excel (Microsoft) and

the equation: μg/ml protein in a 1:500 dilution = (absorbance at 562nm – Y-intercept)/slope (μg/mL protein in a 1:500 dilution)/2 = concentration in μg/μl.

8.3. Protein Samples Preparation for Western Blot

Stock protein lysates were removed from –20^{0}C and thawed at room temperature. Tubes were vortexed and centrifuged quickly, then placed on ice. The amount of protein lysate needed for 50μg or 100μg of total protein was pipetted in a 500μl Eppendorf tube and combined with an appropriate volume of 4X Sample Buffer to yield a final concentration of 1X. 20μl of Pre-Stained Broad Range Protein Marker (New England BioLabs) was pipetted into its own tube and processed with the protein sample tubes. All samples were "boiled" at 100^{0}C for 5 minute in a PTC 100 PCR machine (MJ Research) before loading for electrophoresis.

8.4. Western Blot

To detect psoriasin by western analysis with anti-psoriasin antibodies, 50µg of total protein per lane were run on a 16.5% SDS-polyacrylamide gel using Tricine-SDS-PAGE methodology. Gels were first stacked at 15mA for 20 min and separated for 2-21/2 hr at 30 mA. For all other proteins, 100µg of total protein were run per lane on a 10% SDS-polyacrylamide gel and gels were stacked for 20 min at 15mA and separated for 1 –11/2 hr at 25 mA. To transfer proteins to nitrocellulose membrane (BioRad), a BioRad Mini-Gel Transfer Apparatus was used as specified by the manufacturer's instructions. For psoriasin detection, a 0.2μm pore size nitrocellulose was used, otherwise 0.45μm pore size nitrocellulose was used for all other proteins. All transfers were done in cold 1X

Transfer Buffer with stirring and the entire transfer apparatus was placed in an ice bucket with ice. All transfers were done at 100Volts for 1 hour. After transfers were complete, nitrocellulose membranes were placed in Blocking Buffer for 45-60 minutes with gentle agitation. Membranes were then incubated with primary antibodies (Table 5) diluted in blocking buffer and incubated overnight at 4^0C with gentle shaking. Primary antibody mixture was removed and blots were washed 3 times with 10ml TBST for 5 minutes with gentle shaking at room temperature. After each was step, TBS-T was discarded. Secondary antibody (Goat anti-Rabbit-HRP or Goat anti-Mouse-HRP, BioRad) were diluted 1:5000 in 10ml Blocking Buffer and incubated on blots for 1 hour at room temperature with gentle shaking. Secondary antibody mixture was removed and blots were washed 3 times with 10ml TBS-T for 5 minutes with gentle shaking at room temperature. After each was step, TBST was discarded. For secondary antibody detection, the surface of the blot was completely covered (~2ml) with the HRP substrate Super Signal (Pierce) for 10 minutes at room temperature. Finally, blots were exposed to photographic film (Kodak MR) and developed with a tabletop automated developer in a darkroom for various times then stored at -20^0C.

9. Co-Immunoprecipitation

9.1. Co-Immunoprecipitation of His-hGCP3 with Psoriasin

Cos1 cell were grown to 80% confluency in 10cm dishes and transiently co-transfected (in some experiments) with either equal molar (12 ug total) or (in other experiments) equal ug amounts (24 ug total) of pcc003 and pcDNA3.1-psor using Lipofectamine 2000

(Invitrogen) at a ratio of 3ul Lp2000:1ug DNA. In preparation for co-IPs, protein-G sepharose beads (Amersham/ 75μL of per co-IP) were washed three times with 500μL co-IP buffer. Between each wash, protein-G-Sepharose beads were gently pelleted by centrifugation at 1000rpm for 30 seconds at 4^0C and the supernatant was removed. After the final wash, beads were resuspended in an equal volume of co-IP buffer to yield a 50% bead slurry. Twenty-four hours after transfection cells were lysed on ice for 10 minutes with 1mL of co-IP buffers known to either preserve protein interactions with psoriasin [Buffer 1: 25mM HEPES pH 7.7, 0.4M NaCl, 1.5mM $MgCl_2$, 2mM EDTA, 1% Triton X-100, 0.5mM DTT, and protease inhibitor mixture (Roche)] (Emberley ED et al., 2003a), or with hGCP3 [Buffer 2: 50mM HEPES pH 7.4, 150μM NaCl, 2mM EDTA, 1mM DTT, 0.5% Triton X-100, and protease inhibitor mixture (Roche)] (Murphy SM et al., 1998). All samples were transferred to chilled 1.5 mL Eppendorf tubes and cleared by centrifugation (12,000g, for 10 min at 4^0C). Supernatants were then transferred to pre-chilled 1.5 mL Eppendorf tubes before pre-clearing equal-volumes of whole-cell lysates with 35μL of a 50% bead slurry by end-over-end rotation for 45 minutes at 4^0C. Next, protein-G beads were spun at 16000Xg for 5 minute at 4^0C and pre-cleared supernatants were transferred to pre-chilled 1.5 mL Eppendorf tubes before commencing the co-IP proper. Complexes were immunoprecipitated by adding 1μL of Anti-His antibody (Invitrogen), or 1μl an unrelated control mouse monoclonal IgG antibody to 1ml of pre-cleared supernatant for 2-4 hours with end-over-end rotation at 4^0C at which time 35μL of 50% protein-G bead slurry was added for an additional 1 hour with end-over-end rotation at 4^0C. Captured protein complexes were washed by gently pelleting protein-G/ antibody beads by centrifugation at 1000rpm for 1 minute at 4^0C, removing the

supernatant, and resuspending beads in 500μL of co-IP buffer. This was repeated a total of three times before pelleting the beads (1500g for 1 minute) and pipetting-off as much of the supernatant as possible. In preparation for western analysis, protein was extracted from the G-Sepharose beads by adding 20μL of 2X SDS-PAGE Loading Buffer and boiling samples for 5 minutes at 100^0C. Beads were spun (1500g for 1minute) and as much of the supernatant as possible (20-30μL) was loaded per lane.

9.2. Co-Immunoprecipitation of His-hGCP3 with γ-Tubulin

The co-IP protocol used to co-IP His-hGCP3 and γ-tubulin is essentially that described above (see II-9.1), however there were several differences. Cos1 cell were grown to 80% confluency in 10cm dishes and transiently transfected with 12μg of pcc003 using Lipofectamine 2000 (Invitrogen) at a ratio of 3ul Lp2000:1ug DNA. Moreover, cells were lysed only in co-IP-buffer-2 and additional immunoprecipitating antibodies used were anti-γ-tubulin (clone GTU88; Sigma) antibody.

10. Immunofluorescent Microscopy

10.1. Cell culture

For all imunofluorescent experiments, cells were seeded 48hrs prior to immunofluorescent processing and grown on 22mm round coverslips (Fisher Scientific) under standard culture conditions.

10.2. Microtubules

To visualize microtubules, cells were washed twice with PBS, before fixation in -20^0C methanol for 10 minutes. Cells were permeabilised by dipping coverslips twice in -20^0C acetone for ten seconds then washed twice with PBS. Finally, cells were rehydrated in PBS for at least 30 minutes prior to labeling with antibody. All subsequent procedures were performed in the dark either under infrared light or significantly reduced lighting. Microtubules were directly immunofluorescently-labeled with anti-β-Tubulin-Cy3 (mouse monoclonal clone Tub2.1; Sigma-Aldrich) antibodies diluted 1:1000 in PBS containing 1% bovine serum albumin (BSA). A humid incubation chamber was made by placing moist paper towels in a 144mm dish, and layering a sheet of parafilm over the moist paper towels. 100μL of diluted antibody per coverslip was pipetted onto the sheet of parafilm and coverslips were placed cell side down over the 'antibody droplet'. Coverslips were incubated for 60 minutes at room temperature in the dark and were then washed 3x 5 minutes with PBS. Coverslips were stained with 1 μg/ml DAPI (4',6-diamidino-2-phenylindole-dihydrochloride) for 1 min, then washed three times in PBS. The excess PBS was removed from the coverslip by touching edge of cover slips on a paper towel. Coverslips were mounted on glass slides (Superfrost/Plus; Fisher Scientific) with 25μL FluoroSave Reagent (Calbiochem) and the edges of the coverslip were sealed with a couple dabs of clear nail polish.

10.3. γ-Tubulin, His-hGCP3, and Psoriasin

To visualize all other proteins, indirect immunofluorescence was used. Cells were fixed in -20^0C methanol for 10 min, hydrated in PBS for 1 min, and then blocked in buffer A

(3% BSA in PBS plus 0.1% Triton X-100) for 45 min (except in some experiments 0.2% gelatin or 1% goat serum was substituted for BSA in buffer A). In other experiments to visualize His-hGCP3 or psoriasin, cells were permeabilized with acetone (see II-10.2) instead of mild-detergent treatment, however this did not alter the immunofluorescent signal obtained from either method (data not shown). Primary antibodies were diluted in 3% BSA. Primary antibody incubations were for 1 h, followed by three washes with buffer A. All subsequent manipulation were performed in the dark either under infrared light or significantly reduced lighting. Secondary antibodies (goat anti-rabbit or mouse Cy3) were from Jackson Immunoresearch Laboratories and were diluted 1:1000 in buffer A. Secondary antibody incubations were for 1 h, followed by three washes with buffer A. Coverslips were then process as described in section (see II-10.2).

10.4. Image Capture

Micrographs were taken with an Eclipse E1000 epifluorescent microscope (Nikon) and images were digitized with ACT-1 software (v.2.63; Nikon). Merged images were generated with Photoshop 6.0 (Adobe).

Table 5: Primary antibodies used for western analysis, co-immunoprecipitation and immunofluorescent microscopy

Target protein	Molecular Mass (kDa)	Name of antibody	Source	Species
Psoriasin	11	anti-psoriasin	Custom made	Rabbit
	11	anti-psoriasin [47C1068]	Abcam	Mouse
β-Tubulin	55	anti-β-Tubulin Cy3 [Tub2.1]	Sigma	Mouse
γ-Tubulin	48	anti-γ-Tubulin [GTU88]	Sigma	Mouse
His-hGCP3	110	Anti-HisG	Invitrogen	Mouse

11. Mitotic Spindle Morphology (MSM)

Mitotic spindles were visualised in methanol fixed (-20^{0}C) / acetone permeabilised cells using direct IF labelling of β-tubulin with a Cy3-anti-β-tubulin antibody (Sigma) as described in section II-10.2. DAPI staining was used to visualise DNA. MSM scoring criteria were established in order to minimize observer-introduced-errors. Prophase spindles were excluded from the count as it is often difficult to accurately distinguish the number and orientation of spindles. In prophase cells, centrosomes are en-route to the poles and often have overlapping and indistinguishable spindles. Telophase and cells undergoing cytokenesis were also excluded from the analysis in order to simplify and standardize the scoring. Spindle defects that were scored included monopolar, multipolar, misaligned and unknown defects. Both the frequency and type of aberrant spindles were scored in three separate experiments, in which 100 consecutively viewed metaphase or anaphase spindles were scored per cell line used.

12. MT Regrowth Assay

12.1. Cell culture

This assay was adapted from Shu and Joshi (Shu HB et al., 1995). Briefly, cells were grown on coverslips till they attained roughly ~60% confluency. Microtubules were then depolymerised in living cells with nocodazole (25uM, Sigma) treatment and on ice for 2 hours. Coverslips were washed twice in cold PBS to remove nocodozale and subsequently placed into fresh warm media (37^0C) for exactly 5 minutes before fixation and IF processing (see II-10.2). Particular attention was paid to the regrowth time, as polymerisation of MT under these conditions is time dependent. In this way regrowth of microtubules from naked centrosome takes place in living cells and is subject to the endogenous cytoplasmic environment.

12.2. Image capture

For quantitative purposes, imaging resources housed within the Genomic Centre for Cancer Research and Diagnosis at the Manitoba Institute for Cell Biology were used. Fluorescent micrographs were obtained with an Axioplan II microscope (Zeiss) equipped with a Hamamatsu CCD, Sensi Cam Series 200 camera (Hamamatsu Co.). Images were digitized (16-bits per channel) with Northern Eclipse Image Analysis software, version 6.0 (Empix Imaging Inc.). For quantification of fluorescent intensity for a given area in pixels, the 'XY Mark' application of the Northern Eclipse software was used. All images were captured with 63X Plan-apochrome objective (Zeiss) and exposure times were kept constant. Slides were scanned with the DAPI filter for cells presenting a metaphase or

early anaphase DNA morphology. Next filters were switched to Cy3 channel to reveal centrosomes with nascent nucleated MTs. In order to minimize effects of photobleaching images were rapidly focussed on the nearest centrosome. Often only one in-focus centrosome was captured as centrosomes are typically not in the same exact plane.

12.3. Quantification:

The degree of MT regrowth was measured based on the assumption that the rate of MT elongation (polymerisation) is constant under experimental conditions (time and temperature kept constant). Therefore total fluorescence intensity centred on a centrosome is proportional to the amount newly generated MTs and is a function of the area size measured. As such, the MT regrowth was defined as the total fluorescent intensity from an area centred on the centrosome (Figure 5, C), minus the average background intensities for that same area, arising from both within the cell (where no tubulin polymerisation has occurred; Figure 5, B2) and from outside the cell (Figure 5, B1). In this way, background fluorescent intensities that are the result of intracellular and coverslip/slide variation are compensated for in the analysis. Fluorescent intensity values for each of the areas measured were obtained with the 'XY Mark' application of the Northern Eclipse software and were processed with Microsoft Excel (Microsoft) software.

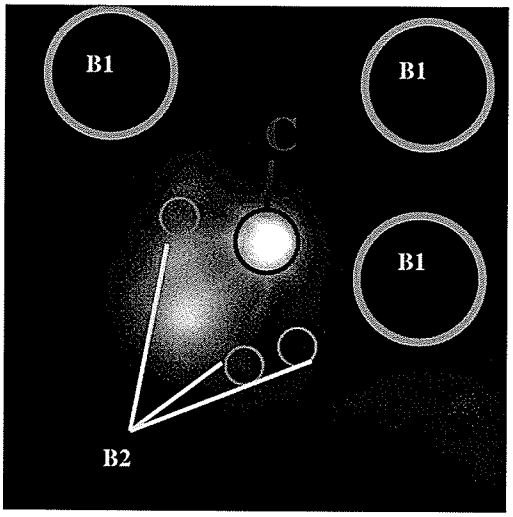

Figure 5: Diagram illustrating the quantification of microtubule regrowth. The average background intensities arising from both within the cell where no tubulin polymerisation has occurred (B2) and from outside the cell (B1) were subtracted from the total fluorescent intensity for a given area centred around the centrosome (C1) where microtubule regrowth has occurred. (B1, background 1; B2, background 2; c, centrosome).

13. Statistical analysis

All statistical analysis was performed with Prism Graphpad software (Graphpad Prism v4.00, Graphpad software) and using One-way ANOVA with either Bonferroni's or Dunnetts post-tests as appropriate. $p < 0.05$ was considered statistically significant.

III. Results

1. Cloning His-hGCP3

There are no commercially available antibodies against hGCP3, nor was it possible to access reagents generated by the laboratories involved in the initial cloning and characterization of hGCP3. As such, it was not possible to detect or monitor levels of endogenous hGCP3 protein. Therefore, to study whether an hGCP3-psoriasin interaction is biologically significant in human breast cancer, it necessitated the construction of a mammalian expression-vector encoding an epitope-tagged hGCP3. For this, two mammalian expression vectors were generated encoding an amino-terminal histidine-tagged hGCP3 protein (His-hGCP3); the first vector (pcDNA4HisMax) is driven by a CMV promoter and designed to constitutively express His-hGCP3, while the second (pTRE2Hyg) is driven by a tetracycline responsive promoter for inducible 'Tet-On' expression.

1.1. pcc001 (pGEM T-easy: hGCP3*)

A PCR-based approach was used to clone full-length hGCP3 as described (section II-2.4). PCR products were ligated into pGem T-Easy and transformed E. Coli were selected on Amp plates. Recombinants were screened, based on the insertional inactivation of the α-peptide coding region for β-galactosidase that flanks the multiple cloning site of pGEM, by blue/ white colony selection on X-Gal agar plates.

White colonies were further analyzed for the presence of a 2.7kb hGCP3 insert using a diagnostic EcoRI restriction; pGem without an insert has only one EcoR1 site, while the 2.7kb hGCP3 insert provides another site to generate three restriction fragments (3kb, 1.9kb, 0.9kb). Two clones (out of four) had the expected EcoR1 restriction pattern (Figure 6A). Sequencing both cloned hGCP3 inserts and alignment with Genbank hGCP3 sequence AF042378, revealed that they each contained a single missense mutation and two silent mutations (Figure 6B). None of the mutations were at sites reported to be polymorphisms (Genbank AF042378).

Although incorporation of three mutations over a 2.7kb amplification product appears to be substantial number of mutations, compared to other polymerase tested (Taq, GC-Rich kit (Roche), Pfu (Invitrogen)), PFx was significantly more accurate. As such, rather than exhaustively repeating the PCR cloning in hopes that a mutation free full-length hGCP3 open reading frame (ORF) could be generated, it was decided that the cloning strategy should continue with existing mutated hGCP3 (hereafter known as hGCP3*) and site-directed-mutagenesis (SDM) would be used to reverse the single missense mutation from clone1.

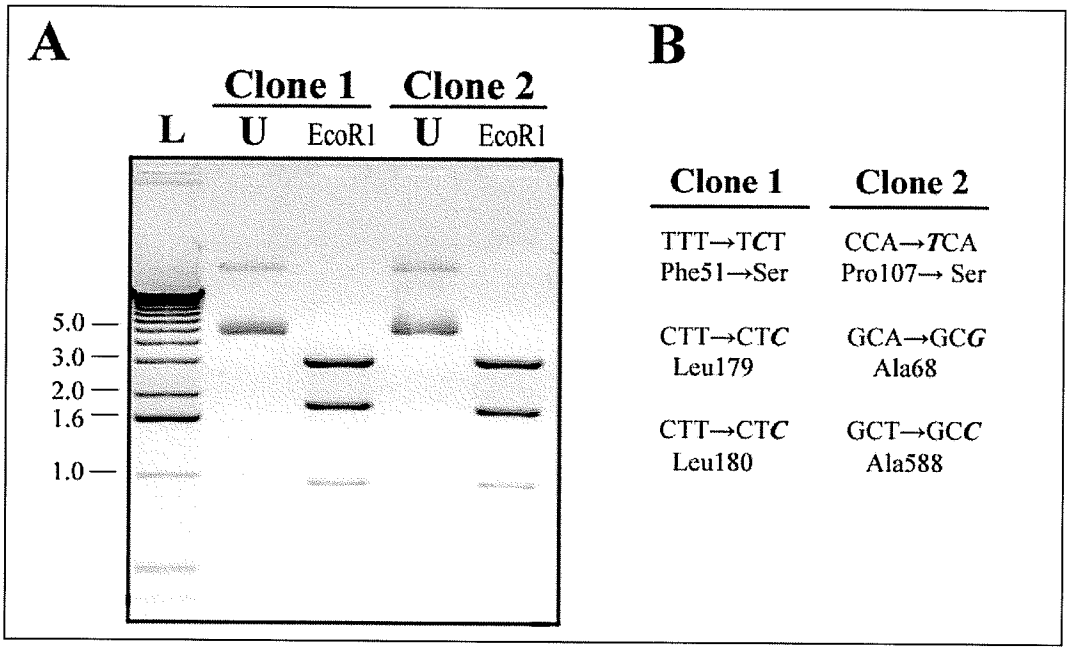

Figure 6: Diagnostic EcoR1 restriction digest of putative pGEM T-easy:hGCP3 ligation clones. **(A)** Putative pGEM T-easy:hGCP3 contain two EcoR1 sites generating three fragments: 3kb, 1.9kb and 0.9kb. **(B)** Sequencing two clones with the desired EcoR1 restriction pattern revealed they each contained a single missense mutation and two silent mutations. Wild-type codons/amino acids are shown on the left, and on the right in bold and italic are the specific mutated nucleotides and resulting amino acid. (L, DNA ladder; U, uncut)

1.2. pcc002 (pcDNA4.0His/MaxA-hGCP3*)

To generate a mammalian expression vector that expresses an N-terminal epitope tagged hGCP3, hGCP3* insert from pcc001 was ligated into pcDNA4His/Max utilizing compatible Not 1 sites. Interestingly, pcc001 did not have the extra deoxythymidine (used for cloning PCR products into pGEM) incorporated 5' of the hGCP3* reading frame. In order to maintain the reading frame, pcDNA4HisMax-A (hereafter referred to

as pcDNA4) was used to subclone the hGCP3* cassette from pcc001 utilizing compatible Not1 restriction sites.

Two out of ten Amp resistant colonies selected contained the hGCP3* insert by PCR analysis (Figure 7A, clones 2 & 5) and by diagnostic Not1 restriction digest (Figure 7B). Orientation of insertion was assessed by diagnostic BamH1 restriction. In the proper orientation, two BamH1 sites, one within the hGCP3* insert and one within the pcDNA4 multicloning site (MCS), are separated by only 140bp; in contrast, the reverse orientation would place the BamH1 sites 2.7kb apart. Therefore in the proper orientation, BamH1 digest produces a 8kb and a 140bp fragment, while the inverse produces a 2.7kb and a 5.3 kb fragments.

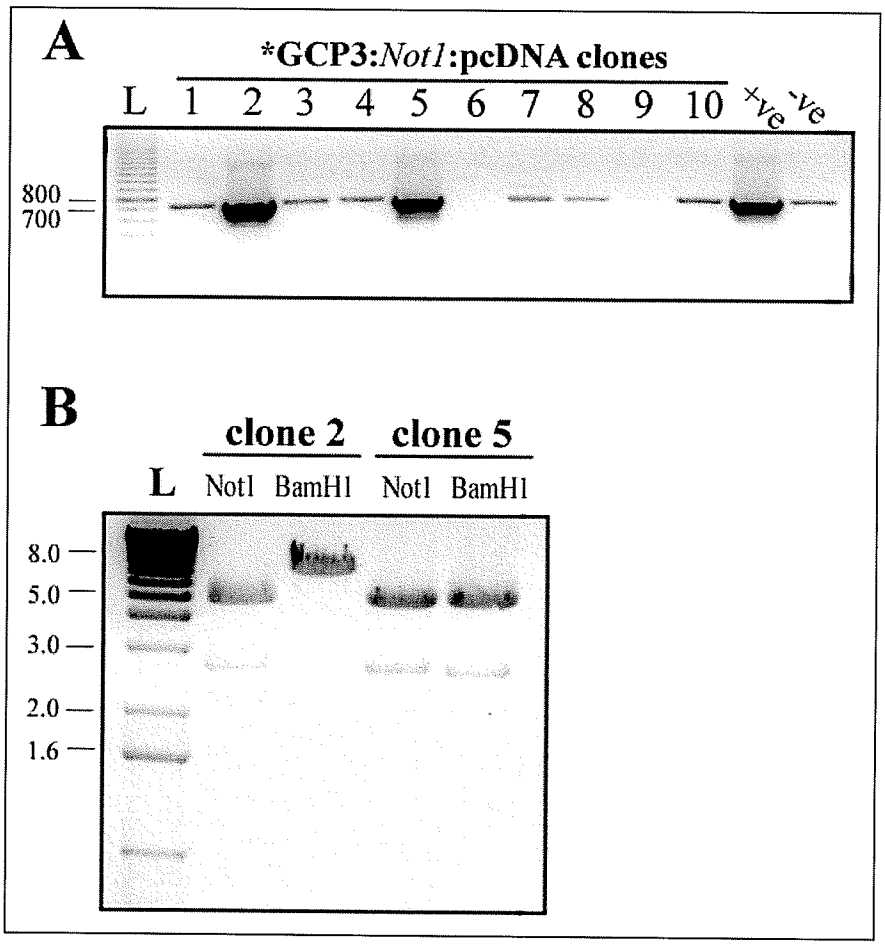

Figure 7: Subcloning the hGCP3* insert from pcc001 into pcDNA4.0HisMaxA using compatible Not1 sites to generate pcc002. **(A)** A rapid PCR screen using GCP3-U/L-Quant primers revealed that two out of ten Amp resistant colonies (clones 2 & 5) contained the hGCP3* insert. pcc001 was used as a positive PCR control (+ ve), while non transformed DH5α was used s a negative PCR control (-ve). **(B)** Not1 restriction digest further confirmed that both clone 2 and 5 contained the hGCP3* insert by the presence of two fragments at 2792bp (hGCP3*) and 5282bp (pcDNA4). However only in clone 2 was the insert placed in the proper orientation as determined by diagnostic BamH1 restriction. In the proper orientation, BamH1 digest produces a 8kb and a 140bp fragment, while the inverse produces a 2.7kb and a 5.3 kb fragments.

1.3. Site-Directed-Mutagenesis (SDM) to Generate pcc003

The 'Transformer site-directed-mutagenesis' kit (Clontech) was used to reverse the single missense mutation at Phe51 in pcc002. The basic principle is to use two primers, designed to simultaneously anneal to one strand of a denatured double-stranded template. One primer introduces the desired mutation while the other mutates a unique restriction site within the vector sequence and serves as the basis for selection of mutated templates. By eliminating this restriction site completely, mutated templates cannot be digested and therefore transform E. coli more efficiently than the linear DNA with no mutations.

The following primers were designed for this purpose: GCP3-REV-MUT and APA1-MUT (Table 4). For clarity, pcc002 will refer to the construct containing the Phe51Ser mutation, pcc002* will refer to site-directed-mutagenized pcc002 products, while confirmed reverse mutated (i.e. wild type) hGCP3 construct is pcc003.

Products from the final mutagenesis step, containing both parental pcc002 and mutated pcc002*, were ApaI restricted before electroporation into DH5α. Transformed colonies able to grow on Amp plates were screened by diagnostic BamH1/ApaI co-restriction. BamHI and ApaI each cut pcc002 once and generate two fragments, 5kb and 3kb. After SDM, 100% of clones analysed had a mutated ApaI site indicated by the presence of a single 8kb band (Figure 8A, top panel). To determine if the mutation present at Phe51 in pcc002 was reverse-mutated, a diagnostic ApoI restriction was performed. Conveniently, the mutation at Phe51 disrupts a ApoI site. By reversing this mutation, the ApoI site is restored making it is possible to distinguish between hGCP3 and hGCP3* via the

presence of a 900bp band. It was found that 100% of the Apa1 mutated pcc002* clones had the 900kb fragment, indicating 100% efficiency in reversing the mutation at Phe51 (Figure 8A, bottom panel). Sequencing of clone 5 confirmed that the hGCP3 sequence within this construct was mutation free and was therefore named pcc003.

To determine if pcc003 specifically expresses a protein with the predicted molecular weight (MW) of His-HGCP3 (MW 109.8kD), both *in vitro* transcribed and translated (TNT), and *in vivo* transient transfection studies were performed. ^{35}S-methionine-labelled-products from *in vitro* TNT'ed pcc003 were resolved by Sodium dodecyl sulphate- polyacrilamide gel electrophoresis (SDS-PAGE) and detected by autoradiography (Figure 8B). A major band corresponding to the largest in vitro TNT product was found to migrate at ~ 110kd. Transient transfection of Cos1 cells with increasing amounts of pcc003 followed by western blot analysis with anti-His antibodies revealed that the expression of a ~110kd His-tagged protein was specific to pcc003 transfection (Figure 8B). A non specific band migrating faster than His-hGCP3 was always detected with the anti-His antibody irrespective of transfection and serves as an internal loading control for subsequent experiments (Figure 8B).

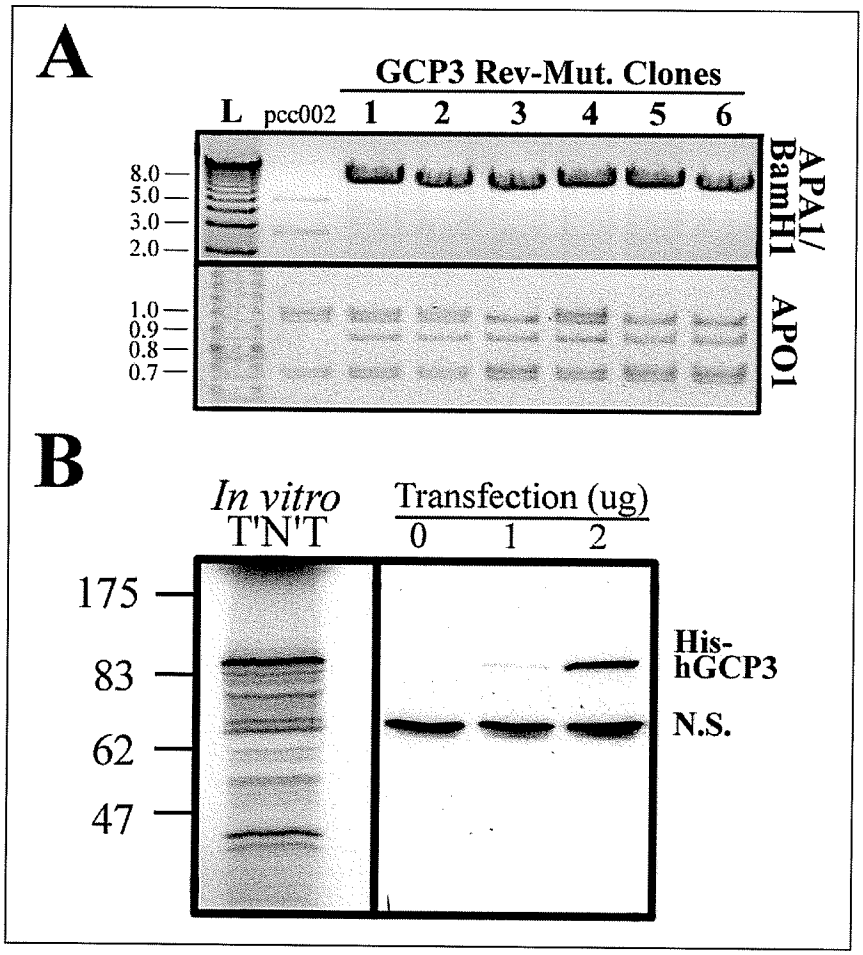

Figure 8: 'Transformer SDM' kit (Roche) results is 100% efficiency in reversing the missense mutation at Phe51, and pc003 (clone 5) expresses a protein of the desired size. **(A)** Diagnostic Apa1/BamHI co-restriction reveals that the unique Apa1 site, used to co-select for desired introduced mutation, is mutated in all clones analysed (Top panel) Conveniently, the mutation at Phe51 disrupts a Apo1 site. By reversing this mutation, the Apo1 site is restored making it is possible to distinguish between hGCP3 and hGCP3* via the presence of a 900bp band. All clones analysed have the desired 900bp band (lower panel). pcc002 is used as a negative control showing two bands for the Apa1/BamHI restriction, and the lack of the 900bp fragment for the Apo1 digest. **(B)** pcc003 encodes a protein with the predicted MW of His-hGCP3 (~110kD) by *in vitro* TNT that is specifically detected by western analysis with anti-His antibodies. (N.S., non-specific)

1.4. pcc005 (pTreHygro-His-hGCP3)

His-tagged hGCP3 from pcc003 was subcloned into a tetracycline inducible expression vector pTre2-Hyg (Promega) using a similar approach previously described for the subcloning of hGCP3*. In contrast however, a blunt end ligation was performed utilizing a unique EcoRV site within pTRE2-hyg multi-cloning-site, and PmeI sites that flank histidine-tagged hGCP3 sequence in pcc003. A total of 10 transformed colonies grew on 25 Amp plates. In order to distinguish the desired construct from possible ligation contaminants, pcc003 and pTre2-Hyg, a diagnostic EcoRI digest was performed. One out of ten Amp resistant colonies had the desired EcoR1 restriction pattern (Figure 9A). Further diagnostic restrictions (Figure 9B) and sequencing confirmed that clone 9 was in fact pTre2-Hyg-His-hGCP3 (hereafter referred to as pcc005).

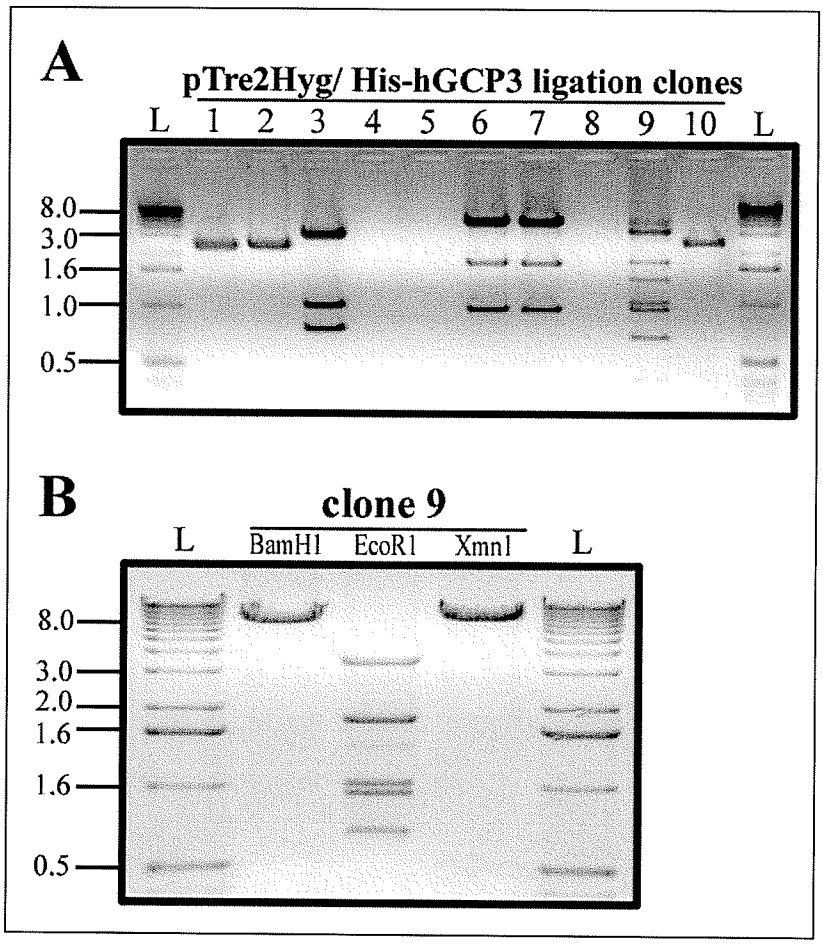

Figure 9. Generating an inducible His-hGCP3 expression construct (pcc005) by subcloning His-hGCP3 cassette from pcc003 into pTRE2Hyg. **(A)** Diagnostic EcoRI digest distinguishes pcc005 (clone 9), from blunt-end ligation contaminants, pcc003 (clone 3), pTre2-Hyg (clone 6, 7), and other AmpR clones. **(B)** Further diagnostic restriction cuts (BamH1 and Xmn1) confirm clone 9 is in fact pcc005 (pTRE2Hyg-His-hGCP3).

2. Characterizing His-hGCP3

It is critical that the histidine-epitope tag and extra N-terminal sequence does not interfere with the recombinant His-hGCP3 ability to function like endogenous hGCP3 otherwise, any results obtained from subsequent experiments with psoriasin may not be biologically accurate. This was tested in two ways: first, co-immunoprecipitation (co-IP) assays were performed to determine if His-hGCP3 retains the ability to interact with γ-tubulin, as is reported in the literature for its endogenous counterpart (Murphy SM et al., 1998; Tassin AM et al., 1998). Co-immunoprecipitation (co-IP) assays were performed based on published procedures used in the original characterization of hGCP3 (Murphy SM et al., 1998; Tassin AM et al., 1998) Second, immunofluorescent (IF) microscopy was used to determine the cellular localization of His-hGCP3 in transiently transfected cells and whether it co-localizes with gamma-tubulin associated with the centrosome as reported in the literature for endogenous hGCP3.

2.1. Co-IP with γ-tubulin

Whole-cell lysates from Cos1 cells that were transiently transfected with either His-HGCP3 or empty vector ((pcDNA4His/Max, Invitrogen), were immunoprecipitated with either Anti-His (Invitrogen), Anti-γ-tubulin (Sigma), or control IgG antibodies. Western analysis with anti-His antibody detected His-HGCP3 in γ-tubulin immunoprecipitates from cells transfected with His-hGCP3 (Figure 1A, Lanes 3-4) but not empty vector (Figure 10A, Lane 1). Control antibody immunoprecipitates (Figure 10A, Lane 2) did not contain His-HGCP3 inferring specificity of γ-tubulin antibody. All immunoprecipitates

were clean as indicated by the absence of the non-specific band present in input lanes (Figure 10A, lanes 5-8). Conversely, western analysis with anti-γ-Tubulin antibody detected γ-tubulin in anti-His-immunoprecipitates (Figure 10B, Lane 2) from cells transfected with His-hGCP3. Although a band corresponding to γ-tubulin is detected in the control-antibody-IP lane (Figure 10B, Lane 1), it is significantly weaker than Anti-His-IP and input lanes (Figure 10B, Lane 3-4).

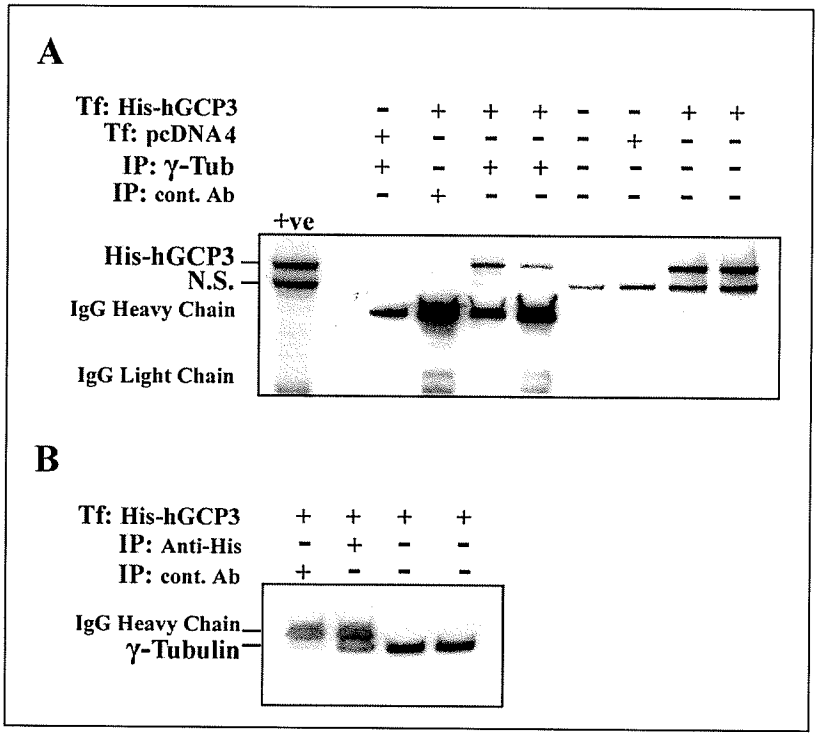

Figure 10: N-terminal Histidine tag does not interfere with His-hGCP3's γ-Tubulin interacting properties in transiently transfected Cos1 cells. **(A)** γ-tubulin immunoprecipitates contain His-hGCP3, while control IP'ed, and mock transfected (pcDNA4) do not (see text for details). **(B)** Conversely, γ-tubulin is detected in anti-His immunoprecipitates in His-hGCP3 transfected cells. (Tf, transfected; pcDNA4, pcDNA4His/Max; γ-tub, γ-tubulin; cont. Ab, control antibody; N.S., non specific

2.2. Immunofluorescent Localization of His-hGCP3

Anti-His antibody specifically detects His-hGCP3 in transiently transfected Cos1 cells by IF microscopy. No signal is detected in primary antibody omission controls (data not shown) or mock transfected Cos1 cells (Figure 11, 1stcolumn). Moreover, not every Cos1 cell in pcc003 transfected dishes show a cy3 signal which is consistent with transfection efficiencies that are typically much less than 100%. (Figure 11, 2ndcolumn). However, His-hGCP3 did not display the expected γ-tubulin IF signal pattern showing punctate foci at centrosomes with diffuse cytoplasmic localization, and decoration of spindle microtubules in mitotic cells (Figure 11, 3rdcolumn). Rather, signal in pcc003 transfected cells was located in the cytoplasm, often in a honey-comb, reticulated pattern, or presented itself as an intense glowing orb in what appeared to be apoptotic cells (Figure 11, 2ndcolumn). The latter likely reflects a decrease in cell volume, serving in effect, to concentrate His-hGCP3 thereby intensifying the signal. Nevertheless the accumulation of overexpressed His-hGCP3 in the cytoplasm may be analogous to that observed when γ-tubulin is overexpressed in mammalian cells (Shu HB et al., 1995). In addition, robust His-hGCP3 signal was never observed in mitotic cells despite extensive scanning of slides.

It is important to note that specific His-hGCP3/ γ-tubulin co-localization experiments were never preformed in Cos1 cells. At the time it was believed that indirect-IF signal obtained with anti-γ-Tubulin antibody (GTU88) in Cos1 cells was an experimental artefact despite using several published experimental conditions (Dictenberg JB et al., 1998; Murphy SM et al., 1998). In contrast to the expected signal, as observed in MCF7

(Figure 11, 3rd column), γ-tubulin signal in non-transfected Cos1 and HeLa cells presented a reticulated filamentous appearance, reminiscent of the microtubule skeleton (Figure 12A). However, the lack of mitotic spindle structures in cells presenting mitotic DNA morphology clearly indicates the γ-tubulin antibody was not immunolablelling MTs (Figure 12A). Although γ-tubulin is generally centrosomal, two reports have shown that γ-tubulin can form tubules having biochemical properties distinct from microtubules (Shu HB et al., 1995) (Figure 12C, top panel), and can form reticulated cytoplasmic structures (Chen D et al., 2001) (Figure 12C, bottom panel). It is interesting to note that in the current study, γ-tubulin structures were only observed in cell lines having two bands detected by western blot analysis with anti-γ-tubulin antibody (Figure 12B).

These results indicate that His-hGCP3 does retain specific biochemical properties associated with it's endogenous counterpart, namely the ability to physically interact with γ-tubulin. Presumably a portion of cytoplasmic His-hGCP3 observed by IF microscopy localizes with endogenous γ-tubulin based on their ability to co-immunoprecipitate. In vertebrate somatic cells, 80% of the γ-tubulin is present in the cytoplasm and is not bound to the centrosome (Khodjakov A et al., 1999; Moudjou M et al., 1996). However, without clear IF co-localization of cytoplasmic His-hGCP3 and endogenous γ-tubulin, these results do not preclude the possibility that both proteins are, for the most part, residing independently in the cytoplasm. It is not clear at present whether the honey-comb structures represent His-hGCP3 exclusion from cellular vacuoles, or an association with another cytoplasmic structure such as the Golgi (Rios RM et al., 2004). Alternatively,

His-hGCP3 IF signal may reflect an association with γ-tubulin in cell lines presenting a non-classical γ-tubulin localization.

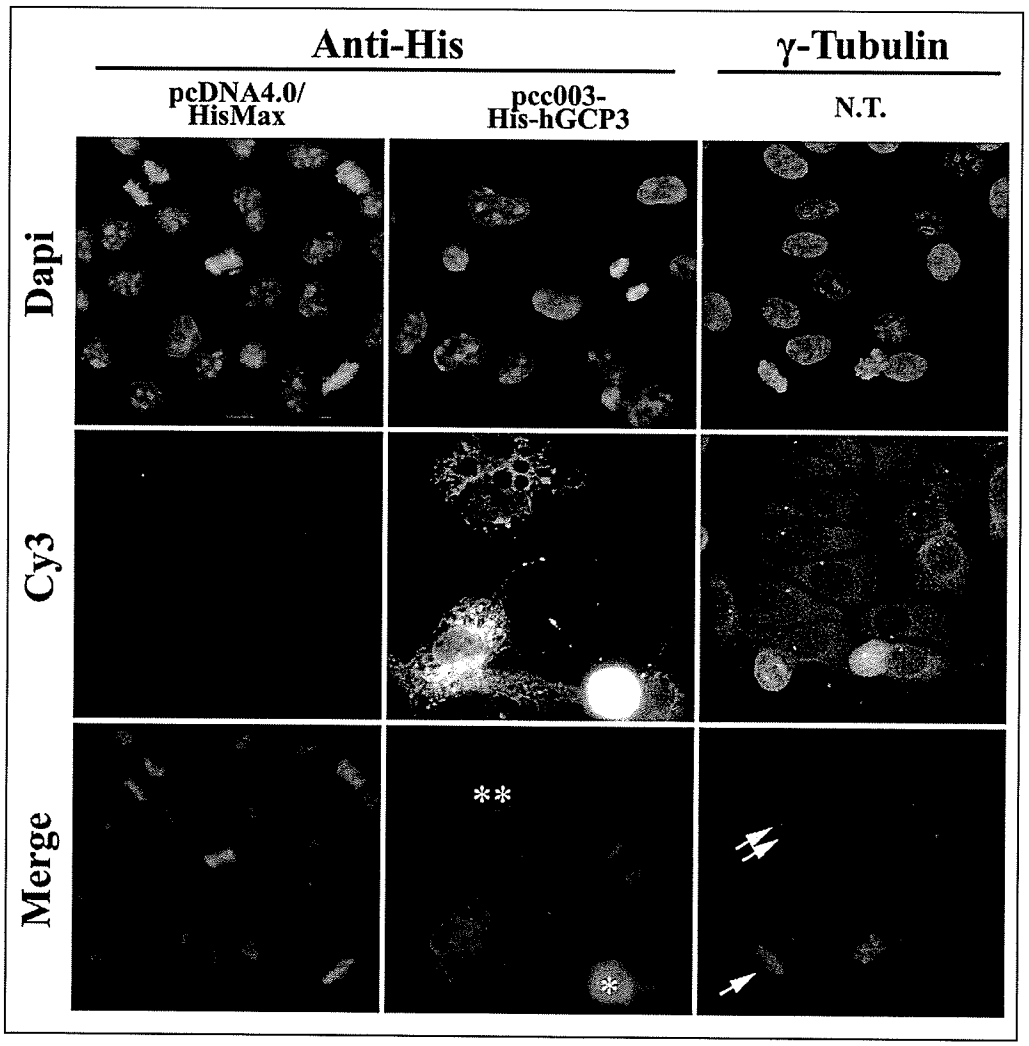

Figure 11: Anti-His antibody specifically detects His-hGCP3 in transiently transfected Cos1 cells by indirect-IF microscopy, but not with the expected γ-tubulin IF signal pattern. No signal is detected in primary antibody omission controls (data not shown) or mock transfected (pcDNA4His/Max) Cos1 cell. In MCF7, γ-tubulin IF signal pattern is present as punctate foci at the centrosome with diffuse cytoplasmic localization (double arrow), and decoration of spindle microtubules in mitotic cells (single arrow). In contrast, His-hGCP3 in Cos1 cells was located in the cytoplasm, often in a honey-comb pattern (**), or presented itself as an intense glowing orb in what appeared to be apoptotic cells (*).

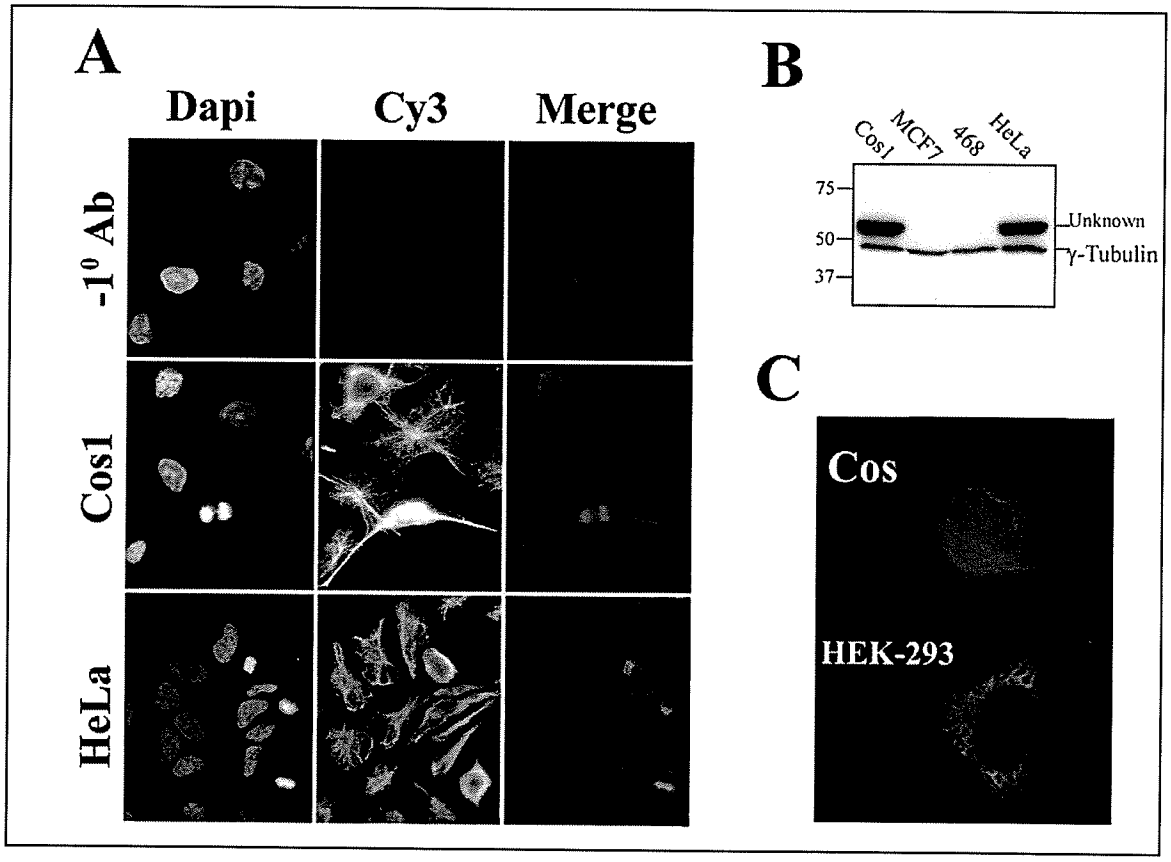

Figure 12: Indirect-IF with Anti-γ-tubulin antibody (GTU88) reveals atypical γ-tubulin localization in Cos1 and Hela cells, and corresponds to the expression of an unidentified protein. **(A)** The filamentous, reticulated structures detected by indirect-IF microscopy in Cos1 and Hela cells is specific to the anti-γ-tubulin antibody as no signal is detected in primary antibody omission controls.**(B)**Western analysis with GTU88 reveals the presence of two bands in cell lines with atypical γ-tubulin localization (Cos1 and Hela), while a single band corresponding to γ-tubulin (48kD) is found in MDA-MB-468, and MCF7; the latter cell line presents typical γ-tubulin localization (Figure 10, 3rdcolumn). **(C)** Examples of similar γ-tubulin structures reported in the literature for Cos cells (Shu HB et al., 1995) and HEK-293(Chen D et al., 2001).

3. Generating His-hGCP3 expressing MCF7 models

The purpose of generating a His-hGCP3 expression model is two fold; first, to determine what effect hGCP3 overexpression has on centrosomal ability to organise the microtubule cytoskeleton; and secondly, to determine whether hGCP3 overexpression influences cellular properties that are compatible with those attributable to psoriasin overexpression and associated with cancer progression.

3.1. Generating a constitutively expressing His-hGCP3 MCF7 line

A standard protocol was used to generate a stable His-hGCP3 model. This protocol has been employed successfully in the past to generate other stable transfection models in the lab (Emberley ED et al., 2003a). MCF7 cells were transfected with pcc003, followed by Zeocin (450ug/mL) selection 24hrs later. Of 14 zeocin resistant MCF7 clones, not a single clone expressed His-HGCP3 as indicated by the lone presence of the non-specific (N.S.) band (Figure 13). Despite loading 100ug of protein from total cell lysates in multiple western analyses, and overexposing the film (data not shown), it was never possible to detect even a faint band corresponding to His-hGCP3.

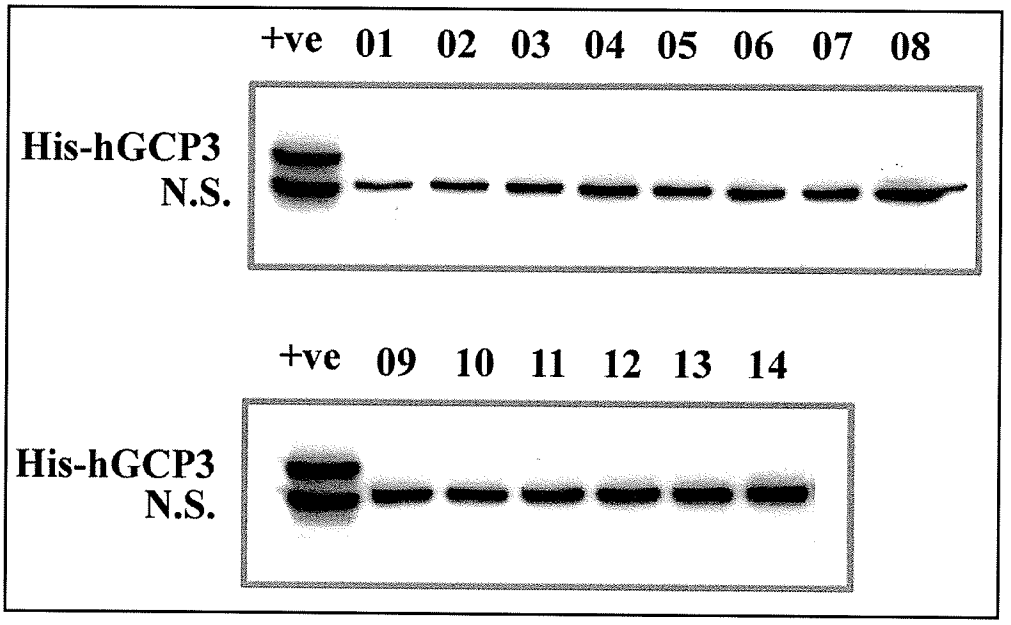

Figure 13: Western analysis of 14 Zeocin resistant MCF7 clones for His-HGCP3 expression reveals only the presence of the non-specific (N.S.) band in all clones. Cos-1 transiently transfected with pcc003 was used as a positive His-hGCP3 control (+ve).

3.2. Generating an inducible expressing His-hGCP3 MCF7 line

MCF7-89 cells were cultured in 'TET-approved' FBS (Hyclone) prior to transfection with pcc005. A total of 73 hygromycin resistant clones, representing a range of fast, medium and slow growing colonies, were successfully transferred to the 96 well format. Unfortunately, bacterial contamination diminished the total number of clones so that only twenty-two clones made it contamination-free to the T25 flask stage. Forty-eight hours prior to harvesting clones for western analysis, doxycycline (1ug/mL) was added to the culture media to induce trans-gene expression. Unfortunately, western analysis with anti-His antibodies failed to reveal inducible His-hGCP3 expression in any of the MCF7-89 clones analysed (Figure 14).

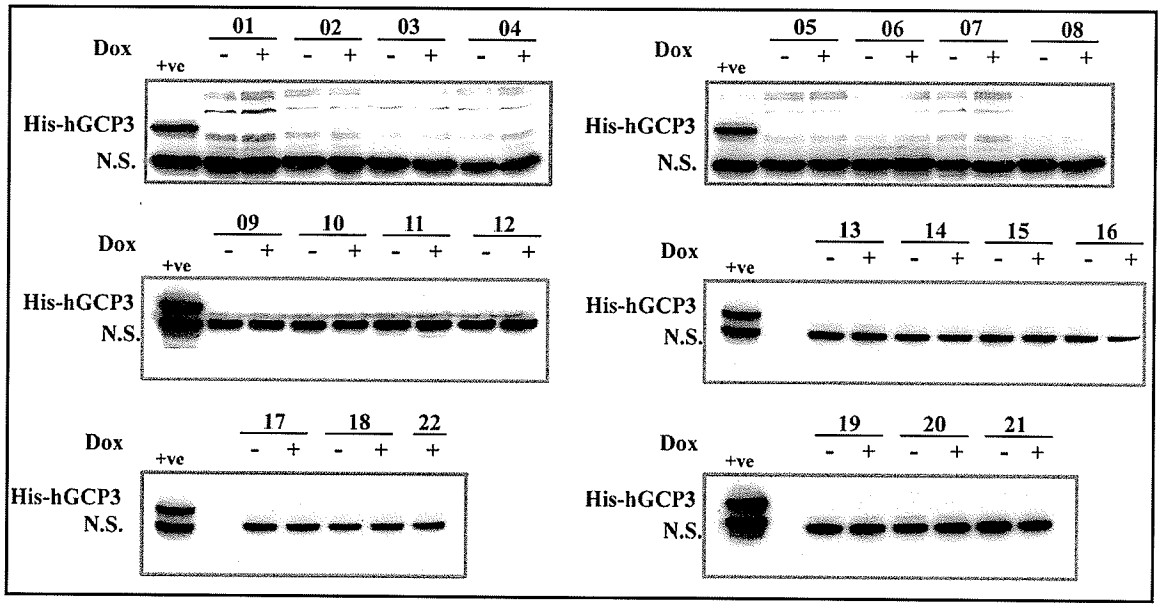

Figure 14: Western Blot analysis of potential MCF7-89 inducible His-hGCP3 clones. Forty-eight hours prior to harvesting clones for western analysis, doxycycline (1μg/mL) was added to the culture media to induce trans-gene expression. Western blot analysis with anti-His antibodies failed to reveal inducible His-hGCP3 expression in any of the MCF7-89 clones analysed despite culturing cells in "Tet-free" media to minimize superfluous His-hGCP3 expression. Cos-1 transiently transfected with pcc003 was used as a positive His-hGCP3 control (+ve).

4. His-hGCP3 Overexpression and Cell Viability

Overexpression of other GCPs has been shown to be toxic in a variety of cells (Fava F et al., 1999; Geissler S et al., 1996; Murphy SM et al., 1998). This raised the concern that overexpression of His-hGCP3 may prove to have the same effect in our cells considering hGCP3s indispensable role within the γ-TuRC. To assess the effect of His-hGCP3 overexpression in mammalian cells, Cos1 cells were transiently transfected with either His-hGCP3 or empty vector (pcDNA4His/Max, Invitrogen). Levels of His-hGCP3

expression were monitored by western blot analysis, and cellular toxicity was inferred by morphological assessment of cells by phase contrast microscopy.

Phase contrast microscopy 24hr post-transfection revealed that overall Cos1 cell populations transfected with His-hGCP3 were less confluent than control plates, and cells adjacent to 'clearings' presented an emaciated, spindly morphology (Figure 15A). In contrast, control cells transfected with the empty vector appeared significantly healthier and were confluent 24h after transfection with cuboidal cell morphology, likely reflecting compressed confluent cell environment (Figure 15A). It was observed, by focussing through the media, that His-hGCP3 transfected plates contained noticeably more floating cells than control transfected plates. Western analysis of the adherent portion of cells with anti-His antibody revealed a robust His-GCP3 signal 24h post transfection in His-hGCP3 transfected cells but not in mock transfected samples (Figure 15B). A significant reduction in His-GCP3 expression is observed 72h post-transfection with no change in the non-specific band intensity.

Taken together these results suggest that robust overexpression of His-hGCP3 is likely to have immediate toxic effects. However, persistent expression of His-hGCP3 72h after transfection suggests that a large portion of transfected cells remain in the adherent population indicating that His-hGP3 expression (likely at modest levels) is not immediately lethal.

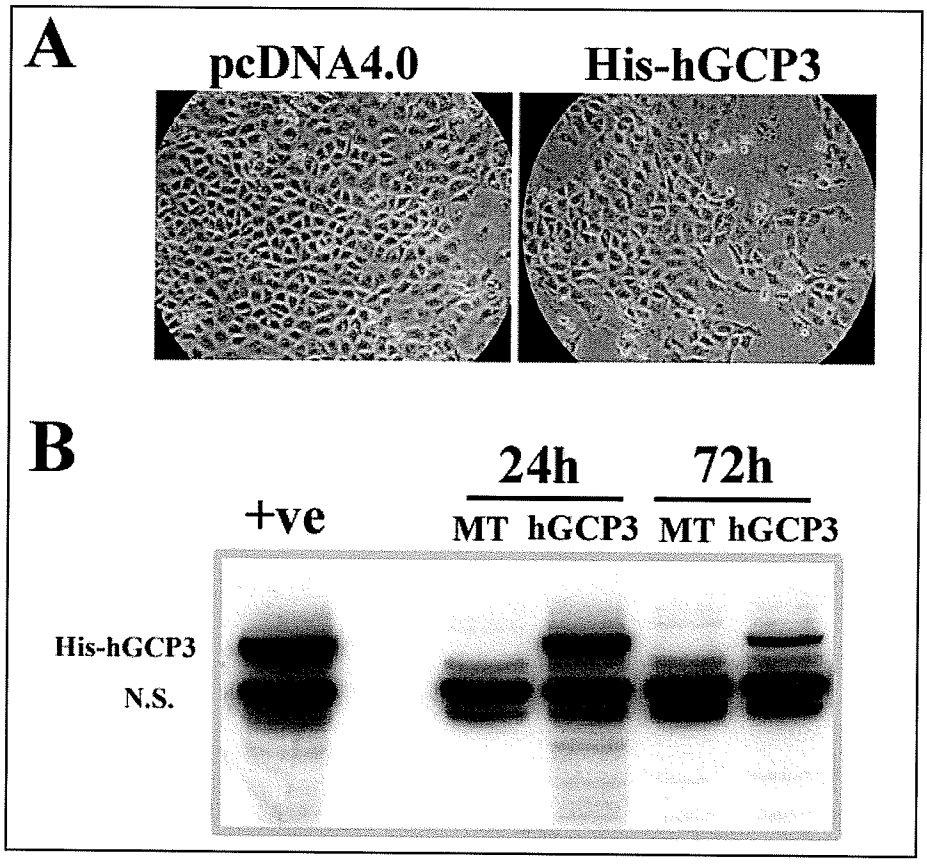

Figure 15: Robust His-hGCP3 expression has immediate cytotoxic effects, but significant portions of cells with modest expression persist in the population 72 hours post-transfection. **(A)** Representative phase contrast images (400X) of Cos1 cells 24 hours post transfection, showing clear signs of toxicity associated with His-hGCP3 expression. **(B)** Representative western blot showing reduction, but persistent His-hGCP3 expression 72 hours post transfection. (MT, mock transfection; h, hours; N.S., non specific

5. Biochemical interaction His-hGCP3 & psoriasin

Results from the yeast two hybrid screen suggested that an interaction between hGCP3 and psoriasin can occur within that experimental context. To assess the merits of an interaction in mammalian cells, two complementary experimental approaches were attempted to achieve this end. First, co-immunoprecipitation analysis on transiently transfected Cos1 cells was performed to determine if a physical interaction between His-

hGCP3 and psoriasin can exist. Secondly, IF co-localization was attempted to determine if His-hGCP3 and psoriasin are in physical proximity to each other within a cell in order for an interaction to be biologically relevant.

5.1. Co-immunoprecipitation with Psoriasin

The central hypothesis of this study is that an interaction between psoriasin and hGCP3 is biologically relevant to breast cancer. It follows an interaction should ideally be demonstrated in a breast cancer cell line. Unfortunately, transfecting pcc003 into epithelial breast cancer cell lines that endogenously express psoriasin (MDA-MB-468) or have been established to constitutively express psoriasin (MDA-MB-231), was exceedingly inefficient. As such, it was decided that co-transfection of Cos1 cells with pcc003 as well as a construct expressing psoriasin (pcDNA3.1-psor) was an adequate alternative. Equal volumes of co-transfected Cos1 cell lysates were immunoprecipitated with either Anti-His or control mouse monoclonal IgG antibodies followed by western analysis with an anti-psoriasin antibody. Despite using several different transfection and IP conditions, reported to preserve other known protein-interactions with either psoriasin or hGCP3, it was not possible to consistently detect psoriasin in anti-His immunoprecipitates. In one experiment, faint bands corresponding to psoriasin were detected in the immunoprecipitates of Cos1 cells co-transfected with either equal molar (Figure 16A, Lane3) or equal ug (Figure 16, Lane 5) amounts of plasmid DNA, but not in the immunoprecipitate of an unrelated mmIgG antibody (Figure 16A, Lane 2). In repeated experiment however, this observation could not be reproduced (Figure 16B, Lane 5-6), even upon robust co-expression of psoriasin and His-hGCP3 (Figure 16B,

Lane 1-3). However, having failed to consistently reproduce a positive interaction by co-immunoprecipitation, it must be concluded that psoriasin and His-hGCP3 do not interact under experimental conditions used here.

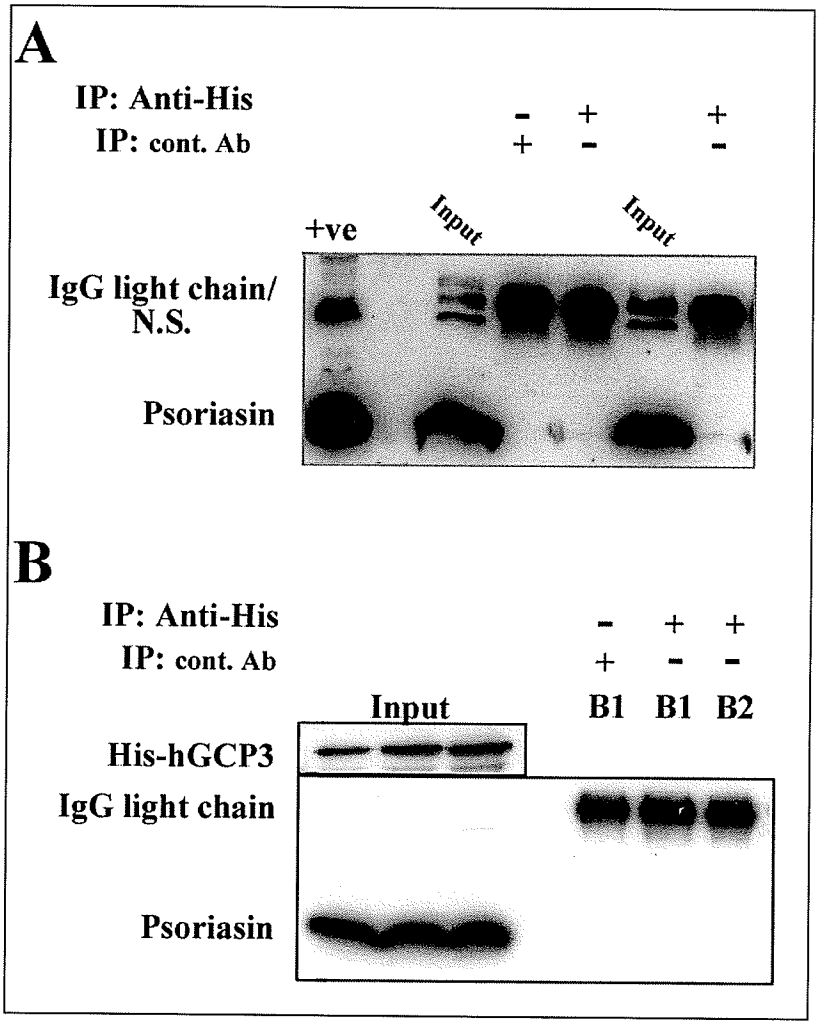

Figure 16: Representative Co-IPs showing (A) positive Psoriasin/ His-hGCP3 interaction and (B) negative Psoriasin/ His-hGCP3 interaction. **(A)** In one experiment, psoriasin was detected in His-hGCP3 immunoprecipitates of Cos1 cells co-transfected with either equal molar (Lane3) or equal ug (Lane 5) of His-hGCP3 and pcDNA3.1-psor plasmids. **(B)** In other cases despite robust His-hGCP3 and psoriasin expression His-hGCP3 immunoprecipitates did not contain psoriasin (Lane 5-6). (IP, immunoprecipitating antibody; B1, co-IP buffer 1; B2, co-IP buffer 2)

5.2. Immunofluorescent Localization of Psoriasin

First it was necessary to determine if available anti-psoriasin antibodies would be suitable for indirect immunofluorescence. Cold methanol fixation is a preferred method of fixation when microtubule and centrosome structures are visualized by IF microscopy as it is rapid and provides excellent structure preservation. This method is typically used when visualizing centrosomal localized proteins including γ-tubulin and pericentrin. Therefore, to determine if psoriasin and hGCP3 co-localize, IF staining and microscopy on cold methanol fixed cells was used. To test antibody specificity, two psoriasin-overexpressing cell models were used from Hela and MB-MDA-231 cell origin that were previously engineered in our lab (see Table 2). Two anti-Psoriasin antibodies were tested for their ability to specifically label psoriasin for indirect-IF under a variety of conditions. The first antibody a rabbit-polyclonal (RP) antibody that recognizes a 14-amino acid peptide corresponding to carboxy-terminus of psoriasin (KQSHGAAPCSGGSQ) was previously developed and characterized in our lab (Emberley ED et al., 2003b) (Figure 17A). The second antibody tested is a commercially available mouse monoclonal (MM) IgG raised against full-length psoriasin (AbCam) (Figure 17B). Psoriasin expression was monitored by western analysis showing no psoriasin expression in Hela.12 or 231-1A1s, but robust expression in Hela.16 and 231-Fa3. In addition, many non-specific bands are detected by western analysis with RP anti-psoriasin antibody, while a single band, corresponding to psoriasin, is detected with the MM antibody.

Unfortunately, neither anti-psoriasin antibody tested showed psoriasin-specificity as detected by indirect-IF labeling. Both the intensity and cellular distribution of signal

remained the same irrespective of the presence of psoriasin and under a range of experimental conditions used. Tested conditions included: different 1^0 and 2^0 antibody concentration, with or without pre-extraction of soluble proteins before fixation, or with acetone or mild detergent (Triton x100) permeabilisation post fixation (data not shown). The non-specific labeling is attributable to 1^0 antibody, as omission controls reveal no signal for the RP antibody (Figure 17A, top panel) or reduced signal for the MM antibody (Figure 17B, top panel). RP had an overall higher background fluorescent intensity, likely a reflection of the many non-specific bands detected by western analysis. These results indicate that neither antibody is suitable for indirect-IF and as such pose a significant obstacle for co-localization studies.

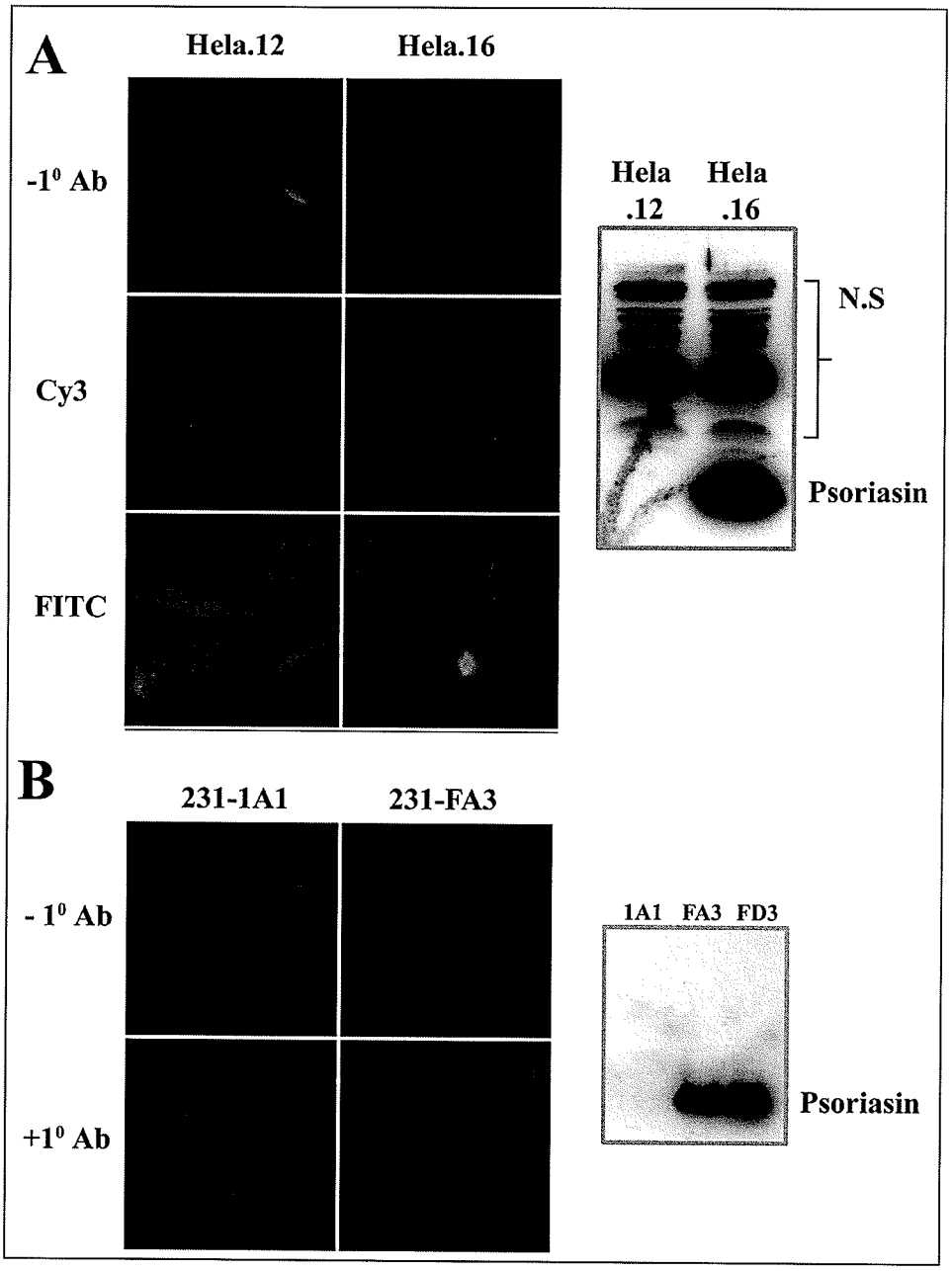

Figure 17: Anti-Psoriasin antibodies tested in this study are not suitable for indirect-IF. Antibodies tested include **(A)** in-lab rabbit-polyclonal antibody and **(B)** commercially available mouse monoclonal antibody (Abcam). For a given antibody, Intensity and cellular distribution of signal remained the same irrespective of the presence of psoriasin (left versus right columns) as monitored by western analysis (Right panels).

6. Assays for γ-TuRC/Centrosomal Function

With the possibility that robust overexpression of His-hGCP3 is cytotoxic, or acts as a dominant negative hGCP3 protein, it was necessary to test for potential biological consequences of psoriasin/hGCP3 interaction using His-hGCP3 independent systems. To date, no specific assay has been developed to measure hGCP3 function directly. In order to determine if psoriasin (over) expression has a biological effect on hGCP3 function, it was rationalized that as an indispensable and intrinsic component of γTuRC, modulation of hGCP3 function would likely affect γTuRC function and therefore translate into altered centrosome function. Evidence for this line of reason comes from studies that show by either mutation or overexpression of specific core GCPs, γTuRC function is altered either by improper localization or decreased activity and phenotypically resulted in spindle defects (Barbosa V et al., 2000; Fava F et al., 1999; Fujita A et al., 2002; Vardy L et al., 2000). Therefore generation of normal bipolar spindle was used as a downstream-biological parameter to correlate psoriasin expression and centrosomal/γTuRC activity. For this, overall mitotic spindle morphology was assessed by IF microscopy and the frequency and type of aberrant spindles were scored. As a second and more direct parameter of centrosomal/γTuRC activity, the capacity to regenerate new microtubule growth from centrosomes stripped of MTs, was additionally measured. This latter assay is known as the MT regrowth assay and the degree of regrowth was quantified using a quantitative IF approach.

6.1. Mitotic Spindle Morphology (MSM)

To determine if aberrant psoriasin expression has a biological effect on mitotic spindle formation, spindle morphology was assessed by IF microscopy in two psoriasin-expressing epithelial breast cancer cell models previously engineered in the lab. Mitotic spindles were visualised in methanol fixed (-20^{0}C) / acetone permeabilised cells using direct IF labelling of β-tubulin with a Cy3-anti-β-tubulin antibody (Sigma). DAPI staining was used to visualise DNA. Spindle defects that were scored included monopolar, multipolar, misaligned and unknown defects (Figure 18A). For this study a psoriasin-inducible MCF7 model (Figure 18B) and a constitutive psoriasin expression MDA-MB-231 model (Figure 18C) were used. Both the frequency and type of aberrant spindles were scored in three separate experiments, in which 100 consecutively viewed metaphase or anaphase spindles were scored per cell line used.

Levels of psoriasin expression were monitored by western analysis with anti-psoriasin antibodies (either a rabbit polyconal or a commercially available mouse monoclonal (Abcam). Shown are representative western blots revealing no psoriasin expression in wild type MCF7, but significant induction of psoriasin expression in the MCF7-MAG clones (Mag06 and Mag07) after 48hr of doxycycline treatment (Figure 18B, Lower Panel). Moreover, no psoriasin expression is detected in wild type MDA-MB-231, or in the 1a1 clone, but robust psoriasin-expression is detected in the Fa3 and Fd3 clones (Figure 18C, Lower Panel).

Analysis of mitotic defects revealed that wild-type MCF7 and derived clones had an overall higher frequency of spindle defects (~30%) (Figure 18B, upper panel) than in the 231s and derived clones (~10%) (Figure 18C, upper panel). In both cell lines however, psoriasin overexpression did not affect the frequency of mitotic spindle defects ($p>0.05$ Anova) or the frequency of specific types of defects analysed ($p>0.05$ Anova). Interestingly, roughly 80% of total spindle defects observed in MCF7 were monopolar spindles; while 231s presented a combination of multi-polar or misaligned spindles. These results suggest that psoriasin expression does not have a biological effect on centrosome function as measured by a mitotic spindle morphology end-point.

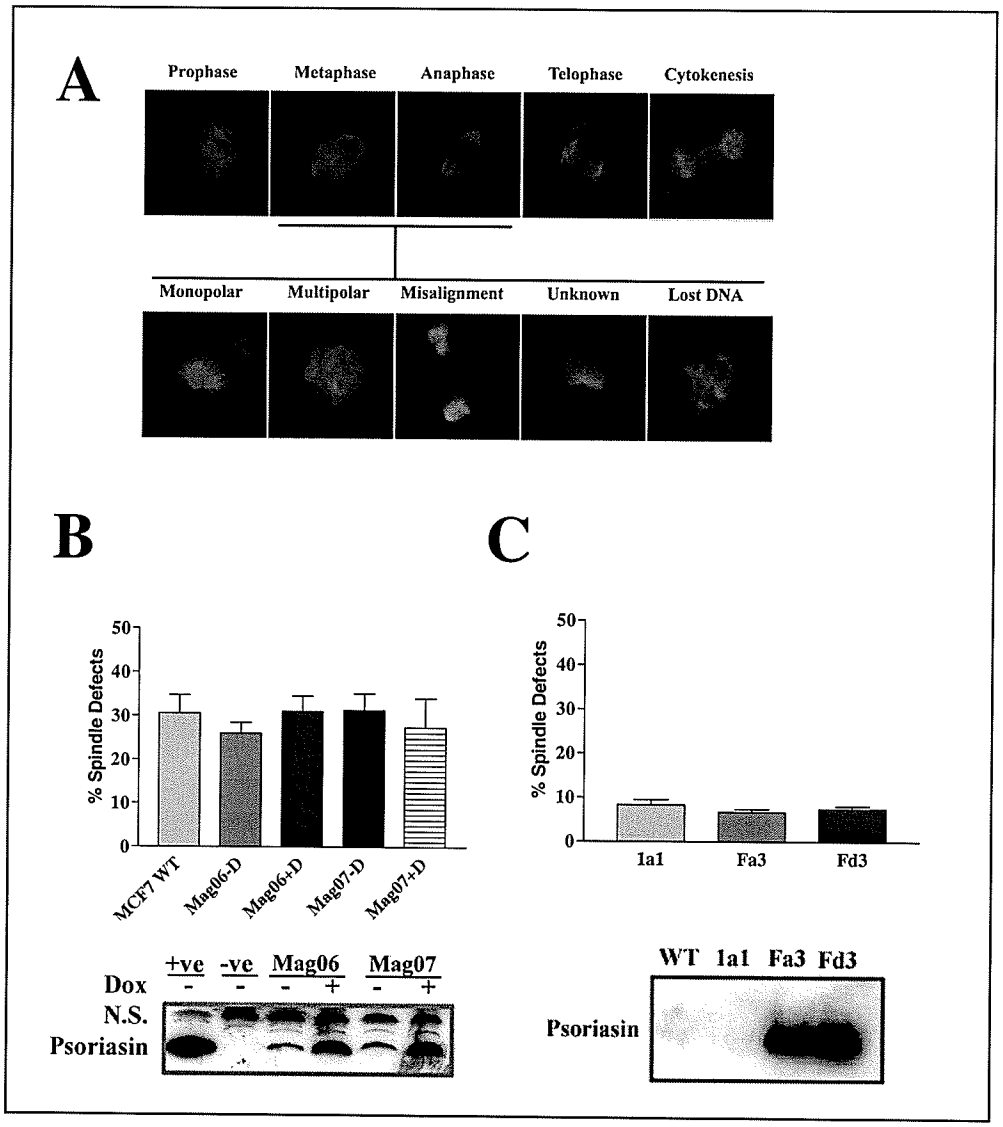

Figure 18: Psoriasin expression does not change the frequency of mitotic spindle defects. **(A)** Mitotic spindle morphology changes throughout mitosis (Top panel) and a range of specific types of spindle defects are observed in metaphase and anaphase cells (Bottom Panel). **(B)** Frequency of spindle defects (~30%) did not change upon psoriasin induction with doxycycline in MCF7-Mag clones as compared to the non-induced ($p>0.05$; N=300) and wild-type MCF7 ($p>0.05$; N=300). **(C)** Same results were obtained with MDA-MB-231 model ($p>0.05$; N=300), however the total frequency of spindle defects observed were significantly lower (~10%). Bars represent the mean +/- S.D. Western blot analysis was used to monitor psoriasin expression (B and C, Lower panel). (D or Dox, doxycycline)

6.2. Microtubule Regrowth Assay

An *in vivo* MT regrowth assay in living cultured cells was used to measure the capacity of mitotic centrosomes to nucleate MT. Briefly, microtubules are depolymerised in living cells with either nocodazole treatment or incubation on ice. Regrowth of microtubules from naked centrosomes takes place in living cells simply by placing the cells into fresh warm media for a set amount of time (typically on the order of minutes) before fixation and IF processing. In this way, the effects of endogenous proteins on MT nucleation can be ascertained *in vivo*.

Therefore, to additionally test if psoriasin has an effect on centrosome function *in vivo*, a MT regrowth assay was performed on three MDA-MB-231 clones (1a1, Fa3, and Fd3) whose psoriasin expression levels are describe above (see Figure 18C). Three independent MT regrowth experiments were performed, in which a total of 60 metaphase or anaphase cells presenting centrosomes with nascent nucleated MTs were quantified per cell line. Only cells in metaphase or anaphase are analysed in order to control for biological variation due to differential nucleation capacity of centrosome at different phases of cell cycle and at different stages of mitosis. It is found that centrosomes in prometaphase to anaphase recruit similar levels of γ-tubulin complexes reflecting a similar capacity to nucleate microtubules (Fava F et al., 1999; Khodjakov A et al., 1999; Lajoie-Mazenc I et al., 1994). If two centrosomes were in focus, the average fluorescent intensity was used for statistical analysis. Figure 19A shows the variation in the degree of MT regrowth observed; some cells have extensive regrowth (Figure 19A Top panels), in contrast to others with minimal regrowth (Figure 19A Top panels). However, there

was no statistically significant difference ($p>0.05$; Anova) in the degree of MT regrowth from centrosomes when psoriasin is present (clones Fa3 and Fd3), or not (1a1) (Figure 19B). These results indicate that psoriasin does not influence centrosome function as defined by the capacity with which a centrosome can nucleate MT.

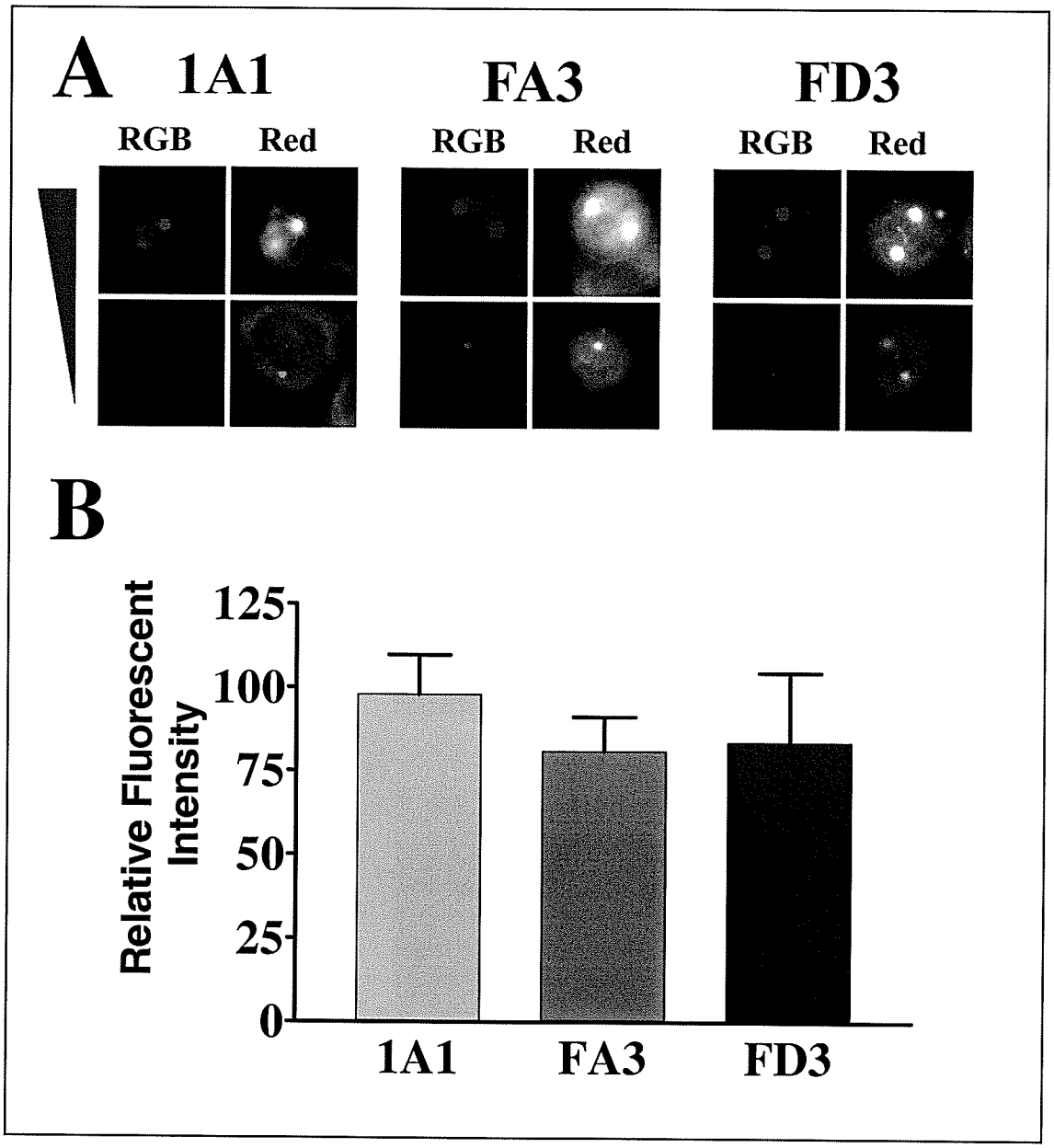

Figure 19: Psoriasin expression does not influence the capacity of centrosomes to nucleate microtubules as measured by a MT regrowth assay in MDA-MB-231 cells. (A) IF images to highlight the observed variability in the degree of MT regrowth, and variability in the intracellular background contributed by unpolymerized tubulin dimers. Top panels show single cells with either one or two centrosomes with extensive MT regrowth, while bottom panels show cells with centrosomes having and minimal regrowth. (B) No statistically significant difference in the degree of MT regrowth is observed in MDA-MB-231 cells when psoriasin is expressed ($p>0.05$, N=60 centrosomes, Anova Dunnetts). Bars represent the Mean +/- S.D. (RGB, red green blue channels; Red, red channel)

7. Summary of Results

- Two mammalian expression vectors were created that express an N-terminal, histidine-tagged hGCP3 (His-hGCP3) recombinant protein; pcc003 (pcDNA4HisMax:hGCP) constitutively expresses His-hGCP3 and is driven by a CMV promoter, while pcc005 (pTRE2Hyg:His-hGCP3) is driven by a minimal Tetracycline responsive promoter and can be induced to express in the presence of doxycycline (Tet-On).

- His-hGCP3 retains the ability to interact with γ-tubulin by co-immunoprecipitation analysis, as is reported in the literature for its endogenous counterpart.

- His-hGCP3 did not display proper cellular distribution/localization by immunofluorescent microscopy that is reported for its endogenous counterpart in transiently transfected cells.

- Indirect-IF with Anti-γ-tubulin antibody (GTU88) reveals atypical γ-tubulin localization in Cos1 and Hela cells, but not in MCF7, and corresponds with the expression of an unidentified protein detected by western analysis with anti-γ-tubulin antibody.

- Efforts to establish an MCF7 cell line which can constitutively overexpress His-hGCP3 (transfected with pcc003), or can be induced to overexpress His-hGCP3 upon treatment with doxycycline (transfected with pcc003) were unsuccessful.

- His-hGCP3 expression likely has immediate cytotoxic effects as assessed by phase contrast microscopy in transiently transfected Cos cells, and His-hGCP3 expression is significantly reduced in the population 72 hours post-transfection.

- His-hGCP3 and psoriasin could not be consistently co-immunoprecipitated indicating they do not interact under the experimental conditions used in this study.

- Anti-psoriasin antibodies tested in this study were not suitable for immunofluorescent localization studies.

- In cultured breast cancer cells, psoriasin had no effect on the frequency or type of mitotic aberrations present (mitotic spindle morphology assay), nor on the capacity of naked centrosomes to regrow microtubules (microtubule regrowth assay).

IV. Discussion

1. Cloning His-hGCP3 Characterizing His-hGCP3

In the initial cloning and characterization of hGCP3, Murphy *et al* created an N-terminal tagged His/ Myc recombinant protein that for all intents and purposes behaved like normal hGCP3; it retained the ability to interact with γ-tubulin, localized with γ-tubulin at the centrosome and was incorporated into endogenous γTuRCs (Murphy SM et al., 1998). We therefore opted to generate our own N-terminal, histidine-tagged hGCP3 (His-hGCP3) construct in order to monitor levels of recombinant hGCP3 overexpression during subsequent experiments.

In all, the final His-hGCP3 mammalian expression vector, pcc003, contained an extra 177 base pairs, encoding 59 extra N-terminal amino acids (see Figure 8). Forty-eight of these amino acids were of pcDNAHisMAx origin and encode for two epitope tags (HisMax and Xpress) in frame with the mutation-free hGCP ORF. The remaining eleven amino acids were accrued during subcloning procedures. Although 59 extra amino acids are substantial, it in fact represents only ~6% of the total hGCP3 protein. It was confirmed that pcc003 expressed a protein of the predicted His-hGCP3 molecular weight (~110kD) by *in vitro* transcription and translation, and could be specifically detected by western analysis with either Anti-His or anti-Xpress (data not shown) antibodies in transiently transfected cells.

Nevertheless, it was paramount to determine that recombinant His-hGCP3 could function like endogenous hGCP3 in order for this construct to be experimentally suitable for subsequent experiments. To this end, co-immunoprecipitation (co-IP) assays confirmed that His-hGCP3 was able to physically interact with endogenous γ-tubulin and therefore retained specific functional properties associated endogenous hGCP3 (see Figure 10).

IF localization data was less clear however, in its support that His-hGCP3 behaves like endogenous hGCP3 (see Figure 11). On one hand, IF localization of His-hGCP in transiently transfected Cos1 cells clearly did not resemble that reported for hGCP3 in the literature; on the other, neither did γ-tubulin. It was expected that signal from both γ-tubulin and His-hGCP3 should localize to centrosomes as punctate foci, with diffuse cytoplasmic localization, and decoration of microtubules in mitotic spindles. Instead, localized His-hGCP3 in transiently transfected Cos1 cells was found in the cytoplasm, often in a distinct honey-comb, reticulated pattern (see Figure 11). It is possible that honey-comb structures simply represent His-hGCP3 exclusion from vacuoles in cells undergoing early stages of apoptosis, or an association with specific cytoplasmic structure such as the Golgi apparatus, as has been reported for γ-tubulin (Rios RM et al., 2004). However, the most compelling explanation for the observed reticulated His-hGCP3 IF-signal pattern is that it indeed reflects an association with γ-tubulin, but as it occurs in cell lines presenting a non-classical γ-tubulin localization, so to is the atypical localization of His-hGCP3. Support for the latter assertion comes from two reports that show γ-tubulin can form tubules (so-called γ-tubules) having distinct biochemical properties than microtubules (Shu HB et al., 1995) and can form reticulated cytoplasmic

structures (Chen D et al., 2001). Although γ-tubulin is generally centrosomal, morphological comparison of the atypical γ-tubulin structures observed in the current study and that reported in the literature for the same cell line (Cos cells) show several distinct similarities (see Figure 12). First, individual filaments can be resolved and appear to form a network that radiates from a central origin. Second, a single focal origin is observed in most interphase Cos cells that is directly adjacent to the nucleus. In contrast, Hela cells often did not present a single focal origin. Rather, a filamentous γ-tubulin network that spanned the entire cytoplasm was observed that was morphologically more similar to that reported in HEK-293 cell (Chen D et al., 2001). Finally, the atypical γ-tubulin structures observed in the current study were distinct from microtubules as inferred by the absence of spindle structures in mitotic cells. This is consistent with the fact that γ-tubules can only be stained by γ-tubulin antibody, but not by α- and β-tubulin antibodies (Shu HB et al., 1995).

Despite these undeniable morphological similarities, it must be emphasised that it is not known at present whether structures observed in the current study are in fact so-called γ-tubules. The main concern is the frequency in which non-transfected Cos or Hela cells presented this 'phenotype,' as it was invariably observed in every cell. In contrast to the literature, γ-tubules were only observed in Cos cells when γ-tubulin was overexpressed, and were never observed in other cell lines (CHO, PtK2, and Hela) under the same conditions (Shu HB et al., 1995). Moreover, only a minority of non-transfected HEK-293 cells presented reticulated γ-tubulin structures (Chen D et al., 2001). It should be noted in

the present study, under the same conditions with the only variable being cell line, MCF7 gave the expected γ-tubulin signal while Hela and Cos cells did not.

Western analysis with anti-γ-tubulin antibodies revealed a second band, in addition to γ-tubulin, in those cell lines specifically presenting atypical γ-tubulin locolisation (see Figure 12). This raises the obvious question as to whether this second band arises from the 'non-specific' detection of a protein that is expressed only in particular cell lines. If this is the case, it cannot be assumed that by using the same anti-γ-tubulin antibody, that the 'non-specific' protein detected by western analysis is the same 'non-specific' protein detected by IF. However given the coincidence of expression and distinct 'cytoskeletal' phenotype, it would be interesting to determine if they are in fact the same protein. More to point of the current study however, this would suggest that His-hGCP3 does not display proper cellular localization and therefore is not behaving like endogenous hGCP3. An alternative explanation is that anti-γ-tubulin antibody is detecting the correct target protein, namely γ-tubulin, in all cases. It is known that γ-tubulin can be post-translationally modified by phosphorylation (Kukharskyy V et al., 2004) or by mono-ubquitination (Hsu LC et al., 2001); (Starita LM et al., 2004). If this is the case, it is interesting to speculate that the γ-tubulin species observed ~52kD is a post-translationally modified γ-tubulin (48kD) that is competent to form these unique γ-tubule structures. To test if structures observed in Cos1 cells are in fact γ-tubules, they should be resistant to conditions known to depolymerise microtubules, such as either cold or nocodazole treatment (Shu HB et al., 1995). If these structures prove to be γ-tubules, this would suggest that they can occur more frequently than previously reported, and possibly

ascribe a novel function to γ-tubulin. This would represent a novel finding that would merit further experimental investigation.

2. Generating His-hGCP3 expressing MCF7 model

MCF7 cells were chosen as a suitable breast cancer model for His-hGCP3 overexpression based on the availability of reverse tetracycline-transacitivator (rtTA) expressing MCF7 clone 89 (MCF7-89) (Venditti M et al., 2002). This allows for the generation of not only a constitutive expressing model in wild type MCF7, but additionally, a doxycycline-inducible model in the MCF7-89. A direct benefit in having both models is the possibility to laterally confirm any results in a separate expression model , thereby ensuring results are strictly not a clonal or expression system phenomenon. Moreover, when establishing constitutively-expressing stable transfectants it is desired to have clones with different levels of transgene expression. However realizing this end it is not always possible and is not experimentally controllable. In contrast, the inducible model is inherently more conducive to experiments in which titratable levels expression are to be correlated with changes in biological function. In the inducible system levels of transgene expression can be modulated simply by varying the concentration of doxycycline. Additionally, an inducible model is better suited for establishing clones in which expression of the protein of interest may have cytotoxic properties. This is achieved simply by culturing cells in Tet-Free conditions to reduce transgene expression.

Nevertheless, our efforts to establish an MCF7 cell line which can overexpress His-hGCP3, or can be induced to overexpress His-hGCP3 were unsuccessful. Arguably the

failure to achieve this end may reflect experimental or technical short-comings. In particular, the total number of clones selected should have been significantly more. However the most probable explanation is that constitutive expression of even low levels of exogenous His-hGCP3 may be lethal. Despite culturing cells in "Tet-free" media to minimize superfluous trans-gene expression, it is likely that some His-hGCP3 was expressed due to uncontrollable promoter leakiness even under these conditions. This is the case observed with other inducible models, namely the psoriasin inducible MCF-89.

Other members in the GCP family have been shown to have "toxic effects" in a variety of cells when overexpressed. In yeast, overexpression of either GCP2 or GCP3 orthologues, Spc97p or Spc98p, is lethal (Geissler S et al., 1996; Knop M et al., 1997a). In cultured human epithelial cells, overexpression of a GFP-tagged hGCP4 was found to induce nuclear fragmentation, a hallmark of apoptosis, in over 80% of cells transfected versus 12% in control cells (Fava F et al., 1999). Moreover, it is reported that introduction of even low levels of foreign γ-tubulin into mammalian cells is lethal as it causes massive reorganization of the cellular microtubule network (Shu HB et al., 1995). Although Murphy *et al* were able to generate an A31 (mouse fibroblast) cell line that stably expresses a Myc/His-tagged hGCP3, they note that expression levels in this clone do not reflect a tolerance to hGCP3 overexpression (Murphy SM et al., 1998). The point is made rather, that hGCP3 overexpression is toxic to cells based on their inability to establish a clone that had levels of foreign Myc/His-hGCP3 higher than endogenous hGCP3 levels (Murphy SM et al., 1998).

Moreover, cellular toxicity associated with His-hGCP3 overexpression was confirmed in transiently transfected Cos1 cells (see Figure 15). It was observed that His-hGCP3 expression significantly dropped off over a short period of time after transfection (72hrs). It believed that this reflects cellular toxicity or growth inhibition in His-hGCP3 expressing cells, thereby allowing non-transfected cells (within the pcc0003 transfected population) to out-grow and effectively dilute His-hGCP3 protein concentration in whole cell lysates. Alternatively, this reduction may simply reflect increased protein turnover combined with decreased production likely through plasmid degradation, a common phenomena in transiently transfected cells. However the later seems unlikely to be the full explanation when taken with morphological observations 24h post-transfection showing clear signs of duress in His-hGCP3 transfected cells not observed in control transfection.

In the current study it is not known whether toxicity associated with His-hGCP3 overexpression is an inherent consequence of hGCP3 overexpression. It is thought that massive unbalanced overproduction of a singular γTuRC subunit can result in loss of γTuC function. This may occur by squelching other structural components of the γTuC thereby disrupting complex structure or by preventing proper localization of the complexes. In yeast, the lethal effect caused by overexpression of either Spc97p or Spc98p, could be counterbalanced when either Tub4p or complementary Spc protein was overexpressed (Geissler S et al., 1996; Knop M et al., 1997a). Alternatively His-hGCP3 may function as a dominant negative protein. Although His-hGCP3 retains the ability to interact with γ-tubulin, it is not clear whether His-hGCP3 can localize to the centrosome.

Therefore it cannot be ruled out that His-hGCP3 simply does not retain the ability to interact with the large coiled-coil proteins (CG-NAP (Takahashi M et al., 2002), pericentrin (Zimmerman WC et al., 2004), or kendrin (Takahashi M et al., 2002)) that make the centromatrix and serve as docking sites for γTuRCs. If the case, it is conceivable that His-hGCP3 when incorporated into γTuRC effectively reduces or prevents γTuRC localization to the centrosome. This would ultimately translate into cells entering mitosis with centrosomes having an insufficient capacity to generate MT for mitotic spindles. It is reported that loss of γ-TuRCs from centrosomes caused by overexpressing the GCP2/3 binding domain of pericentrin triggers a G2/interphase checkpoint arrest and ultimately induces apoptosis in somatic cells (Zimmerman WC et al., 2004). In either case, the toxicity associated with overexpression of individual γTuC subunits may not be completely surprising considering the fundamental cellular importance of γTuCs and their indispensable role in generating MTs

3. Biochemical interaction His-hGCP3 & psoriasin

It was not possible to consistently detect by western analysis, psoriasin in anti-His immunoprecipitates despite using IP conditions reported to preserve known psoriasin (Emberley ED et al., 2004) or hGCP3 (Murphy SM et al., 1998) protein-interactions. It should not be forgotten the hGCP3 amino acid sequence identified by the initial Y2H screen that interacts with psoriasin is the reported putative γ-tubulin binding domain (see Figure 3 and Figure 4 (Tassin AM et al., 1999)). It serves to reason that IP conditions able to preserve an interaction between His-hGCP3 and γ-tubulin should preserve an interaction with His-hGCP3 and psoriasin. However results obtained in this study show

this is not the case. Although a positive interaction by co-immunoprecipitation was identified in two separate experiments, it was never reliably reproduced with all necessary controls. More often than not, an interaction failed to be detected even under robust co-expression of psoriasin and His-hGCP3.

There are two possible explanations that rationalize these contradictory results. First, an interaction does occur; however, the interaction is not kinetically favoured under experimental conditions, or takes places at a specific stage in the cell-cycle that was not enriched for in subsequent negative co-IPs. Circumstantial support for a cell-cycle dependent role for psoriasin comes from the observation that endogenous psoriasin expression in the epithelial breast cancer line MDA-MB-468 is enriched in mitotic cells (Dr. P.H. Watson personal communication). This may explain why only faint bands corresponding to psoriasin were ever detected in His-hGCP3 immunoprecipitates. To a lesser extent, this rationale explains the irreproducibility of positive co-IP. The alternative explanation, simply stated, is that positive co-IPs are due to experimental error and psoriasin and hGCP3 do not interact. It certainly appears that sample cross-contamination or lane-bleeding may very well explain positive co-IP results presented in Figure 16A. This later assertion has direct implications on the biological meaning of the initial interaction identified by the Y2H screen and is discussed below (see section IV-5)

Although anti-psoriasin antibodies did not lend themselves to indirect IF microscopy (see Figure 17), it is unlikely that negative co-IP are the result of improper psoriasin localization in transiently transfected Cos1 cells. Psoriasin is known to have both

cytoplasmic and nuclear localization, as well as being secreted (Emberley ED et al., 2003a). The construct used to express psoriasin, pcDNA3.1-psor, has been used to establish stable psoriasin-expressing cell lines (MDA-MB-231). In these cell lines, foreign psoriasin expression is found by IHC to have proper cellular localization (Emberley ED et al., 2003a). It is not known at present why rabbit polyclonal anti-psoriasin antibody specifically detects psoriasin by immunohistochemistry (IHC) and not by IF; however, differential cell fixation techniques may account for this discrepancy. It still remains to be determined if psoriasin and His-hGCP3 co-localize within the cell. However, without data showing a clear interaction between psoriasin and His-hGCP3, there is less need for further localization studies.

4. Assays for γ-TuRC/Centrosomal Function

Psoriasin expression did not influence endogenous hGCP3 function as measured by two assays for centrosome function: the microtubule regrowth assay (MRG), and mitotic spindle morphology assay (MSM) (see Figure 18 & 19). The hypothesis that psoriasin influences centrosomal function mediated through hGCP3 is at the heart of this study's relevance to breast cancer research. However, it was necessary to test this hypothesis using His-hGCP3 independent systems. This is not a trivial point considering the cytotoxicity associated with robust His-hGCP3 overexpression, and the possibility that His-hGCP3 may act as a dominant negative protein with altered functionality. As such, using breast cancer cell models with endogenous levels of hGCP3, and titratable levels of psoriasin expression presented a clear benefit over a transient transfection approach, in order to assay for changes in centrosome function in relation to psoriasin expression.

Nevertheless, two major experimental shortcomings could not be overcome. First, the two assays employed to measure centrosome function can only be considered indirect measures of hGCP3 activity. No specific assay has been developed to measure hGCP3 function directly. Therefore, the lack of correlation between psoriasin expression and altered hGCP3 function may simply reflect the wrong biological end-point measured. However, evidence in the literature supports the central line of reasoning that altered function of specific core GCPs, such as GCP3, compromises γTuRC function either by improper localization or decreased activity, and translates into altered centrosomal function (Barbosa V et al., 2000; Fava F et al., 1999; Fujita A et al., 2002; Vardy L et al., 2000). In fission yeast, mutations in either GCP2, GCP3 or GCP6 orthologues, alp4, alp6 and alp16, result in defective formation of bipolar spindles leading to mitotic cells with monopolar spindles (Fujita A et al., 2002; Vardy L et al., 2000). Mutations in the Drosophila GCP3 orthologue Dgrip91 were found to deplete the centrosomal associated fraction of γTuRCs, resulting in mitotic spindles with abnormally few MTs and centrosomes missing centrioles (Barbosa V et al., 2000). Moreover, overexpression of hGCP4 was found to induce the formation of multipolar mitoses in certain mammalian cell lines (Fava F et al., 1999). The second experimental shortcoming is that the level of psoriasin expression within an individual cell assayed was not known, nor was the proportion of cells expressing psoriasin in the population. Although levels of psoriasin were monitored by western analysis, this information can only provide insight into the overall expression levels of the population. Therefore, it is possible that levels of psoriasin detected by western analysis are the result of few cells expressing massive

quantities of psoriasin. If this is the case, the experimental sample size used in statistical analyses may not be large enough to tease apart actual differences in centrosome function in relation to psoriasin expression. However this does appear to be the case, at least for the MDA-MB-231 psoriasin expressing clones, as they present by IHC, a fairly uniform psoriasin expression throughout the population (Emberley ED et al., 2003a).

Therefore the lack of correlation between psoriasin expression and change in centrosome function likely is not a reflection of improper choice of biological end-points measured, nor a highly skewed expression distribution within the cell population; rather, it reflects a lack of biological significance between psoriasin expression and hGCP3 activity. These results are consistent with the inability to confirm an interaction between psoriasin and His-hGCP3 by co-immunoprecipitation analysis in transiently transfected cells.

Despite a lack of correlation between psoriasin expression and altered hGCP3 function, several interesting observations were made on the nature of mitotic spindles in two routinely cultured epithelial breast cancer lines, MCF7 and MDA-MB-231. MCF7 and derived clones had an overall higher frequency of spindle defects (~30%) (Figure 6B, upper panel) than in the 231s and derived clones (~10%) (see Figure 18). Interestingly, roughly 80% of total spindle defects observed in MCF7 were monopolar spindles; while 231s were a combination of multi-polar or misaligned spindles were observed.

The high frequency of monopolar spindles observed in MCF-7 cells and derived psoriasin-inducible clones was unexpected. It is not known at present whether monopolar

spindle phenotype in MCF7 is the result of a specific genetic defect. Monopolar spindle phenotype have been described in conjunction with molecular alterations of proteins involved in the cell cycle dependent regulation of centrosome cohesion, and physical separation of centrosome during mitosis. Examples include Nek2a kinase, a member of the NiMA (never in mitosis A) kinase family) that regulates parental-centriole cohesion via phosphorylation of a large structural protein C-Nap1 found at centriole ends (Faragher AJ et al., 2003; Fry AM et al., 1998). Functional inactivation of the kinase domain inhibits centrosome separation leading to the formation of monopolar spindles and interferes with chromosome segregation leading to overall changes in DNA content of the cell population (Faragher AJ et al., 2003). Additionally, the mitotic motor Eg5, a member of the BiMC (blocked in mitosis) family of plus end-directed kinesins has been implicated in separation of spindle poles (Miyamoto DT et al., 2003). Inhibiting Eg5 with microinjected antibodies (Blangy A et al., 1995; Gaglio T et al., 1996), or specific small molecule inhibitors (Mayer TU et al., 1999) results in spindle poles collapsing together and the formation of monopolar asters.

It appears that monopolar spindles observed were not the result of failed centrosome duplication but rather failed centrosome separation. This is supported by the observation that the frequency of cells with a single MT-regrowth-foci observed in the MRG assay did not reflect the frequency of MCF7s with monopolar spindles observed in the MSM assay. In addition to depolymerizing microtubules, nocodazole also induces centrosome splitting, only if centrosomes have been duplicated, and at the dose administered to cell for the MRG assay (Meraldi P et al., 2001).

5. Biological of Significance of Y2H

Results presented in this thesis suggest that an interaction between psoriasin and hGCP3 does not occur in breast cancer cell. This is based on their inability to be co-immunoprecipitated in transiently transfected Cos1 cells, and the lack of any biological correlation between psoriasin expression with altered hGCP3 function. These results challenge the assertion that the interaction identified by the Y2H screen may have biological meaning in human breast cancer.

There are several reasons why an interaction was identified in yeast, but could not be corroborated in a mammalian cell. Recall, the hGCP3 sequence found to interact with psoriasin in yeast clone 6-4, did not encode a full length protein (hGCP3 aa516-584). With the assumption that clone 6-4 is a true Y2H positive colony, this interaction may simply reflect differential biochemical properties associated with the truncated protein. A truncated protein may reveal hidden or cryptic recognition sequences that are masked within the full length protein, potentially allowing accessibility to otherwise sterically defined binding sites. Moreover, the Y2H assay extensively relies on the use of chimeric proteins that may have altered conformations as a result of artificially fusing two proteins together (van Criekinge W et al., 1999). This in turn may result in altered functional properties of the prey and/or bait protein. Additionally, the two-hybrid system requires fusion proteins to be targeted to the yeast nucleus. As such the interaction occurs in a cellular environment that is distinct from that assayed for interaction in mammalian cells by co-immunoprecipitation analysis. Coupled with the fact that only reporter gene activity is measured, it is impossible to exclude the possibility that a bridging protein,

unique in the yeast, facilitates the interaction (van Criekinge W et al., 1999). Alternatively, the discrepancy between an interaction detected in the yeast system and co-IP assay in mammalian cells, may simply reflect the sensitivities of these assays. It is reported that the sensitivity of the Y2H system leads to the detection of interactions with dissociation constants around 10^{-7}M, in the range of the most weak protein interactions found in the cell (Phizicky E et al., 2003). This is more sensitive than co-immunoprecipitation in which interacting proteins need to be co-purified, which requires stability of a complex through dilution from cell lysis, and subsequent purification step (Phizicky E et al., 2003). It is possible that the interaction identified in the yeast is an artefact caused by the overproduction of proteins in-vivo coupled with the sensitivity of the assay.

However the most compelling reason why an interaction between hGCP3 and psoriasin could not be corroborated in a mammalian cell, is provided by a recent review of the initial Y2H data (only performed during the course of this write-up). It was found (again) that reintroduction of the psoriasin-bait plasmid and prey plasmid from clone 6-4 into a different yeast did not reconstitute β-galactosidase activity (Figure 20). Failure to reconstitute β-gal activity challenges the very assertion that clone 6-4 is a true-Y2H positive. To understand this, recall the Y2H assay exploits the fact that the DNA-binding domain of GAL4 (fused in-frame with psoriasin) is incapable of activating transcription unless physically, but not necessary covalently associated with an activating domain (fused to the prey cDNA sequence library). When both domains are in close proximity, due to physical interaction between their respective chimeric partner-proteins, the β-

galactosidase reporter gene is activated and leads to colorimetric detection (white to blue) on X-gal medium. Simply put, if the bait and prey plasmids encode for fusion proteins that can interact, β-galactosidase activity should be maintained irrespective of yeast used. Therefore an interaction between hGCP3 and psoriasin could not be corroborated in a mammalian cell because it did not occur in yeast. The most likely explanation why initial 6-4 clone presented B-gal activity is that this yeast could autoactivate the β-gal reporter due to spurious transcription. Hence the need for prey-bait plasmid reconstitution analysis. Alternatively this yeast may have contained more than one prey-plasmid, one of which conferred the ability to interact with psoriasin, but was not preferentially isolated and sequenced in subsequent steps.

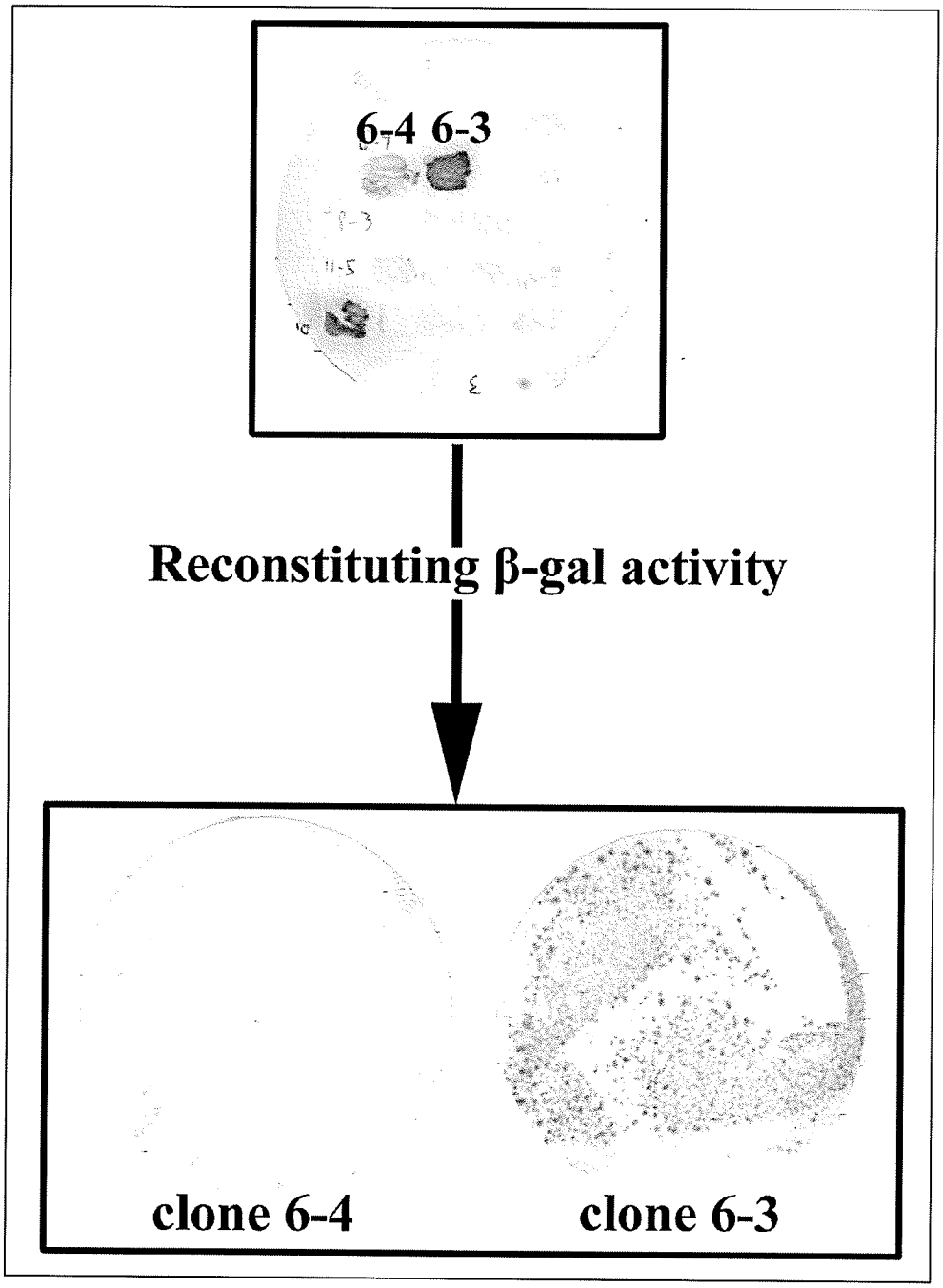

Figure 20: Reintroduction of the bait/psoriasin plasmid and prey plasmid from clone 6-4 (hGCP3 a.a. 516-584) into yeast did not reconstitute β-galactosidase activity. Top panel shows the initial activation of B-galactosidase for clones 6-3 and 6-4 as indicated by the presence of blue colorimetric conversion product. Lower panel shows that upon reintroduction of bait and prey plasmids B-gal activity was maintained in clone 6-3 but not clone 6-4.

V. Conclusions

It was never possible to consistently co-IP psoriasin and His-hGCP3. We do not believe this is on account of issues associated with cell viability. Although it was never possible to establish a His-hGCP3 overexpressing MCF7 clone, and immediate cytotoxic effects were observed upon transient transfection of pcc003 into Cos1 cells, we'd argue that co-IP assays were occurring in viable cells since a significant portion of adherent transfected cells retained persistent His-hGCP3 expression even at 72hr post transfection. Moreover we do not believe that failure to co-IP His-hGCP3 and psoriasin is the result of altered functionality associated with His-hGCP3 recombinant protein. We feel that the constructs generated in this study are suitable for this project. This is based on the expressed tagged-protein's ability to retain γ-tubulin interacting properties. Although His-hGCP3 did not properly localize within the cell as is reported for its endogenous counterpart, this was in the context of cell lines that additionally had atypical γ-tubulin localization. Therefore, it is concluded that these two proteins do not interact, or an interaction cannot be detected under experimental conditions used. This is consistent with results obtained from assays for centrosome function, showing that psoriasin overexpression in epithelial breast cancer cells does not influence overall mitotic spindle morphology or the capacity in which centrosomes devoid of MTs can reinitiate MT nucleation. Therefore it is concluded, that although an interaction between hGCP3 and psoriasin can occur in the Y2H system (and this is subject to question), it does not appear that this interaction is conserved in mammalian cells. By extrapolation, it is concluded that an interaction between hGCP3 and psoriasin is not biologically relevant to breast cancer and merits no further investigation.

Reference List

1. Al Haddad, S., Zhang, Z., Leygue, E., Snell, L., Huang, A., Niu, Y., Hiller-Hitchcock, T., Hole, K., Murphy, L.C., & Watson, P.H. Psoriasin (S100A7) expression and invasive breast cancer. Am.J.Pathol. **155**, 2057-2066 (1999).

2. Algermissen, B., Sitzmann, J., LeMotte, P., & Czarnetzki, B. Differential expression of CRABP II, psoriasin and cytokeratin 1 mRNA in human skin diseases. Arch.Dermatol.Res. **288**, 426-430 (1996).

3. Allred, D.C., Mohsin, S.K., & Fuqua, S.A. Histological and biological evolution of human premalignant breast disease. Endocr.Relat Cancer **8**, 47-61 (2001).

4. Alowami, S., Qing, G., Emberley, E., Snell, L., & Watson, P.H. Psoriasin (S100A7) expression is altered during skin tumorigenesis. BMC.Dermatol. **3**, 1- (2003).

5. Barbosa, V., Yamamoto, R.R., Henderson, D.S., & Glover, D.M. Mutation of a Drosophila gamma tubulin ring complex subunit encoded by discs degenerate-4 differentially disrupts centrosomal protein localization. Genes Dev. **14**, 3126-3139 (2000).

6. Blangy, A., Lane, H.A., d'Herin, P., Harper, M., Kress, M., & Nigg, E.A. Phosphorylation by p34cdc2 regulates spindle association of human Eg5, a kinesin-related motor essential for bipolar spindle formation in vivo. Cell **83**, 1159-1169 (1995).

7. Boniface, K., Bernard, F.X., Garcia, M., Gurney, A.L., Lecron, J.C., & Morel, F. IL-22 inhibits epidermal differentiation and induces proinflammatory gene expression and migration of human keratinocytes. J.Immunol. **174**, 3695-3702 (2005).

8. Bonnett, M., Wallis, T., Rossmann, M., Pernick, N.L., Carolin, K.A., Segel, M., Bouwman, D., & Visscher, D. Histologic and radiographic analysis of ductal carcinoma in situ diagnosed using stereotactic incisional core breast biopsy. Mod.Pathol. **15**, 95-101 (2002).

9. Breen, E.C. & Tang, K. Calcyclin (S100A6) regulates pulmonary fibroblast proliferation, morphology, and cytoskeletal organization in vitro. J.Cell Biochem. **88**, 848-854 (2003).

10. Buerger, H., Otterbach, F., Simon, R., Poremba, C., Diallo, R., Decker, T., Riethdorf, L., Brinkschmidt, C., Dockhorn-Dworniczak, B., & Boecker, W. Comparative genomic hybridization of ductal carcinoma in situ of the breast-evidence of multiple genetic pathways. J.Pathol. **187**, 396-402 (1999).

11. Canaday, J., Stoppin-Mellet, V., Mutterer, J., Lambert, A.M., & Schmit, A.C. Higher plant cells: gamma-tubulin and microtubule nucleation in the absence of centrosomes. Microsc.Res.Tech. **49**, 487-495 (2000).

12. Carroll, P.E., Okuda, M., Horn, H.F., Biddinger, P., Stambrook, P.J., Gleich, L.L., Li, Y.Q., Tarapore, P., & Fukasawa, K. Centrosome hyperamplification in human cancer: chromosome instability induced by p53 mutation and/or Mdm2 overexpression. Oncogene **18**, 1935-1944 (1999).

13. Celis, J.E., Rasmussen, H.H., Vorum, H., Madsen, P., Honore, B., Wolf, H., & Orntoft, T.F. Bladder squamous cell carcinomas express psoriasin and externalize it to the urine. J.Urol. **155**, 2105-2112 (1996).

14. Chamovitz, D.A. & Segal, D. JAB1/CSN5 and the COP9 signalosome. A complex situation. EMBO Rep. **2**, 96-101 (2001).

15. Chen, D., Xu, W., He, P., Medrano, E.E., & Whiteheart, S.W. Gaf-1, a gamma - SNAP-binding protein associated with the mitochondria. J.Biol.Chem. **276**, 13127-13135 (2001).

16. Davies, B.R., O'Donnell, M., Durkan, G.C., Rudland, P.S., Barraclough, R., Neal, D.E., & Mellon, J.K. Expression of S100A4 protein is associated with metastasis and reduced survival in human bladder cancer. J.Pathol. **196**, 292-299 (2002).

17. Dictenberg, J.B., Zimmerman, W., Sparks, C.A., Young, A., Vidair, C., Zheng, Y., Carrington, W., Fay, F.S., & Doxsey, S.J. Pericentrin and gamma-tubulin form a protein complex and are organized into a novel lattice at the centrosome. J.Cell Biol. **141**, 163-174 (1998).

18. Donato, R. S100: a multigenic family of calcium-modulated proteins of the EF-hand type with intracellular and extracellular functional roles. Int.J.Biochem.Cell Biol. **33**, 637-668 (2001).

19. Donato, R. Intracellular and extracellular roles of S100 proteins. Microsc.Res.Tech. **60**, 540-551 (2003).

20. El Rifai, W., Moskaluk, C.A., Abdrabbo, M.K., Harper, J., Yoshida, C., Riggins, G.J., Frierson, H.F., Jr., & Powell, S.M. Gastric cancers overexpress S100A calcium-binding proteins. Cancer Res. **62**, 6823-6826 (2002).

21. Emberley, E.D., Alowami, S., Snell, L., Murphy, L.C., & Watson, P.H. S100A7 (psoriasin) expression is associated with aggressive features and alteration of Jab1 in ductal carcinoma in situ of the breast. Breast Cancer Res. **6**, R308-R315 (2004).

22. Emberley, E.D., Gietz, R.D., Campbell, J.D., HayGlass, K.T., Murphy, L.C., & Watson, P.H. RanBPM interacts with psoriasin in vitro and their expression

correlates with specific clinical features in vivo in breast cancer. BMC.Cancer **2**, 28-(2002).

23. Emberley, E.D., Niu, Y., Curtis, L., Troup, S., Mandal, S.K., Myers, J.N., Gibson, S.B., Murphy, L.C., & Watson, P.H. The S100A7-c-Jun activation domain binding protein 1 pathway enhances prosurvival pathways in breast cancer. Cancer Res. **65**, 5696-5702 (2005).

24. Emberley, E.D., Niu, Y., Leygue, E., Tomes, L., Gietz, R.D., Murphy, L.C., & Watson, P.H. Psoriasin interacts with Jab1 and influences breast cancer progression. Cancer Res. **63**, 1954-1961 (2003a).

25. Emberley, E.D., Niu, Y., Njue, C., Kliewer, E.V., Murphy, L.C., & Watson, P.H. Psoriasin (S100A7) expression is associated with poor outcome in estrogen receptor-negative invasive breast cancer. Clin.Cancer Res. **9**, 2627-2631 (2003b).

26. Enerback, C., Porter, D.A., Seth, P., Sgroi, D., Gaudet, J., Weremowicz, S., Morton, C.C., Schnitt, S., Pitts, R.L., Stampl, J., Barnhart, K., & Polyak, K. Psoriasin expression in mammary epithelial cells in vitro and in vivo. Cancer Res. **62**, 43-47 (2002).

27. Erhardt, M., Stoppin-Mellet, V., Campagne, S., Canaday, J., Mutterer, J., Fabian, T., Sauter, M., Muller, T., Peter, C., Lambert, A.M., & Schmit, A.C. The plant Spc98p homologue colocalizes with gamma-tubulin at microtubule nucleation sites and is required for microtubule nucleation. J.Cell Sci. **115**, 2423-2431 (2002).

28. Ernster, V.L., Ballard-Barbash, R., Barlow, W.E., Zheng, Y., Weaver, D.L., Cutter, G., Yankaskas, B.C., Rosenberg, R., Carney, P.A., Kerlikowske, K., Taplin, S.H., Urban, N., & Geller, B.M. Detection of ductal carcinoma in situ in women undergoing screening mammography. J.Natl.Cancer Inst. **94**, 1546-1554 (2002).

29. Ernster, V.L. & Barclay, J. Increases in ductal carcinoma in situ (DCIS) of the breast in relation to mammography: a dilemma. J.Natl.Cancer Inst.Monogr151-156 (1997).

30. Ernster, V.L., Barclay, J., Kerlikowske, K., Grady, D., & Henderson, C. Incidence of and treatment for ductal carcinoma in situ of the breast. JAMA **275**, 913-918 (1996).

31. Evans, L., Mitchison, T., & Kirschner, M. Influence of the centrosome on the structure of nucleated microtubules. J.Cell Biol. **100**, 1185-1191 (1985).

32. Fanara, P., Oback, B., Ashman, K., Podtelejnikov, A., & Brandt, R. Identification of MINUS, a small polypeptide that functions as a microtubule nucleation suppressor. EMBO J. **18**, 565-577 (1999).

33. Faragher, A.J. & Fry, A.M. Nek2A kinase stimulates centrosome disjunction and is required for formation of bipolar mitotic spindles. Mol.Biol.Cell **14**, 2876-2889 (2003).

34. Fava, F., Raynaud-Messina, B., Leung-Tack, J., Mazzolini, L., Li, M., Guillemot, J.C., Cachot, D., Tollon, Y., Ferrara, P., & Wright, M. Human 76p: A new member of the gamma-tubulin-associated protein family. J.Cell Biol. **147**, 857-868 (1999).

35. Feng, G., Xu, X., Youssef, E.M., & Lotan, R. Diminished expression of S100A2, a putative tumor suppressor, at early stage of human lung carcinogenesis. Cancer Res. **61**, 7999-8004 (2001).

36. Fry, A.M., Mayor, T., Meraldi, P., Stierhof, Y.D., Tanaka, K., & Nigg, E.A. C-Nap1, a novel centrosomal coiled-coil protein and candidate substrate of the cell cycle-regulated protein kinase Nek2. J.Cell Biol. **141**, 1563-1574 (1998).

37. Fujita, A., Vardy, L., Garcia, M.A., & Toda, T. A fourth component of the fission yeast gamma-tubulin complex, Alp16, is required for cytoplasmic microtubule integrity and becomes indispensable when gamma-tubulin function is compromised. Mol.Biol.Cell **13**, 2360-2373 (2002).

38. Fukasawa, K., Choi, T., Kuriyama, R., Rulong, S., & Vande Woude, G.F. Abnormal centrosome amplification in the absence of p53. Science **271**, 1744-1747 (1996).

39. Gaglio, T., Saredi, A., Bingham, J.B., Hasbani, M.J., Gill, S.R., Schroer, T.A., & Compton, D.A. Opposing motor activities are required for the organization of the mammalian mitotic spindle pole. J.Cell Biol. **135**, 399-414 (1996).

40. Geissler, S., Pereira, G., Spang, A., Knop, M., Soues, S., Kilmartin, J., & Schiebel, E. The spindle pole body component Spc98p interacts with the gamma-tubulin-like Tub4p of Saccharomyces cerevisiae at the sites of microtubule attachment. EMBO J. **15**, 3899-3911 (1996).

41. Gergely, F., Karlsson, C., Still, I., Cowell, J., Kilmartin, J., & Raff, J.W. The TACC domain identifies a family of centrosomal proteins that can interact with microtubules. Proc.Natl.Acad.Sci.U.S.A **97**, 14352-14357 (2000).

42. Ghadimi, B.M., Sackett, D.L., Difilippantonio, M.J., Schrock, E., Neumann, T., Jauho, A., Auer, G., & Ried, T. Centrosome amplification and instability occurs exclusively in aneuploid, but not in diploid colorectal cancer cell lines, and correlates with numerical chromosomal aberrations. Genes Chromosomes.Cancer **27**, 183-190 (2000).

43. Glaser, R., Harder, J., Lange, H., Bartels, J., Christophers, E., & Schroder, J.M. Antimicrobial psoriasin (S100A7) protects human skin from Escherichia coli infection. Nat.Immunol. **6**, 57-64 (2005).

44. Goepfert, T.M., Adigun, Y.E., Zhong, L., Gay, J., Medina, D., & Brinkley, W.R. Centrosome amplification and overexpression of aurora A are early events in rat mammary carcinogenesis. Cancer Res. **62**, 4115-4122 (2002).

45. Grigorian, M., Andresen, S., Tulchinsky, E., Kriajevska, M., Carlberg, C., Kruse, C., Cohn, M., Ambartsumian, N., Christensen, A., Selivanova, G., & Lukanidin, E. Tumor suppressor p53 protein is a new target for the metastasis-associated Mts1/S100A4 protein: functional consequences of their interaction. J.Biol.Chem. **276**, 22699-22708 (2001).

46. Gupta, S., Hussain, T., MacLennan, G.T., Fu, P., Patel, J., & Mukhtar, H. Differential expression of S100A2 and S100A4 during progression of human prostate adenocarcinoma. J.Clin.Oncol. **21**, 106-112 (2003).

47. Gupta, S.K., Douglas-Jones, A.G., Fenn, N., Morgan, J.M., & Mansel, R.E. The clinical behavior of breast carcinoma is probably determined at the preinvasive stage (ductal carcinoma in situ). Cancer **80**, 1740-1745 (1997).

48. Gustafson, L.M., Gleich, L.L., Fukasawa, K., Chadwell, J., Miller, M.A., Stambrook, P.J., & Gluckman, J.L. Centrosome hyperamplification in head and neck squamous cell carcinoma: a potential phenotypic marker of tumor aggressiveness. Laryngoscope **110**, 1798-1801 (2000).

49. Holland, R. & Hendriks, J.H. Microcalcifications associated with ductal carcinoma in situ: mammographic-pathologic correlation. Semin.Diagn.Pathol. **11**, 181-192 (1994).

50. Hsu, L.C., Doan, T.P., & White, R.L. Identification of a gamma-tubulin-binding domain in BRCA1. Cancer Res. **61**, 7713-7718 (2001).

51. Hsu, L.C. & White, R.L. BRCA1 is associated with the centrosome during mitosis. Proc.Natl.Acad.Sci.U.S.A **95**, 12983-12988 (1998).

52. Hu, W., Kavanagh, J.J., Deaver, M., Johnston, D.A., Freedman, R.S., Verschraegen, C.F., & Sen, S. Frequent overexpression of STK15/Aurora-A/BTAK and chromosomal instability in tumorigenic cell cultures derived from human ovarian cancer. Oncol.Res. **15**, 49-57 (2005).

53. Hwang, E.S., DeVries, S., Chew, K.L., Moore, D.H., Kerlikowske, K., Thor, A., Ljung, B.M., & Waldman, F.M. Patterns of chromosomal alterations in breast ductal carcinoma in situ. Clin.Cancer Res. **10**, 5160-5167 (2004).

54. Ilg, E.C., Schafer, B.W., & Heizmann, C.W. Expression pattern of S100 calcium-binding proteins in human tumors. Int.J.Cancer **68**, 325-332 (1996).

55. James, L.A., Mitchell, E.L., Menasce, L., & Varley, J.M. Comparative genomic hybridisation of ductal carcinoma in situ of the breast: identification of regions of

DNA amplification and deletion in common with invasive breast carcinoma. Oncogene **14**, 1059-1065 (1997).

56. Jinquan, T., Vorum, H., Larsen, C.G., Madsen, P., Rasmussen, H.H., Gesser, B., Etzerodt, M., Honore, B., Celis, J.E., & Thestrup-Pedersen, K. Psoriasin: a novel chemotactic protein. J.Invest Dermatol. **107**, 5-10 (1996).

57. Kellogg, D.R., Moritz, M., & Alberts, B.M. The centrosome and cellular organization. Annu.Rev.Biochem. **63**, 639-674 (1994).

58. Khodjakov, A. & Rieder, C.L. The sudden recruitment of gamma-tubulin to the centrosome at the onset of mitosis and its dynamic exchange throughout the cell cycle, do not require microtubules. J.Cell Biol. **146**, 585-596 (1999).

59. Knop, M., Pereira, G., Geissler, S., Grein, K., & Schiebel, E. The spindle pole body component Spc97p interacts with the gamma-tubulin of Saccharomyces cerevisiae and functions in microtubule organization and spindle pole body duplication. EMBO J. **16**, 1550-1564 (1997a).

60. Knop, M. & Schiebel, E. Spc98p and Spc97p of the yeast gamma-tubulin complex mediate binding to the spindle pole body via their interaction with Spc110p. EMBO J. **16**, 6985-6995 (1997b).

61. Korver, W., Guevara, C., Chen, Y., Neuteboom, S., Bookstein, R., Tavtigian, S., & Lees, E. The product of the candidate prostate cancer susceptibility gene ELAC2 interacts with the gamma-tubulin complex. Int.J.Cancer **104**, 283-288 (2003).

62. Kukharskyy, V., Sulimenko, V., Macurek, L., Sulimenko, T., Draberova, E., & Draber, P. Complexes of gamma-tubulin with nonreceptor protein tyrosine kinases Src and Fyn in differentiating P19 embryonal carcinoma cells. Exp.Cell Res. **298**, 218-228 (2004).

63. Lajoie-Mazenc, I., Tollon, Y., Detraves, C., Julian, M., Moisand, A., Gueth-Hallonet, C., Debec, A., Salles-Passador, I., Puget, A., Mazarguil, H., & . Recruitment of antigenic gamma-tubulin during mitosis in animal cells: presence of gamma-tubulin in the mitotic spindle. J.Cell Sci. **107 (Pt 10)**, 2825-2837 (1994).

64. Lakshmi, M.S., Parker, C., & Sherbet, G.V. Metastasis associated MTS1 and NM23 genes affect tubulin polymerisation in B16 melanomas: a possible mechanism of their regulation of metastatic behaviour of tumours. Anticancer Res. **13**, 299-303 (1993).

65. Lengauer, C., Kinzler, K.W., & Vogelstein, B. Genetic instabilities in human cancers. Nature **396**, 643-649 (1998).

66. Levett, D., Flecknell, P.A., Rudland, P.S., Barraclough, R., Neal, D.E., Mellon, J.K., & Davies, B.R. Transfection of S100A4 produces metastatic variants of an orthotopic model of bladder cancer. Am.J.Pathol. **160**, 693-700 (2002).

67. Leygue, E., Snell, L., Hiller, T., Dotzlaw, H., Hole, K., Murphy, L.C., & Watson, P.H. Differential expression of psoriasin messenger RNA between in situ and invasive human breast carcinoma. Cancer Res. **56**, 4606-4609 (1996).

68. Lin, J., Blake, M., Tang, C., Zimmer, D., Rustandi, R.R., Weber, D.J., & Carrier, F. Inhibition of p53 transcriptional activity by the S100B calcium-binding protein. J.Biol.Chem. **276**, 35037-35041 (2001).

69. Lingle, W.L., Barrett, S.L., Negron, V.C., D'Assoro, A.B., Boeneman, K., Liu, W., Whitehead, C.M., Reynolds, C., & Salisbury, J.L. Centrosome amplification drives chromosomal instability in breast tumor development. Proc.Natl.Acad.Sci.U.S.A **99**, 1978-1983 (2002).

70. Lingle, W.L., Lutz, W.H., Ingle, J.N., Maihle, N.J., & Salisbury, J.L. Centrosome hypertrophy in human breast tumors: implications for genomic stability and cell polarity. Proc.Natl.Acad.Sci.U.S.A **95**, 2950-2955 (1998).

71. Lingle, W.L. & Salisbury, J.L. Altered centrosome structure is associated with abnormal mitoses in human breast tumors. Am.J.Pathol. **155**, 1941-1951 (1999).

72. Madsen, P., Rasmussen, H.H., Leffers, H., Honore, B., Dejgaard, K., Olsen, E., Kiil, J., Walbum, E., Andersen, A.H., Basse, B., & . Molecular cloning, occurrence, and expression of a novel partially secreted protein "psoriasin" that is highly up-regulated in psoriatic skin. J.Invest Dermatol. **97**, 701-712 (1991).

73. Martin, O.C., Gunawardane, R.N., Iwamatsu, A., & Zheng, Y. Xgrip109: a gamma tubulin-associated protein with an essential role in gamma tubulin ring complex (gammaTuRC) assembly and centrosome function. J.Cell Biol. **141**, 675-687 (1998).

74. Martinsson, H., Yhr, M., & Enerback, C. Expression patterns of S100A7 (psoriasin) and S100A9 (calgranulin-B) in keratinocyte differentiation. Exp.Dermatol. **14**, 161-168 (2005).

75. Mayer, T.U., Kapoor, T.M., Haggarty, S.J., King, R.W., Schreiber, S.L., & Mitchison, T.J. Small molecule inhibitor of mitotic spindle bipolarity identified in a phenotype-based screen. Science **286**, 971-974 (1999).

76. Mayor, T., Hacker, U., Stierhof, Y.D., & Nigg, E.A. The mechanism regulating the dissociation of the centrosomal protein C-Nap1 from mitotic spindle poles. J.Cell Sci. **115**, 3275-3284 (2002).

77. Meraldi, P. & Nigg, E.A. Centrosome cohesion is regulated by a balance of kinase and phosphatase activities. J.Cell Sci. **114**, 3749-3757 (2001).

78. Miyamoto, D.T., Perlman, Z.E., Mitchison, T.J., & Shirasu-Hiza, M. Dynamics of the mitotic spindle--potential therapeutic targets. Prog.Cell Cycle Res. **5**, 349-360 (2003).

79. Moog-Lutz, C., Bouillet, P., Regnier, C.H., Tomasetto, C., Mattei, M.G., Chenard, M.P., Anglard, P., Rio, M.C., & Basset, P. Comparative expression of the psoriasin (S100A7) and S100C genes in breast carcinoma and co-localization to human chromosome 1q21-q22. Int.J.Cancer **63**, 297-303 (1995).

80. Moritz, M., Braunfeld, M.B., Guenebaut, V., Heuser, J., & Agard, D.A. Structure of the gamma-tubulin ring complex: a template for microtubule nucleation. Nat.Cell Biol. **2**, 365-370 (2000).

81. Moritz, M., Zheng, Y., Alberts, B.M., & Oegema, K. Recruitment of the gamma-tubulin ring complex to Drosophila salt-stripped centrosome scaffolds. J.Cell Biol. **142**, 775-786 (1998).

82. Moudjou, M., Bordes, N., Paintrand, M., & Bornens, M. gamma-Tubulin in mammalian cells: the centrosomal and the cytosolic forms. J.Cell Sci. **109 (Pt 4)**, 875-887 (1996).

83. Murphy, S.M., Preble, A.M., Patel, U.K., O'Connell, K.L., Dias, D.P., Moritz, M., Agard, D., Stults, J.T., & Stearns, T. GCP5 and GCP6: two new members of the human gamma-tubulin complex. Mol.Biol.Cell **12**, 3340-3352 (2001).

84. Murphy, S.M., Urbani, L., & Stearns, T. The mammalian gamma-tubulin complex contains homologues of the yeast spindle pole body components spc97p and spc98p. J.Cell Biol. **141**, 663-674 (1998).

85. Nagy, N., Brenner, C., Markadieu, N., Chaboteaux, C., Camby, I., Schafer, B.W., Pochet, R., Heizmann, C.W., Salmon, I., Kiss, R., & Decaestecker, C. S100A2, a putative tumor suppressor gene, regulates in vitro squamous cell carcinoma migration. Lab Invest **81**, 599-612 (2001).

86. Nigg, E.A. Centrosome aberrations: cause or consequence of cancer progression? Nat.Rev.Cancer **2**, 815-825 (2002).

87. Nikitenko, L.L., Lloyd, B.H., Rudland, P.S., Fear, S., & Barraclough, R. Localisation by in situ hybridisation of S100A4 (p9Ka) mRNA in primary human breast tumour specimens. Int.J.Cancer **86**, 219-228 (2000).

88. Oegema, K., Wiese, C., Martin, O.C., Milligan, R.A., Iwamatsu, A., Mitchison, T.J., & Zheng, Y. Characterization of two related Drosophila gamma-tubulin complexes that differ in their ability to nucleate microtubules. J.Cell Biol. **144**, 721-733 (1999).

89. Ohta, T., Essner, R., Ryu, J.H., Palazzo, R.E., Uetake, Y., & Kuriyama, R. Characterization of Cep135, a novel coiled-coil centrosomal protein involved in microtubule organization in mammalian cells. J.Cell Biol. **156**, 87-99 (2002).

90. Olivotto, I. & Levine, M. Clinical practice guidelines for the care and treatment of breast cancer: the management of ductal carcinoma in situ (summary of the 2001 update). CMAJ. **165**, 912-913 (2001).

91. Olsen, E., Rasmussen, H.H., & Celis, J.E. Identification of proteins that are abnormally regulated in differentiated cultured human keratinocytes. Electrophoresis **16**, 2241-2248 (1995).

92. Phizicky, E., Bastiaens, P.I., Zhu, H., Snyder, M., & Fields, S. Protein analysis on a proteomic scale. Nature **422**, 208-215 (2003).

93. Pihan, G.A., Purohit, A., Wallace, J., Knecht, H., Woda, B., Quesenberry, P., & Doxsey, S.J. Centrosome defects and genetic instability in malignant tumors. Cancer Res. **58**, 3974-3985 (1998).

94. Pihan, G.A., Purohit, A., Wallace, J., Malhotra, R., Liotta, L., & Doxsey, S.J. Centrosome defects can account for cellular and genetic changes that characterize prostate cancer progression. Cancer Res. **61**, 2212-2219 (2001).

95. Pihan, G.A., Wallace, J., Zhou, Y., & Doxsey, S.J. Centrosome abnormalities and chromosome instability occur together in pre-invasive carcinomas. Cancer Res. **63**, 1398-1404 (2003).

96. Rieder, C.L., Faruki, S., & Khodjakov, A. The centrosome in vertebrates: more than a microtubule-organizing center. Trends Cell Biol. **11**, 413-419 (2001).

97. Rios, R.M., Sanchis, A., Tassin, A.M., Fedriani, C., & Bornens, M. GMAP-210 recruits gamma-tubulin complexes to cis-Golgi membranes and is required for Golgi ribbon formation. Cell **118**, 323-335 (2004).

98. Roymans, D., Vissenberg, K., De Jonghe, C., Willems, R., Engler, G., Kimura, N., Grobben, B., Claes, P., Verbelen, J.P., Van Broeckhoven, C., & Slegers, H. Identification of the tumor metastasis suppressor Nm23-H1/Nm23-R1 as a constituent of the centrosome. Exp.Cell Res. **262**, 145-153 (2001).

99. Ruse, M., Broome, A.M., & Eckert, R.L. S100A7 (psoriasin) interacts with epidermal fatty acid binding protein and localizes in focal adhesion-like structures in cultured keratinocytes. J.Invest Dermatol. **121**, 132-141 (2003).

100. Salisbury, J.L. The contribution of epigenetic changes to abnormal centrosomes and genomic instability in breast cancer. J.Mammary.Gland.Biol.Neoplasia. **6**, 203-212 (2001).

101. Salisbury, J.L., D'Assoro, A.B., & Lingle, W.L. Centrosome amplification and the origin of chromosomal instability in breast cancer. J.Mammary.Gland.Biol.Neoplasia. **9**, 275-283 (2004).

102. Sanders, M.E., Schuyler, P.A., Dupont, W.D., & Page, D.L. The natural history of low-grade ductal carcinoma in situ of the breast in women treated by biopsy only revealed over 30 years of long-term follow-up. Cancer **103**, 2481-2484 (2005).

103. Sato, N., Mizumoto, K., Nakamura, M., Maehara, N., Minamishima, Y.A., Nishio, S., Nagai, E., & Tanaka, M. Correlation between centrosome abnormalities and chromosomal instability in human pancreatic cancer cells. Cancer Genet.Cytogenet. **126**, 13-19 (2001).

104. Schnackenberg, B.J. & Palazzo, R.E. Identification and function of the centrosome centromatrix. Biol.Cell **91**, 429-438 (1999).

105. Shono, M., Sato, N., Mizumoto, K., Maehara, N., Nakamura, M., Nagai, E., & Tanaka, M. Stepwise progression of centrosome defects associated with local tumor growth and metastatic process of human pancreatic carcinoma cells transplanted orthotopically into nude mice. Lab Invest **81**, 945-952 (2001).

106. Shu, H.B. & Joshi, H.C. Gamma-tubulin can both nucleate microtubule assembly and self-assemble into novel tubular structures in mammalian cells. J.Cell Biol. **130**, 1137-1147 (1995).

107. Sorci, G., Agneletti, A.L., Bianchi, R., & Donato, R. Association of S100B with intermediate filaments and microtubules in glial cells. Biochim.Biophys.Acta **1448**, 277-289 (1998).

108. Sorci, G., Agneletti, A.L., & Donato, R. Effects of S100A1 and S100B on microtubule stability. An in vitro study using triton-cytoskeletons from astrocyte and myoblast cell lines. Neuroscience **99**, 773-783 (2000).

109. Starita, L.M., Machida, Y., Sankaran, S., Elias, J.E., Griffin, K., Schlegel, B.P., Gygi, S.P., & Parvin, J.D. BRCA1-dependent ubiquitination of gamma-tubulin regulates centrosome number. Mol.Cell Biol. **24**, 8457-8466 (2004).

110. Takahashi, M., Yamagiwa, A., Nishimura, T., Mukai, H., & Ono, Y. Centrosomal proteins CG-NAP and kendrin provide microtubule nucleation sites by anchoring gamma-tubulin ring complex. Mol.Biol.Cell **13**, 3235-3245 (2002).

111. Takenaga, K., Nakamura, Y., & Sakiyama, S. Expression of antisense RNA to S100A4 gene encoding an S100-related calcium-binding protein suppresses metastatic potential of high-metastatic Lewis lung carcinoma cells. Oncogene **14**, 331-337 (1997a).

112. Takenaga, K., Nakanishi, H., Wada, K., Suzuki, M., Matsuzaki, O., Matsuura, A., & Endo, H. Increased expression of S100A4, a metastasis-associated gene, in human colorectal adenocarcinomas. Clin.Cancer Res. **3**, 2309-2316 (1997b).

113. Tarapore, P., Horn, H.F., Tokuyama, Y., & Fukasawa, K. Direct regulation of the centrosome duplication cycle by the p53-p21Waf1/Cip1 pathway. Oncogene **20**, 3173-3184 (2001).

114. Tassin, A.M. & Bornens, M. Centrosome structure and microtubule nucleation in animal cells. Biol.Cell **91**, 343-354 (1999).

115. Tassin, A.M., Celati, C., Moudjou, M., & Bornens, M. Characterization of the human homologue of the yeast spc98p and its association with gamma-tubulin. J.Cell Biol. **141**, 689-701 (1998).

116. Tonini, G.P., Casalaro, A., Cara, A., & Di Martino, D. Inducible expression of calcyclin, a gene with strong homology to S-100 protein, during neuroblastoma cell differentiation and its prevalent expression in Schwann-like cell lines. Cancer Res. **51**, 1733-1737 (1991).

117. Tutt, A., Gabriel, A., Bertwistle, D., Connor, F., Paterson, H., Peacock, J., Ross, G., & Ashworth, A. Absence of Brca2 causes genome instability by chromosome breakage and loss associated with centrosome amplification. Curr.Biol. **9**, 1107-1110 (1999).

118. van Criekinge, W. & Beyaert, R. Yeast Two-Hybrid: State of the Art. Biol.Proced.Online. **2**, 1-38 (1999).

119. Van Ruissen, F., de Jongh, G.J., Zeeuwen, P.L., van Erp, P.E., Madsen, P., & Schalkwijk, J. Induction of normal and psoriatic phenotypes in submerged keratinocyte cultures. J.Cell Physiol **168**, 442-452 (1996).

120. Vardy, L. & Toda, T. The fission yeast gamma-tubulin complex is required in G(1) phase and is a component of the spindle assembly checkpoint. EMBO J. **19**, 6098-6111 (2000).

121. Vassilev, A., Kimble, M., Silflow, C.D., LaVoie, M., & Kuriyama, R. Identification of intrinsic dimer and overexpressed monomeric forms of gamma-tubulin in Sf9 cells infected with baculovirus containing the Chlamydomonas gamma-tubulin sequence. J.Cell Sci. **108 (Pt 3)**, 1083-1092 (1995).

122. Venditti, M., Iwasiow, B., Orr, F.W., & Shiu, R.P. C-myc gene expression alone is sufficient to confer resistance to antiestrogen in human breast cancer cells. Int.J.Cancer **99**, 35-42 (2002).

123. Vogel, J.M., Stearns, T., Rieder, C.L., & Palazzo, R.E. Centrosomes isolated from Spisula solidissima oocytes contain rings and an unusual stoichiometric ratio of alpha/beta tubulin. J.Cell Biol. **137**, 193-202 (1997).

124. Wang, X.W., Zhan, Q., Coursen, J.D., Khan, M.A., Kontny, H.U., Yu, L., Hollander, M.C., O'Connor, P.M., Fornace, A.J., Jr., & Harris, C.C. GADD45 induction of a G2/M cell cycle checkpoint. Proc.Natl.Acad.Sci.U.S.A **96**, 3706-3711 (1999).

125. Weber, R.G., Bridger, J.M., Benner, A., Weisenberger, D., Ehemann, V., Reifenberger, G., & Lichter, P. Centrosome amplification as a possible mechanism for numerical chromosome aberrations in cerebral primitive neuroectodermal tumors with TP53 mutations. Cytogenet.Cell Genet. **83**, 266-269 (1998).

126. Wiese, C. & Zheng, Y. A new function for the gamma-tubulin ring complex as a microtubule minus-end cap. Nat.Cell Biol. **2**, 358-364 (2000).

127. Wrone-Smith, T., Mitra, R.S., Thompson, C.B., Jasty, R., Castle, V.P., & Nickoloff, B.J. Keratinocytes derived from psoriatic plaques are resistant to apoptosis compared with normal skin. Am.J.Pathol. **151**, 1321-1329 (1997).

128. Young, A., Dictenberg, J.B., Purohit, A., Tuft, R., & Doxsey, S.J. Cytoplasmic dynein-mediated assembly of pericentrin and gamma tubulin onto centrosomes. Mol.Biol.Cell **11**, 2047-2056 (2000).

129. Zheng, Y., Wong, M.L., Alberts, B., & Mitchison, T. Nucleation of microtubule assembly by a gamma-tubulin-containing ring complex. Nature **378**, 578-583 (1995).

130. Zhou, J., Shu, H.B., & Joshi, H.C. Regulation of tubulin synthesis and cell cycle progression in mammalian cells by gamma-tubulin-mediated microtubule nucleation. J.Cell Biochem. **84**, 472-483 (2002).

131. Zimmerman, W.C., Sillibourne, J., Rosa, J., & Doxsey, S.J. Mitosis-specific anchoring of gamma tubulin complexes by pericentrin controls spindle organization and mitotic entry. Mol.Biol.Cell **15**, 3642-3657 (2004).